METHOD DEVELOPMENT FOR ELECTROCHEMICAL IMPEDANCE SPECTROSCOPY STUDIES OF BOVINE SERUM ALBUMIN ON PLATINUM ELECTRODE SURFACES

by

Michelle Ann MacDonald

Submitted in partial fulfilment of the requirements
for the degree of Doctor of Philosophy

at

Dalhousie University
Halifax, Nova Scotia
March 2014

TABLE OF CONTENTS

LIST OF FIGURES

LIST OF TABLES

ABSTRACT

In this thesis, a method is presented for studying protein adsorption on solid surfaces by Electrochemical Impedance Spectroscopy (EIS), using a model system of Bovine Serum Albumin (BSA) on platinum electrode surfaces. EIS is a commonly used analytical technique for electrochemical biosensors, particularly useful because of the ability to model the electrochemical data with Equivalent Electrical Circuits (EECs) and extract meaningful quantitative values for physical processes that are occurring in the electrochemical system (for example, double-layer capacitance C_{dl} or charge-transfer resistance R_{ct}). In this thesis, a comprehensive method for EEC selection is developed by which the data are found to be Kramers-Kronig compliant, a library of possible circuits is selected, and then residual errors, parameter values, and standard deviations based on replicate measurements are used to find the circuit which best models the electrochemical system.

The influence of number of factors related to experimental set-up and EIS conditions on BSA adsorption is examined, and suggestions are given as to avoid signal convolution by these factors. Most influentially, performing EIS in Phosphate Buffered Saline (PBS) before exposure to BSA results in a significant decrease in BSA film formation. BSA adsorption is strongly influenced by potential, with more positive potentials resulting in greater BSA adsorption. The application of ac vs. dc potential, however, does not influence the BSA film. Surface-Enhanced Raman Spectroscopy (SERS) experiments of BSA and Human Serum Albumin (HSA) adsorption on gold Sphere Segment Void (SSV) substrates are also presented. Finally, BSA adsorption on platinum surfaces is monitored over time using EIS. Results suggest that, after incubation, BSA desorbs from the electrode surface but the rate of desorption is dependent on the concentration gradient between the surface and the bulk solution. Results also suggest that BSA adsorption is strongly affected by concentration, with higher concentrations resulting in greater BSA adsorption on the electrode surface and greater BSA desorption upon change to a less positive potential.

LIST OF ABBREVIATIONS AND SYMBOLS USED

Abbreviations

BSA	Bovine Serum Albumin
CPE	Constant Phase Element
Cy3	Cyanine 3
CV	Cyclic Voltammogram
DNA	Deoxyribonucleic Acid
EEC	Equivalent Electrical Circuit
EIS	Electrochemical Impedance Spectroscopy
EQCM	Electrochemical Quartz Crystal Microbalance
HSA	Human Serum Albumin
HS-PTFE	Heat Shrink-Polytetrafluoroethylene
IgG	Immunoglobulin G
PBS	Phosphate Buffered Saline
Rh6G	Rhodamine 6G
SERS	Surface-Enhanced Raman Spectroscopy
XPS	X-Ray Photoelectron Spectroscopy

Symbols

θ	Phase angle
A	Area of electrode
C	Capacitance
C_{dl}	Double-layer capacitance

C_f	Film capacitance
d	Distance
ε	Dielectric constant
ε_o	Permittivity of a vacuum
e	Applied potential
E	Amplitude of applied potential
E_{oc}	Open-circuit Potential
E_{eq}	Equilibrium Potential of Redox Species
i	Current
I	Amplitude of current
R	Resistance
R_{ct}	Charge-transfer resistance
ΔR_{ct}	Change in charge-transfer resistance
R_f	Film resistance
R_s	Solution resistance
σ_{im}	Residual error in imaginary component of EIS
σ_{real}	Residual error in real component of EIS
T	Time
ω	Frequency
ω_{max}	Frequency at which Z_{im} is at a maximum
$Z(\omega)$	Total impedance
$Z_{im}(\omega)$	Imaginary component of impedance
$Z_{real}(\omega)$	Real component of impedance

ACKNOWLEDGEMENTS

Firstly, I would like to thank my supervisor Dr. Heather Andreas for the opportunity to carry out research in a field in which I am genuinely interested. Her support, encouragement, and expertise have been unending and I am so grateful to have had the opportunity to learn from her. I would particularly like to thank Dr. Andreas for allowing me to begin research in a new field in her lab, and for working so hard to help me through all of the obstacles that come with setting up a new project.

I would like to acknowledge and thank the members of my supervisory committee: Dr. Donald Weaver, Dr. Peter Wentzell, and Dr. Peng Zhang. Thank-you also to Dr. Phil Bartlett and the Bartlett Research Group at the University of Southampton. I am so grateful to the Department of Chemistry for the opportunity to study in the welcoming and encouraging environment that is here at Dalhousie University. I would also like to acknowledge the Vanier Canada Graduate Scholarships and the Killam Trusts for their financial support of this degree.

I have been so fortunate along this journey to have worked with many wonderful people. Justin Tom, Jennifer Black, and Robert Johnson: thank you for all of the laughter, ideas, help, and insight. Alicia Oickle: you, in particular, have not only impacted my academic career, but have become a wonderful friend. I could not have been nearly as happy or successful at Dalhousie without you on my team.

To all my friends and family who have been unbelievably supportive of me over the past few years: thank you. I am so lucky to have such a wonderful support system, and I couldn't have gotten here without you.

Finally, I want to express my undying gratitude to my parents (Jane and Rob) and to my amazing husband, Andrew. There is absolutely no way that I would be at this point without your love, patience, and support. Thank you for celebrating the small victories with me, and for pushing me to persevere when it didn't seem worth it. Each of you was instrumental in every step of this process, and I am who and where I am today because of you.

Chapter 1 INTRODUCTION

The adsorption of proteins onto solid surfaces has been an area of interest for several decades because of its diverse applications in medicine, food processing, and biotechnology.[1] In particular, protein adsorption plays a large role in the development of electrochemical biosensors.[2] A biosensor is a device which transforms chemical information into an analytical signal; an electrochemical biosensor, then, is simply a biosensor that uses an electrochemical transducer.[3] Electrochemical biosensors have emerged at the forefront of biosensor research because of their potential for fast, accurate, and analyte-specific analysis of biomolecules both *in vivo* and *in vitro*.[4,5]

The field of electrochemical biosensor research is extremely broad, spanning a wide variety of analytical techniques, electrode materials, analyte materials, and detection platforms. For each specific analyte, a novel biosensor must be developed and new challenges overcome. Common to many electrochemical biosensor platforms, however, is the challenge of non-specific adsorption. Non-specific adsorption is the adsorption of solution molecules, other than the molecule of interest, onto the electrode surface, causing a change in signal which may be wrongly attributed to analyte signal.[6,7]

In a typical biological sample there may be hundreds of different biomolecules present and biosensors are required to differentiate among these molecules and "find" the analyte of interest. To overcome this challenge, electrode surfaces are typically modified by immobilizing a recognition element on the electrode prior to analyte detection.[8] This modification can take many forms, but is commonly the immobilization of an antibody structure on the electrode surface in order to make the surface specific for the corresponding antigen.[8–10]

Surface modification helps to decrease non-specific adsorption, but does not eliminate the problem as solution molecules are still able to find their way through the immobilized antibodies and adsorb on the electrode surface, generating a change in signal. To mitigate the effects of non-specific adsorption, surface modification is often followed by the formation of a blocking layer on the electrode surface – such that no remaining bare electrode surface is available for adsorption.[7,9,11,12] Commonly, the blocking molecule used for electrochemical biosensors is Bovine Serum Albumin (BSA)[11–17] – this protein will be the focus of the work presented in this thesis.

At the foundation of biosensor research is the necessity to understand how biomolecules interact with surfaces. For example, without thorough knowledge of how BSA adsorbs on electrode surfaces, its efficiency as a blocking molecule cannot be predicted. Protein adsorption has been under investigation for decades, but continues to be an important field of study for biosensor development as well as many other applications including fouling[18,19] and food processing.[1,20] BSA adsorption, in particular, has been the subject of much research over the past three decades, but questions still remain as to what factors influence BSA adsorption on solid surfaces and how BSA adsorption changes over time.

There are three commonly used electrochemical techniques in electrochemical biosensor research: cyclic voltammetry,[8,21–25] Electrochemical Quartz Crystal Microbalance (EQCM),[26–28] and Electrochemical Impedance Spectroscopy (EIS).[7,11,29–32] EIS will be the primary electrochemical technique described in this work. EIS measures the current that results from the application of an oscillating potential to the electrode

surface and uses changes in this current to understand the processes that occur at the biosensor surface (discussed in greater detail in Section 2.4).

One of the greatest advantages of EIS is the ability to fit data to an Equivalent Electrical Circuit (EEC) that models the physical processes occurring in the electrochemical system. Fitting the data to an EEC enables researchers to extract quantitative values for physical parameters such as double-layer capacitance (C_{dl}), charge-transfer resistance (R_{ct}), and solution resistance (R_s). The method by which an EEC is chosen, however, remains inconsistent in biosensor literature.

The goal of the research presented in this thesis was to develop a comprehensive method by which EECs can be chosen for protein/surface studies, using a model system of BSA on a platinum electrode surface. Chapter 2 provides background information on the topics and techniques discussed in this thesis, and Chapter 3 reports all Experimental Methods. Chapters 4 and 5 present the developed method for EEC choice. Once a suitable EEC was chosen for the system, the focus changed towards examining how EIS measurements influence BSA adsorption, and determining how to form reproducible BSA films by modifying experimental procedures – this research is presented in Chapter 6. Chapter 7 discusses preliminary work completed with the Bartlett Group at the University of Southampton focusing on using electrochemical Surface-Enhanced Raman Spectroscopy (SERS) to study BSA adsorption on gold electrode surfaces. Finally, the goal of the research presented in Chapter 8 was to determine how BSA films change over time. Overall conclusions and suggestions on future work are presented in Chapter 9.

Chapter 2 BACKGROUND

2.1 Electrochemical Biosensors

Biosensors are analytical devices that incorporate biological sensing elements, and convert a biological response into a useful (typically electrical) signal. Electrochemical biosensors, in particular, use electrochemical techniques (for example, EIS or cyclic voltammetry) as methods for bioanalyte detection.

Biosensors have diverse potential applications in the medical, food, and environmental fields.[4,33,34] In the medical field, biosensors are being optimized for detection of chemicals in the body – as is employed with the blood glucose sensor for diabetic patients.[35–37] In the food industry biosensors are being developed, for example, to detect levels of growth hormones in milk[38] or to study the bio-fouling of foods by processing techniques.[19] An example of a potential biosensor application in the environmental industry includes the detection of environmental endocrine disrupters in drinking water.[39]

Biosensors to date have employed a wide variety of analytical techniques. Among those presented in the literature are Surface Enhanced Raman Spectroscopy (SERS),[40–47] fluorescence microscopy and spectroscopy,[48,49] Surface Plasmon Resonance,[50–52] and Mass Spectrometry.[53–56] Over the course of biosensor development, however, electrochemical techniques have emerged for biomolecule analysis due to their speed of measurement and high sensitivity.[4] The most common electrochemical techniques in biosensor research are Cyclic Voltammetry,[20–25,57,58] EIS,[9,11,16,22,30,32,35,57,59–69] and EQCM.[26–28,70]

What many biosensors have in common is that they rely on a thorough understanding of biomolecule (most often, protein) adsorption at the electrode surface. Protein adsorption can occur for analyte detection, through non-specific adsorption, or as a secondary process such as when BSA is applied to the electrode surface as a blocking layer. In each case, protein adsorption impacts the function of the electrochemical biosensor. For this reason, an understanding of protein adsorption is crucial to the development of electrochemical biosensors.

The study of protein adsorption is by no means a new field. Beginning with amino acids (the building blocks of proteins), researchers in many fields have attempted to elucidate the adsorption behavior of proteins since the late 1960s.[71] A fundamental understanding of how proteins adsorb is not only crucial to aid in biosensor development, but also plays a major role in other fields of study including medicine, separations, and food processing.[1] For example, understanding protein adsorption is crucial for the development of medical implants as biocompatibility of these devices is strongly dependent on how proteins adsorb to them in the body.[72,73] In separations, protein adhesion onto chromatographic columns, for example, can affect the separation efficiency.[1] The presence of casein and lactoglobulin can result in the fouling of metal surfaces during the processing of milk[18] – providing motivation to understand the adsorption properties of these proteins.

The nature of interactions between a protein and a solid surface is dependent on the amino acid sequence of the protein as well as the fully-folded tertiary and quaternary protein structures.[71] Since each protein has a unique amino acid sequence and folded structure, it is expected that each protein interacts in a different way with solid surfaces.

For globular proteins such as BSA, it is generally agreed upon that electrostatic and hydrophobic interactions drive adsorption[1] (discussed in greater detail in Section 2.2.1). The proceeding sections will focus on serum albumin adsorption specifically, as serum albumins are the primary proteins discussed in this thesis.

2.2 Serum Albumin

BSA is a globular protein that is composed of 583 amino acids[74] and has an average molecular weight of 66 kDa.[13] Serum Albumin is one of the most abundant proteins in mammalian plasma.[74] A fully-folded BSA monomer has dimensions 4 nm x 4 nm x 14 nm.[13] The isoelectric point of BSA is 4.6;[26] the molecule carries a net negative charge at pH values above 4.6, and a net positive charge at pH values below 4.6.

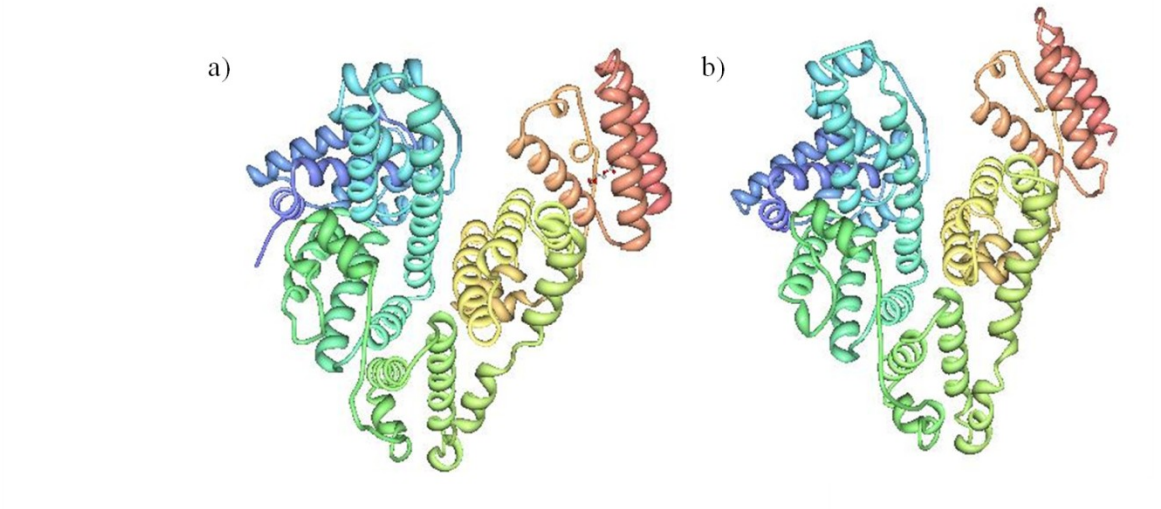

Figure 2.1: Crystal structure of a) BSA (Protein Databank ID: 4F5S) and b) HSA (Protein Databank ID: 1AO6).

Human Serum Albumin, (HSA) is the human-variant of BSA and contains two extra amino acids (for a total of 585).[74] It was recently determined that BSA exhibits about 75.8% identity as compared with HSA.[74] HSA has an isoelectric point of 4.7.[75]

As mentioned previously, the motivation behind the study of serum albumin adsorption is multi-faceted;[1] it has been studied for a wide variety of applications including, but not limited to, cell targeting,[26] corrosion of medical implants and biocompatibility,[31,76,77] fouling of food processing equipment,[31,76] and biosensing.[6,7,13,14,30,31,62,66,76,78] The proceeding sections will summarize the current understanding of serum albumin adsorption on bulk solid surfaces.

2.2.1 Serum Albumin Adsorption Mechanism

To achieve protein adsorption, the adsorbed protein state must be thermodynamically favorable over the solution state.[2] The interactions that make this possible are primarily electrostatic and hydrophobic in nature.[1] For metal surfaces in particular, protein adsorption is closely related to the charge on the surface.[1,2] Additionally, the greatest protein adsorption occurs at the isoelectric point (4.6 for BSA, 4.7 for HSA) of the protein, as the protein has a net neutral charge at this pH and protein-protein repulsions are minimized.[79]

Inconsistency exists in the literature about the nature of interactions between serum albumin and bulk noble metal surfaces (Au and Pt). Several groups suggest that the interaction is electrostatic in nature,[12,23,28,80,81] while others report adsorption with a mechanism of electron transfer through the carboxyl groups of the protein.[82,83] Those who support an electrostatic mechanism suggest that an increase in potential leads to an

increase in serum albumin adsorption on the electrode surface.[12,28,80,81] Additionally, Ying *et al.*[81] suggest that HSA can adsorb to both positively and negatively charged gold surfaces because of the flexibility of the protein to rearrange on the surface.

Studies of serum albumin adsorption on non-noble metals also debate whether chemisorption or electrostatic interactions are responsible for serum albumin adsorption. Researchers show that BSA adsorbs on a CrCoMo surface through a chemisorption accompanied by a transfer of charge to form protein-metal bonds.[84] The chemisorption mechanism is supported with BSA on stainless steel surfaces[85] where adsorption is reported to be accompanied by a charge-transfer from the carboxylate groups of the protein to the electrode surface. On titanium surfaces, however, an electrostatic mechanism is proposed as increasing negative charges on the BSA molecules results in less adsorption to the negatively-charged titanium surface.[86] An earlier study of BSA on titanium, however, suggested that chemisorption occurs through the basic amino groups of the protein.[77]

Serum albumin adsorption on metal oxide surfaces (titania, alumina, zirconia, silica) was shown to increase linearly with increasing densities of positive surface charge,[87] suggesting a possible electrostatic interaction. Further studies of BSA on alumina suggested that the carboxyl groups on the BSA interact electrostatically with the alumina.[88] Studies of HSA on titania surfaces showed that greater adsorption occurs when the BSA and the surface are oppositely charged, but that specific HSA-TiO_2 interactions prevail over electrostatic ones.[75] Studies of BSA adsorption on silica suggest that the amount of adsorbed protein is dependent on the electrostatic interactions between the protein and the surface, the repulsive interactions between protein molecules, and

hydrophobic interactions.[89] Finally, examination of BSA on tin oxide surfaces showed chemical bonds between the BSA and the surface.[90]

Examination of serum albumin adsorption on hydrophobic and hydrophilic surfaces suggest that, in these cases, hydrophobic interactions govern adsorption.[13,91] Jeyachandran *et al.*[13] suggest that BSA as a higher interaction strength with the hydrophilic (KOH) surfaces due to the formation of BSA-surface complexes. Ying *et al.*,[91] on the other hand, suggest that BSA adsorption is two times greater on hydrophobic surfaces, owing to the affinity between the protein and the surface.

Particular to the system presented in this thesis (BSA on Pt) past research suggests an electrostatic adsorption mechanism[28,80] or chemisorption facilitated through charge-transfer between the carboxylate groups on the BSA and the electrode suface.[83] It is relevant to be mindful of possible hydrophobic interactions as well, as hydrophobic interactions do impact serum albumin adsorption on a number of surfaces.[1,13,91]

2.2.2 Evidence of Serum Albumin Adsorption

It is well established in the literature that serum albumin adsorption on an electrode surface results in a blocking of that surface such that reactions that occur on the protein-free surface are either decreased or eliminated.[7,12,13,23,66,77,85,92–95] This effect is demonstrated by Figure 2.2 which presents cyclic voltammograms of a platinum electrode in Phosphate Buffered Saline (PBS) solution before and after protein adsorption, without (a) and with (b) a ferricyanide redox couple in solution. The cyclic voltammograms collected without ferricyanide (Figure 2.2a) show a decrease in the platinum oxide formation (*ca.* 0.2 V and above on the anodic sweep) and reduction (*ca*.

0.3 V and below peaks on the cathodic sweep) after BSA adsorption, confirming that less platinum oxide is formed and reduced when BSA is adsorbed on the electrode surface. Similarly, there is a decrease in the peak heights of the ferri/ferrocyanide redox peaks (centered at *ca*. 0.17 V in Figure 2.2b) after BSA adsorption, confirming that BSA on the surface also blocks this reaction.

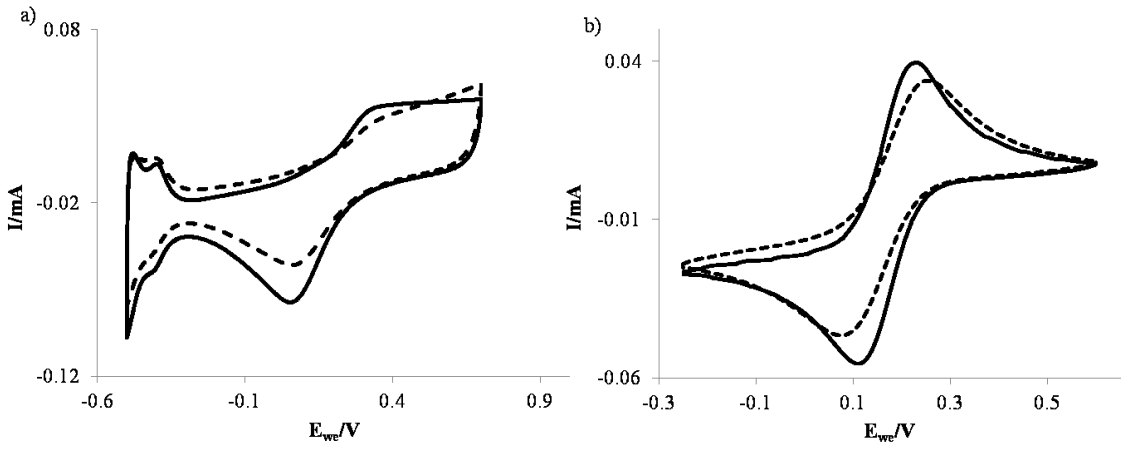

Figure 2.2: Cyclic voltammograms for a Pt electrode in PBS electrolyte without (a) and with (b) 3 mM ferri/ferrocyanide redox couple. Solid lines indicate bare Pt electrode and dashed lines indicate experiments in which a BSA film is present on the electrode surface.

2.2.3 Other Factors Influencing Serum Albumin Adsorption

In general, temperature changes can have a significant impact on protein adsorption, particularly at temperatures which are much greater than room temperature.[96] BSA has a denaturation temperature of 351 K (78 °C), above which the protein unfolds and forms a gel-like substance on the substrate surface.[58] The temperature dependence of BSA adsorption on platinum electrodes, specifically, was explored by Rouhana *et al*.[58] using cyclic voltammetry. The results showed that the surface coverage of BSA reached a

plateau over the temperature range 299 to 323 K (26 to 50 °C), at protein concentrations from *ca.* 0 to 0.20 g L^{-1}.

Solution pH has an impact on BSA adsorption as changes in pH affect the net charge of the protein in solution. Since BSA has a pI of 4.6, it carries a net negative charge at pH values above 4.6 and a net positive charge at pH values below 4.6. The greatest amount of protein adsorption is expected to occur at the isoelectric point,[97] when pH = 4.6. At pH 7, as is used in the experiments presented in this thesis, BSA carries a net negative charge. Assuming an electrostatic adsorption mechanism, greater BSA adsorption is expected at higher electrode potentials.

In general, greater protein adsorption can be observed with higher solution protein concentration.[96] Proteins generally form monolayers on material surfaces, as most proteins do not adsorb to surfaces in conformations that facilitate protein-protein binding.[96] For globular protein such as BSA, maximum adsorption typically corresponds to a close-packed monolayer of protein molecules on the surface.[97] While multilayers have not been reported for BSA specifically, they have been observed for other globular proteins such as β-lactoglobulin.[98]

2.3 Overview of Relevant Electrochemical Concepts

2.3.1 Double-Layer Capacitance

The capacitance (C) of an electrode/electrolyte boundary is a measure of the amount of charge stored on a surface at a particular potential.[99] As an electrode surface is charged, ions from solution are coulombically attracted to the electrode surface and reside in solution near the surface to balance the charge on the surface. This results in a

"double-layer" of charge, as illustrated in Figure 2.3 The so-called "double-layer" is actually very complex and includes specifically adsorbed anions, ions which have a hydration shell, adsorbed molecules, solvent layers, *etc*. However, for the purposes of biosensors and many other applications, the double-layer is simplified to the model shown in Figure 2.3, called the Helmholtz model. In this simple model, the double-layer is expected to behave as a parallel plate capacitor, and the principals that govern the charging and capacitance of a parallel plate capacitor are expected to apply.

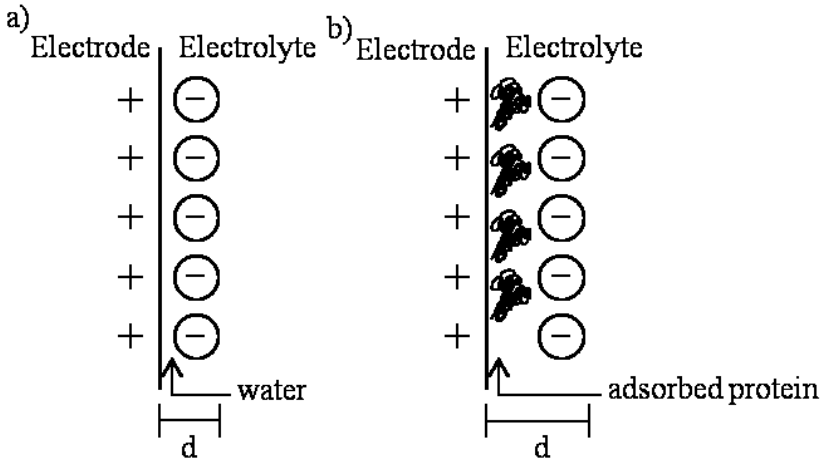

Figure 2.3: Simplified diagrams of the (a) electrochemical double-layer and (b) modified electrochemical double-layer with adsorbed protein layer. Note that neither diagram is presented to scale. For example, the size of BSA *ca.* 4 nm x 4 nm x 14 nm, the diameter of a chloride ion is *ca*. 180 pm, and the size of a water molecule is *ca.* 1-3 Å.

Capacitance is dependent on both the dielectric constant of the material (ε) between the two layers of charge in the double-layer (water in Figure 2.3a and adsorbed protein in Figure 2.3b) and the distance between these layers (d), through the equation

$$C = \frac{\varepsilon\varepsilon^{\circ}A}{d}, \tag{2.1}$$

where ε° is the permittivity of free space (8.85 x 10^{-12} F m^{-1}), and A is the area on which the charge is stored. When analyte protein molecules adsorb to the electrode surface (Figure 2.3b), both ε and d of the system will change.

Double-layer capacitance (C_{dl}) is often used to indicate protein adsorption.[23,27,62,69,95,100–103] Protein adsorption results in both an increase in d (as proteins adsorb on the electrode surface),[69] and a decrease in A (as adsorbed proteins reduce the amount of surface area in contact with the electrolyte);[103] consequently, protein adsorption results in an overall decrease in C_{dl}. The magnitude of change in C_{dl} can be related to the amount of protein adsorption, with higher values of C_{dl} resulting from less protein adsorption.[23]

2.3.2 Solution Resistance

As ions move through solution they encounter friction which causes them to lose energy as heat.[104] The friction that the ions encounter is represented by a resistance, R_s, which is termed the solution resistance. Ions travelling in a more viscous solution, for example, would experience a higher R_s than those travelling in a less viscous solution. The loss in energy that occurs is seen electrochemically as a loss in potential, and is termed the IR_s drop (where I is current). A low solution resistance is required for electrochemistry experiments, so that potential applied to the working electrode is all applied across the working electrode surface, rather than some of that potential being lost as charge moves through solution. The loss in potential due to solution resistance can be minimized by using an appropriate concentration of ions with high mobility in the electrolyte solution.[105]

2.3.3 Charge-Transfer Resistance

Charge-transfer resistance (R_{ct}) can be defined as the resistance to electron transfer across the electrode/electrolyte interface. In general, R_{ct} is impacted by both the energy-barrier associated with electron transfer at the electrode surface, and that associated with transport of the redox species to the electrode surface.[66] R_{ct} can be impacted by adsorption; for proteins, in particular, the presence of adsorbed proteins on the electrode surface increases R_{ct} by blocking the surface and making it more difficult for solution species to reach the electrode surface.[106] Accordingly, R_{ct} is commonly used to track protein adsorption at electrode surfaces; typically, R_{ct} values before and after adsorption are compared and an increase in R_{ct} is generally sufficient to indicate that protein has adsorbed on the electrode surface.[20,22,23,27,84,107]

Changes in R_{ct} are most often used to track protein adsorption in studies which employ EIS as the primary technique. In these cases, a redox couple is often added to solution to provide a simple means for tracking R_{ct}.[106] By far the most common redox couple used in EIS biosensor (or protein adsorption) research is the ferri/ferrocyanide redox couple.[9,10,35,57,65,108–110] This redox couple is easily soluble in aqueous media and is required in low concentrations (less than 4 mM) for EIS studies.[7] The downfall to use of the ferri/ferrocyanide redox couple is that it and may compete with analyte molecules for adsorption (see Chapter 6).

2.4 Electrochemical Impedance Spectroscopy

2.4.1 Overview

EIS is an analytical technique that measures the current that results from the application of an oscillating potential to the electrode surface. When an oscillating (ac) potential is applied to an electrode surface, the resulting current has the same frequency as the applied potential, but may be shifted in phase.[111] The amount of phase-shift is dependent on the relative resistive and capacitive features of the electrochemical system.[111] Consequently, the phase-shift can be used to monitor physical processes at the electrode surface, as each process (for example, protein adsorption) results in a change in the capacitance and/or resistance, and therefore a change in the phase-shift of the measured current.

As mentioned previously (Sections 2.3.1 and 2.3.3), protein adsorption on electrode surfaces results in changes in both C_{dl} and R_{ct}. EIS, then, is an excellent tool for studying protein adsorption, as impedance is sensitive to changes in resistance and capacitance. Further, changes in impedance can be used to quantitatively determine C_{dl} and R_{ct} values, by modeling the EIS data with an EEC (discussed further in Section 2.4.3).

By definition, impedance is defined as the ability of a circuit element to resist the flow of current.[99] Impedance is similar to resistance (it is a ratio between voltage and current), but is also impacted by the ability of a circuit to store energy.[111] In EIS, a sinusoidal (ac) voltage, e, of small magnitude, E, is applied to an electrode over a range of frequencies (ω), and the resulting sinusoidal current is measured. The resulting current, i, is of the same frequncy as the applied potential, but may be shifted in phase

(Figure 2.3). The phase-shift is reported as the phase angle (θ) as it relates to the period of the sinusoidal waves. The phase-shift (phase angle) represents the relative capacitive, resistive, and inductive character of the electrochemical system.[99]

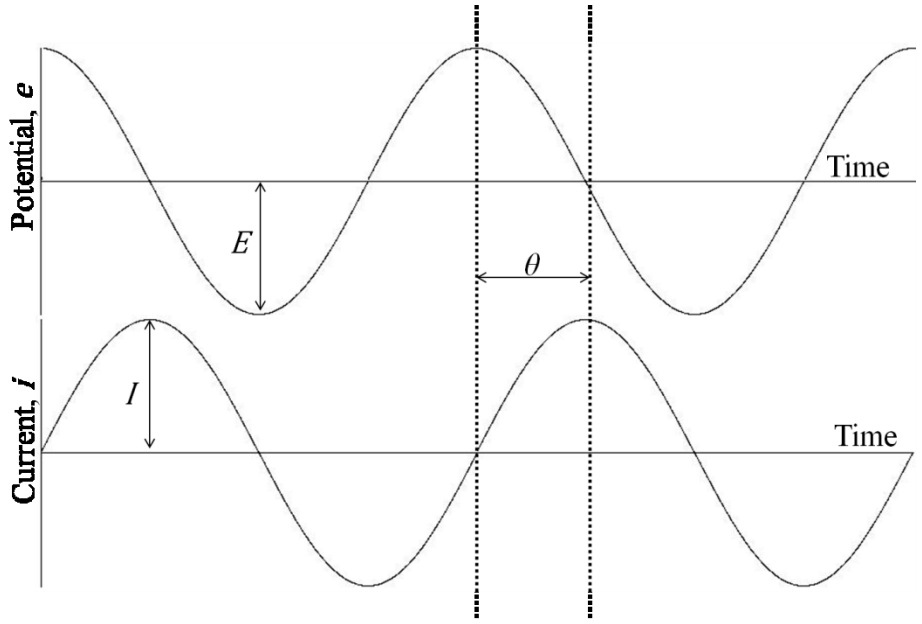

Figure 2.4: An example of applied potential and resulting current for an EIS experiment. Modeled after Bard *et al*.[99]

Equations 2.2 and 2.3 describe the applied potential (e) and resulting current (i), respectively, where t is time, I is the magnitude of the current oscillations, and ω is the frequency of the oscillations. These equations help guide an understanding of the impedance of two simple systems: a resistor and a capacitor.

$$e = Esin(\omega t) \tag{2.2}$$

$$i = Isin(\omega t + \theta) \tag{2.3}$$

If a potential is applied across a pure resistor, the phase angle is zero and the resulting current is in phase with the applied potential, as is suggested by Ohm's Law (Equation 2.4) through which potential (e) is directly proportional to current (i):

$$e = iR, \tag{2.4}$$

where R is the resistance. The resulting current (i), then, is described by Equation 2.5, where E is the magnitude of applied potential and R is the resistance.[99]

$$i = \frac{E}{R}\sin(\omega t) \tag{2.5}$$

In the case of a pure capacitor, however, current is equal to the capacitance (C) multiplied by the derivative of the potential (Equation 2.6), and therefore the resulting current is out of phase with the applied potential.[99]

$$i = C\frac{de}{dt} \tag{2.6}$$

$$i = C\omega E cos(\omega t) \tag{2.7}$$

$$i = C\omega E sin(\omega t + \frac{\pi}{2}) \tag{2.8}$$

Taking the derivative of a sine function yields a cosine function (Equation 2.7). Further, in impedance experiments the frequency of the resulting current is the same as that of the applied potential; it is possible to convert the cosine function (Equation 2.7) into a sine function which is shifted in phase by π/2 radians (Equation 2.8). Therefore, the phase angle for a pure capacitor is π/2.

The impedance of a system is expressed in complex notation.[99] The real impedance is denoted Z_{real} and the imaginary impedance is denoted Z_{im}. The overall impedance is expressed as a linear combination of the real and imaginary components:

$$Z(\omega) = Z_{real}(\omega) - jZ_{im}(\omega). \tag{2.9}$$

Although mathematically impedance is referred to as having real and imaginary components, both quantities are real as they can be measured by the phase angle.[99]

2.4.2 Impedance Plots

Impedance plots typically take one of two forms: Nyquist plots (Figure 2.4a) or Bode plots (Figure 2.4b). Nyquist plots are plots of $-Z_{im}$ on the y-axis versus Z_{real} on the x-axis; Bode plots show the phase angle and overall impedance on y-axes, against frequency on the x-axis.[111] For protein adsorption and biosensor studies, Nyquist plots are the most common plots presented in the literature,[10,11,16,22,30,37,65,75,78,110,112] although Bode plots are sometimes presented as they offer explicit information about the frequency.[31,72,95]

In a Nyquist plot, each point on the plot corresponds to a different measurement frequency;[111] typically, the frequency decreases with increasing real impedance along the x-axis, although the relationship between the two depends on the system under study. Mathematically, the real impedance, Z_{real}, is related to the resistance of the system (R) (Equation 2.10), and the imaginary impedance, Z_{im} is related to the capacitance of the system (C), where $j = \sqrt{-1}$ (Equation 2.11).

$$Z_{real} = R \tag{2.10}$$

$$Z_{im} = \frac{1}{j\omega C} \tag{2.11}$$

Figure 2.4 shows a sample Nyquist plot for a simple circuit involving a solution resistance (R_s) in series with one capacitor and one resistor in parallel. For an electrochemical system, the diameter of the semi-circle is often equated to the charge-

transfer resistance (R_{ct}, discussed in Section 2.3.3).[111] Further, the first x-intercept of the semi-circle (50 Ω in Figure 2.4) represents the solution resistance (R_s, discussed in Section 2.3.2). C_{dl} can be calculated using the maximum value of Z_{im} (at the top of the semi-circle) and the frequency at this point (obtained from the experimental data or the corresponding Bode plot), where C_{dl} is inversely proportional to Z_{im} (Equation 2.11).[99]

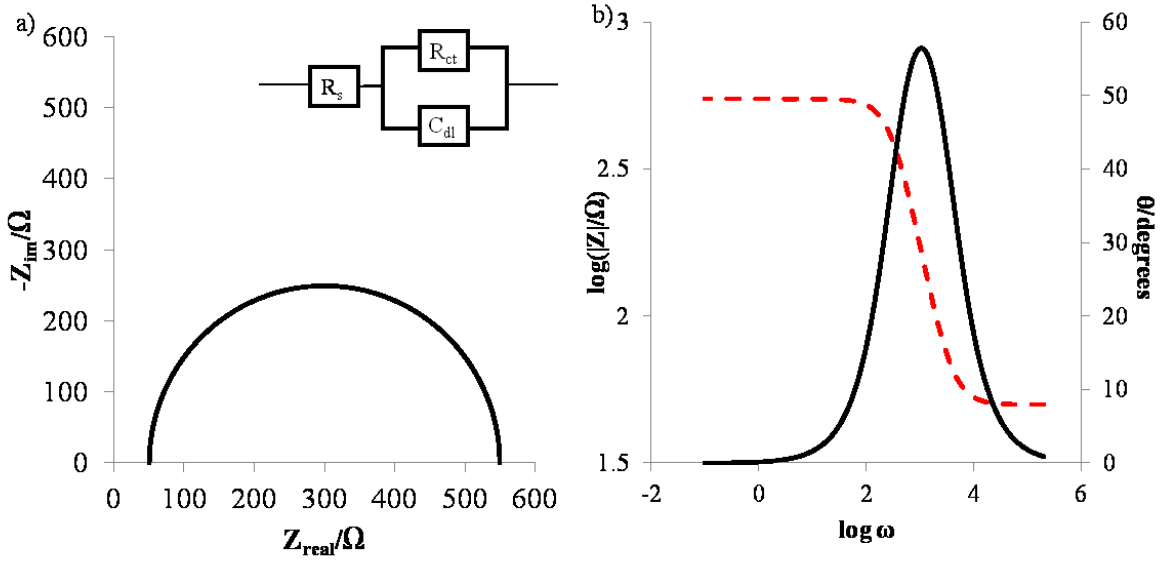

Figure 2.5: Simulated Nyquist (a) and Bode (b) plots for circuit with one capacitor and one resistor in parallel. Circuit is shown in the inset of (a), R_s = 50 Ω, R_{ct} = 500 Ω, C_{dl} = 1 μF. Plots were simulated using the ZSim function in EC-Lab.

As previously discussed (Section 2.3.3), protein adsorption on an electrode surface is expected to result in an increase in R_{ct}; therefore, protein adsorption is indicated on a Nyquist plot by an increase in the diameter of the semi-circle.[7] It follows, then, that Nyquist plots are very useful when studying protein adsorption data, as a quick comparison of semi-circles indicates (qualitatively) whether or not protein adsorption has occurred. Changes in C_{dl} are less obvious from a Nyquist plot and often require further (qualitative) analysis.

2.4.3 Equivalent Electrical Circuits and Modelling of Impedance Data

One of the greatest advantages of EIS is the ability to fit the experimental data to an Equivalent Electrical Circuit (EEC) which models the physical processes occurring in the electrochemical system. By fitting the data to an EEC, researchers are able to extract quantitative values for physical parameters that describe the system, and therefore are able to gain a better understanding of the processes which occur in the system. For example, in protein adsorption studies, the data can be modeled before and after exposure to protein, and R_{ct} values from each experiment can be extracted and compared. Since an increase in R_{ct} is expected to indicate blocking of the surface by proteins, this method can confirm the presence of protein molecules on the electrode surface.

Choosing a circuit by which to model impedance data is not a simple task. A review of the literature shows that, most often, circuits are chosen based on a combination of knowledge of the electrochemical system and a comparison between the fit and empirical data.[10,22,23,27,113,114] Most important in choosing a circuit to model the electrochemical system is that there is physical significance for each of the circuit elements in the EEC. For example, an excellent fit may be obtained using a large number of circuit elements, but those elements may not represent a process which is occurring in the system that is being modeled. When this over-fitting occurs, no chemical knowledge can be gained by fitting the EIS data to an EEC. EEC choice and fitting will be discussed in greater detail in Chapter 5.

2.5 Surface-Enhanced Raman Spectroscopy (SERS)

Raman spectroscopy is the study of inelastic scattering of light from molecules.[115] When a molecule is irradiated with electromagnetic radiation, energy is absorbed by the molecule and promotes the molecule into a higher (unstable, virtual) energy state. Typically, the molecule then releases the same amount of energy (as photons) as was absorbed, and relaxes back to its ground state.[116] This is called Rayleigh scattering.

Occasionally, however, the excited molecule releases less energy than was absorbed, and relaxes to a vibrational state instead of the ground state. The release of this energy is called Raman scattering. Raman scattering also occurs when a molecule which is already in a vibrational state is promoted to a virtual state and then relaxes back to the ground state, thus giving off a greater quantity of energy than was absorbed.[115] Rayleigh and Raman scattering are depicted in Figure 2.5. Raman scattering can be further divided into Stokes and Anti-Stokes scattering, when the energy released is less or more than that adsorbed, respectively.

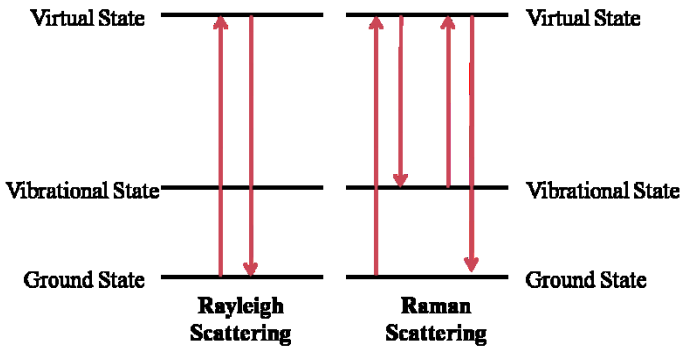

Figure 2.6: Diagram of Rayleigh and Raman scattering.

In order for a molecule to be Raman-active, it must undergo a change in polarizability upon irradiation. The subsequent Stokes and Anti-Stokes energy that is

given off is characteristic of a particular molecule and therefore Raman scattering can be used as a finger-print to identify molecules.[116]

The major pitfall of Raman spectroscopy is that Raman scattering is typically very weak and so requires a large amount of sample to obtain a measureable signal. Since the discovery of the Raman Effect in 1921, advances have been made to improve the Raman signal. For example, Resonance Raman Scattering (RRS) occurs when the energy of the virtual state coincides with an electronic level of the molecule[115] in which case the Raman signal is increased by a few orders of magnitude.[116]

A more general manner in which to obtain an improved Raman signal came in 1974 when Fleischmann *et al*.[117] obtained an unexpectedly large signal when studying pyridine adsorbed on electrochemically roughened silver surfaces. This work was followed by Jeanmaire and Van Duyne[118] and Albrecht and Creighton[119] who found that the increase in signal could not be due to an increase in surface area alone and that, instead, a surface enhancement was occurring. Thus, the term Surface-Enhanced Raman Spectroscopy (SERS) was coined.

Many years later the nature of the surface enhancement is well-understood. The greatest contribution to the enhancement comes from an enhancement in the local electric field around the molecule; specifically, the excitation of local plasmons which interfere constructively with the incoming radiation to magnify its intensity and subsequently the intensity of inelastic scattering from the molecule.[115,116] This so-called electromagnetic enhancement can increase the signal by six or more orders of magnitude.

With this understanding comes the push to design SERS substrates with enhanced electric fields at the surface. Generally, a SERS substrate can be any metallic surface

which produces an electromagnetic enhancement; gold and silver colloidal surfaces, for example, are very common in SERS research.[115] The major challenge in developing substrates for SERS comes with developing surfaces that have a uniform and reproducible enhancement across the entire surface.[116] The SERS substrates used in the experiments presented in this thesis (discussed further in Chapter 7) show standard deviations of less than 10 % across the surface.

SERS has been used to study biomolecules since its discovery in 1974[117] and has been used extensively for protein identification.[40,44–46,120–124] For protein SERS, the size of the protein molecule and the orientation of the adsorbed molecule greatly influence the SERS spectrum, as only amino acid residues residing close enough to the substrate surface to be enhanced will have peaks in the spectrum.[45] Therefore, in theory, SERS can not only be used to detect proteins, but also to determine the orientation of adsorbed molecules.

Particular to the serum albumin studies presented in this thesis, SERS spectra of BSA on gold nanocylinders,[44] gold nanoparticles,[125] nitrocellulose,[120] colloidal silver,[126] silver hydrosols,[127] and gold nanograin-aggregates[121,128] have been reported in the literature. In many cases, however, BSA has been used as a model protein to demonstrate the enhancement or reproducibility of a particular substrate.[44,120,128] Opportunities remain to use SERS as a tool for understanding serum albumin adsorption on SERS substrate surfaces.

Chapter 3 EXPERIMENTAL METHODS

3.1 Electrochemical Impedance Spectroscopy Experiments

3.1.1 General

Unless otherwise noted, all experiments were completed at room temperature, 22 ± 3 °C. All solutions were made using 18.2 MΩ-cm Millipore water. All PBS and BSA solutions were stored at 4 °C; PBS solutions were used within one month of the date they were made, and BSA solutions were used within 2 weeks. BSA solutions were allowed to come to room temperature before use in experiments, and were checked for evidence of protein denaturation (indicated by cloudy suspensions in solution) before use. Solid BSA was also stored at 4 °C. All other chemicals were stored at room temperature in vented chemical storage cupboards.

3.1.2 Electrodes and Cells

Working electrodes were 0.5 mm diameter Pt wire covered in heat-shrink polytetrafluoroethylene (HS-PTFE, Zeus Engineered Extrusions, 28 guage). The working electrode was prepared by sliding a small (*ca.* 5 cm long) piece of HS-PTFE onto a platinum wire and exposing the HS-PTFE to heat by rotating it above a butane flame for *ca*. 15 seconds. The HS-PTFE is expected to create an excellent seal around the wire as the final inner diameter after shrinking is 0.46 mm and the wire diameter is 0.5 mm. For each experiment, *ca.* 4 mm of the wire was left uncovered, resulting in an electrochemical surface area of *ca.* 0.08 cm^2 (determined by method described in Section 3.1.5).

The counter electrode was either a coiled Pt wire or Pt mesh, with surface area at least 10 times greater than that of the working electrode. The reference electrodes used were homemade Ag/AgCl reference electrodes with 0.15 M KCl (99.999%, Aldrich) filling solution. The potential of the reference electrodes was 0.271 V vs. Standard Hydrogen Electrode (SHE). The concentration of the filling solution was chosen to be the same as the concentration of Cl^- in the electrolyte solution. All potentials in the thesis are reported against this reference electrode.

All EIS experiments were run in all-glass three-compartment electrochemical cells (Figure 3.1). The total volume of PBS in the electrochemical cell was *ca*. 7 mL. The electrochemical cell had one compartment for each electrode (working, counter, reference), with the compartments for the counter and reference electrodes separated from the working electrode compartment by ground glass joints. The advantage of using a three-compartment cell for protein experiments was to minimize the reference and counter electrode exposure to protein by slowing the movement of protein into these compartments. Similarly, any species which may be formed at the counter electrode will not interfere with the processes occurring at the reference electrode.

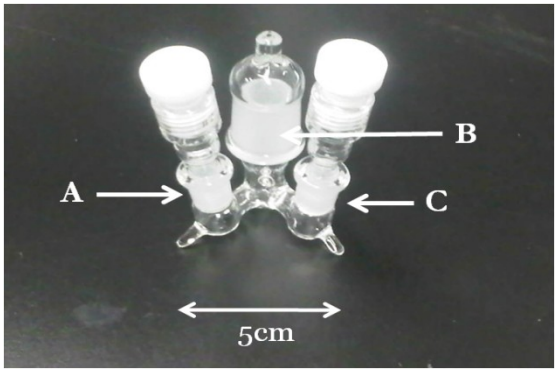

Figure 3.1. Example of a three-compartment electrochemical cell used in this work. A) counter-electrode compartment, B) working-electrode compartment, C) reference-electrode compartment.

3.1.3 Instrumentation

All electrochemical impedance measurements were performed using a Bio-Logic VMP3 multipotentiostat. Data were collected using EC-Lab software.

3.1.4 Electrochemical Cleaning

Electrochemical cleaning was completed in either the three-compartment cell or in a glass beaker cell. Electrochemical cleaning was performed on all platinum electrodes in deaerated 1 M H_2SO_4 (99.999%, Aldrich) before all EIS experiments. The cleaning was completed by cycling from -0.3 to 1.3 V at 1 V s^{-1} for at 200 cycles, or until a clean Pt cyclic voltammogram (-0.3 to 1.3 V at 0.1 V s^{-1}) was in evidence. After electrochemical cleaning, the electrode was rinsed thoroughly with 18 MΩ-cm water before proceeding with other experiments.

3.1.5 Electrochemical Surface Area Determination

The electrochemical surface area of the platinum working electrodes was determined by first cycling the electrode from -0.3 to 1.3 V at 0.1 V s^{-1} in 1 M H_2SO_4. EC-lab software was used to determine the area under the hydrogen under-potential deposition region of the curve (*ca.* -0.25 V to 0.04 V); integrating under the cyclic voltammogram in this region gives a measure of charge passed during the potential sweep in mA V. This value was then normalized for sweep rate by dividing by the sweep rate (0.1 V s^{-1}), resulting in a value of mA s, or mC (1 A s = 1 C). Finally, the charge was divided by 0.22 as 0.22 mC cm^{-2} is required to oxidize a monolayer of hydrogen from

polycrystalline platinum.[129] The final surface area for each of the electrodes was *ca*. 0.08 cm^2.

3.1.5 Electrochemical Impedance Measurements

EIS experiments were performed in phosphate-buffered saline (PBS) solution containing 0.2 M KH_2PO_4 (Sigma), 0.2 M K_2HPO_4 (Anhydrous, BDH Chemicals), and 0.15 M KCl (Aldrich, 99.999% metals basis). $K_3Fe(CN)_6$ was added to the PBS solution to provide a redox couple, with a final concentration of 3 mM. The pH of the PBS solution was *ca.*6.8, as measured using a SympHony pH electrode and meter.

EIS was run at the equilibrium potential of the ferri/ferrocyanide redox couple (E_{eq}, 0.171 V), using a frequency range of 500 kHz to 100 mHz and a potential perturbation amplitude of 10 mV. EIS was run in "single sine" mode such that only one frequency was sampled at a time. The equilibrium potential of the redox couple was determined by running a cyclic voltammogram from -0.5 V to 0.7 V at 0.1 V s^{-1} in PBS containing 3 mM ferricyanide and calculated the median potential between the oxidation and reduction peaks.

The EIS was repeated four consecutive times, followed by a 10 minute "rest" period at open-circuit potential, E_{oc}. The total time for one "set" plus one "rest" was *ca*. 23 minutes. For 20 hour experiments, the set/rest pattern was repeated a minimum of 55 times. For shorter experiments, only one set was completed. The length of each experiment will be noted throughout the thesis.

3.2.2.1 Incubation Experiments

In incubation experiments, BSA was introduced to the electrode surface by incubation in a 1, 10, 20, or 40 g L^{-1} solution of BSA (98% fatty acid free, Sigma) in PBS for 30 minutes. Incubation is a common method of protein film formation,[7,11,23,92] and past studies suggest that 30 minutes is a sufficient incubation time to form a BSA film on the electrode surface.[13,23] After incubation, the working electrode was transferred directly from the incubation solution to the electrolyte solution, and the EIS was run.

3.2.2.2 In Cell Experiments

Experiments were also completed during which BSA was present directly in the electrochemical cell. In this case, the electrochemical cell was either filled with BSA-containing PBS prior to EIS measurements (solution prepared as described in Section 3.2.2.1), or BSA was injected into the PBS solution in the electrochemical cell (700 µL of 10 g L^{-1} BSA for a total BSA concentration of 1 g L^{-1} in the electrochemical cell).

3.2.2.3 EEC Fitting

Before modeling EIS data, the data were determined to be Kramers-Kronig compliant, as is discussed in Chapter 4. All modeling of EIS data was completed using the Zfit function in EC-Lab with a simplex fit and 50,000 iterations, weighted by |Z|. For each circuit, all parameters were constrained to be positive, and initial estimates were given based on similar literature values and based on results obtained from non-EIS electrochemical experiments. Estimates were given as follows:

- R_s – Solution resistance was estimated from constant current charge/discharge experiments (presented in Section 5.3) in the three-compartment electrochemical cell. The resulting R_s values were determined to be 40 to 60 Ω, depending on the positioning of the electrode in the cell. For this reason, the initial estimate of R_{ct} used for the fitting procedure was 50 Ω. The solution resistance was determined by applying a constant positive current of 0.05 mA (or 0.5 mA) to the platinum electrode surface (in PBS electrolyte) and measuring the instantaneous drop in potential after the current was switched to negative 0.05 mA (or 0.5 mA). The drop in potential is equal to $2IR_s$, where I is the applied current and R_s is the solution resistance.
- R_{ct} – for each Nyquist plot, R_{ct} was estimated from the diameter of the semi-circular portion of the plot, by manually extrapolating the semi-circular region down to the x-axis and determining the x-intercept.
- C_{dl} – Literature suggests that the value for C_{dl} for a metal in solution should be in the range of 10 to 40 μF cm^{-2}.[99] The surface area of the Pt electrode used in EIS experiments was 0.08 cm^{-2}, suggesting an expected C_{dl} of 0.8 to 2.3 μF. For this reason C_{dl} was initialized at 1 μF for each fit.
- C_f – Film capacitance (C_f) was obtained by Xie *et al*.[27] to have a maximum value of 20 to 80 μF for BSA in a gold electrode of diameter equal to 0.65 cm^2. Assuming a round electrode, this suggests a capacitance range of *ca*. 60 to 240 μF cm^{-2}. A similar maximum value was obtained for Pt electrodes. Therefore, for the 0.08 cm^2 electrode used in this thesis, C_f can be estimated to be *ca.* 5 to 20 μF. Accordingly, C_f was initialized at 10 μF for each fit. When a

constant-phase element (CPE) was used in place of C_f, n was initialized at 0.8, as the CPE was not expected to model a pure capacitor (n=1) and the behaviour otherwise, was unknown.

- R_f – Film resistance (R_f) was obtained in the literature to be 3 to 7 Ω for BSA on a Pt electrode surface.[27] Accordingly, R_f was initialized to be 10 Ω.
- W – The Warburg impedance (W) was estimated by fitting only the low-frequency, linear region of the Nyquist plot to a single Warburg element. This resulted in a W-value of *ca*. 1200-2000 Ω $s^{-0.5}$ for various replicates. For this reason, the Warburg element was initialized at 1500 Ω $s^{-0.5}$ for each fit.

It is important to note that many different initial estimates were made in an effort to determine the impact of the initial value on the outcome of the fit. It was determined that the initial value did not impact the resulting parameter values unless the guess was several orders of magnitude off. For example, initial values of 1 μF, 10 μF, 100 μF, and 1000 μF all resulted in the same optimized C_f-value.

3.2 Surface Enhanced Raman Spectroscopy (SERS)

3.2.1 Instrumentation

All Raman experiments were completed using a Renishaw 2000 microscope instrument equipped with a 632.8 nm He-Ne laser. All data were collected using a 50x objective and a spot size of 1 μm. Raman data were collected using Renishaw WiRE 3.1. All electrochemical data was collected using General Purpose Electrochemical System (GPES) software.

3.2.2 Chemicals and Solutions

Proteins used in this work were BSA, HSA labeled with Rhodamine 6G (Rh6G), and Immunoglobulin G (IgG) labeled with Cyanine3 (Cy3). All proteins were commercially available from Abcam. Dithiol-modified Cy3-DNA was synthesized by the Bartlett Group, as per the procedure outlined in their publications.[47,130]

A 0.2 M PBS containing 0.2 M each of Na_2HPO_4 (98 %, Sigma) and NaH_2PO_4 (98 %, Sigma), 0.15 M KCl (99 %, Sigma), and 0.25 g L^{-1} Rh6G-HSA was prepared for use as the electrolyte in Electrochemical SERS experiments. 0.25 g L^{-1} solutions of Cy3-IgG and Rh6G-HSA for competitive adsorption experiments, and 1 g L^{-1} unlabelled BSA was prepared for BSA detection experiments. A solution of 10 mM tris(hydroxymethyl)aminomethane (TRIS) buffer (Sigma, pH *ca.* 7.2), 1 M NaCl (98 %, Sigma), and 1 μM dithoil-modified DNA was prepared for DNA adsorption experiments.

3.2.3 Sphere Segment Void Substrates

All SERS experiments were completed using gold Sphere Segment Void (SSV) substrates, prepared as described by Abdelsalam *et al*.[131] In summary, gold-coated microscope slides prepared were cut into eight pieces and sonicated in ethanol to remove any surface impurities. A capillary force method (utilizing a 15 degree angle and a temperature of 15 °C) was used to immobilize polystyrene spheres (600 nm diameter, Fisher) on the gold surface. Gold was then electrodeposited at -0.72 V vs. a saturated calomel electrode using a commercial gold plating solution (cyanide-free, Metalor ECF 60) and a commercial brightener (Brightener E3, Metalor); 10 μL of plating solution and

50 μL of brightener were used for each deposition. The purpose of the brightener was to aid the onset of nucleation and give a smooth, bright finish to the plated gold surface.[116] The potential was applied for 100 seconds, which corresponded to a film thickness of *ca.* 420 nm. Finally, the polystyrene spheres were dissolved from the surface by soaking the chip in dimethylformamide (DMF, Rathburn) for 30 minutes. The prepared gold surfaces were cleaned by soaking in DMF for 30 minutes, followed by collection of a SERS spectrum (using parameters described below) to ensure no peaks were evident above the background.

3.2.4 Non-electrochemical Raman Measurements

Raman measurements were made using the instrument described in Section 3.2.1. A spot size of 1 μm and an accumulation time of 30 seconds were used to collect each spectrum. After one spectrum was collected, the laser was moved approximately 2 μm in order to avoid denaturation of the protein molecules. Therefore, each spectrum was collected at a different spot on the gold chip, accounting for some variation among repeated spectra.

3.2.4.1 Two-protein Studies

For competitive adsorption experiments of HSA and IgG (Section 7.6) the gold SSV substrate was soaked in a 0.25 g L^{-1} solution of either Rh6G-HSA or Cy3-IgG for 30 minutes. After the 30 minutes, the substrate was removed and dried with Argon, and a SERS spectrum was recorded. Subsequently, the substrate was soaked in a 0.25 g L^{-1}

solution of the other protein (Rh6G-HSA or Cy3-IgG) for 30 minutes, after which the substrate was dried with argon and a SERS spectrum was recorded.

For competitive adsorption experiments involving DNA, the gold substrate was soaked in a 1 μM solution of dithiol-modified DNA for 48 hours to allow the thiol to chemisorb to the gold surface. Substrates were then rinsed in 1 M NaCl and SERS spectra were recorded. Rh6G-HSA was then introduced to the substrate by 30 minute incubation in a 0.25 g L^{-1} solution of Rh6G HSA. After 30 minutes, the substrate was removed and dried with argon, and SERS spectra were recorded.

3.2.5 Electrochemical Raman Measurements

3.2.5.1 Electrodes and Cells

For spectroelectrochemical measurements, the working electrode was a gold SSV substrate (Section 3.2.3). The counter electrode was a platinum wire, and the reference electrode was an Ag/AgCl electrode in contact with the electrolyte solution containing 0.15 M KCl. The potential of the reference electrode was *ca*. 0.45 V vs SHE; potentials reported for SERS experiments are comparable to those reported for EIS experiments.

Electrochemical SERS was completed in a specially-built spectroelectrochemical cell, pictured in Figure 3.2. The cell was built to be used as a flow cell (for temperature experiments), but this function was not utilized. The cell was assembled by placing the gold SSV substrate into the middle and applying pressure with tweezers while a small (*ca*. 150 μL) volume of electrolyte was injected onto the substrate. The whole cell was then covered with a microscope slide cover to seal the electrolyte into the cell. Electrical

contact was made between the gold SSV substrate and the "working electrode contact" (labelled in Figure 3.2) by placing a narrow piece of gold foil between the two.

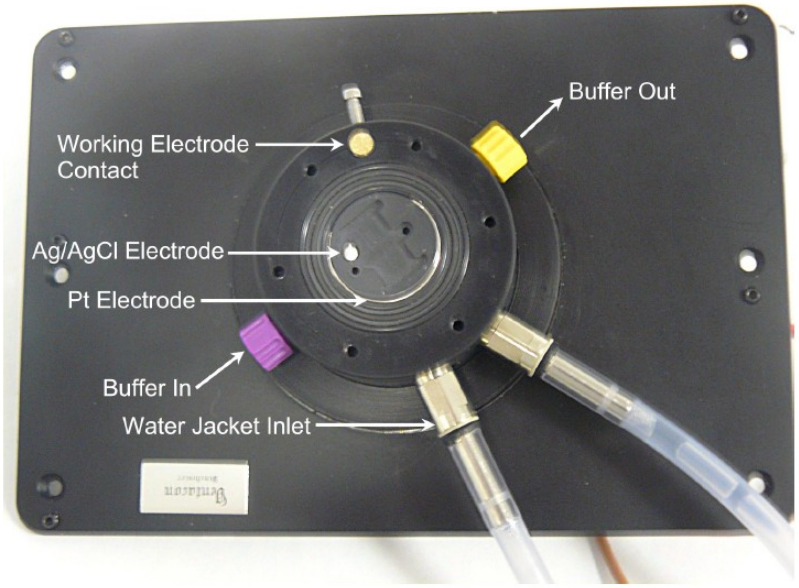

Figure 3.2: Spectroelectrochemical cell used for electrochemical SERS experiments.

3.2.5.2 Cyclic Voltammetry and Potential Hold Experiments

For cyclic voltammetry experiments, the electrode was cycled from -0.3 to 0.9 V at 0.01 V s^{-1}. During one cycle, seven SERS spectra were recorded, using the same conditions as described for non-electrochemical experiments.

For potential hold experiments, a potentiostatic hold at either -0.3 V or 0.9 V was applied to the electrode surface for 120 seconds. During this time, four SERS spectra were recorded, using the same conditions as described for non-electrochemical experiments.

For SERS experiments completed in the spectroelectrochemical cell, the clean, bare gold chip was put in the electrochemical cell, and the cell was filled with 0.25 g L^{-1}

protein in PBS. The cell was left for 30 minutes before SERS measurements were performed to allow the protein time to adsorb on the gold surface.

Chapter 4 KRAMERS-KRONIG COMPLIANCE

4.1 Introduction

The Kramers-Kronig relations were originally developed for the field of optics,[132,133] but over the past severial decades have been applied extensively to EIS to test whether or not the systems being studied satisfy the conditions of stability, causality, and linearity.[111,132–136]

The Kramers-Kronig relations are integral relations which calculate one part of the impedance from the other (experimentally determined) part. For example, the Kramers-Kronig relations can be used to calculate the real impedance from the experimentally determined imaginary impedance, or vice versa. In performing this calculation, any deviation of the calculated values from the experimental values suggests that one of the conditions (stability, causality, or linearity) is violated.[111] The Kramers-Kronig relations are expressed in Equations 4.1 and 4.2,[111] where Z_{im} is the imaginary component of the impedance, ω is the frequency, Z_{real} is the real component of the impedance, and *x* is an independent variable representing the complex frequency.

$$Z_{im}(\omega) = \frac{2\omega}{\pi}\int_0^{\infty} \frac{Z_{real}(x) - Z_{real}(\omega)}{x^2 - \omega^2} dx \tag{4.1}$$

$$Z_{real}(\omega) = Z_{real}(\infty) + \frac{2}{\pi}\int_0^{\infty} \frac{xZ_{im}(x) - \omega Z_{im}(\omega)}{x^2 - \omega^2} dx \tag{4.2}$$

As is expressed in Equations 4.1 and 4.2, the evaluation of the Kramers-Kronig relations requires integration over an infinite frequency range. In the case of the data presented in this thesis, and any experimental data presented in the literature, the frequency range used experimentally is not sufficient to integrate over zero to infinity. Several methods have been proposed in the literature to extrapolate experimental data to an infinite frequency range such that the Kramers-Kronig relations can be evaluated.[133,137–139] A different approach, not requiring any extrapolation, was suggested by Agarwal *et al.,*[140] and is called the measurement model method. Using this approach, the EIS data are fit to a circuit containing a solution resistance (R_s, Section 2.3.2) in series with a number of Voight elements: the "measurement model", as depicted in Figure 4.1. A Voight element is one resistor in parallel with one capacitor. Agarwal suggests that since each Voight element is Kramers-Kronig compliant, then the sum of these must also be Kramers-Kronig compliant.[140] Therefore, if the experimental data can be modeled by such a circuit as is shown in Figure 4.1 (where $n \leq m$ and m is the number of experimental data points), the system under study is stable, causal, and linear.

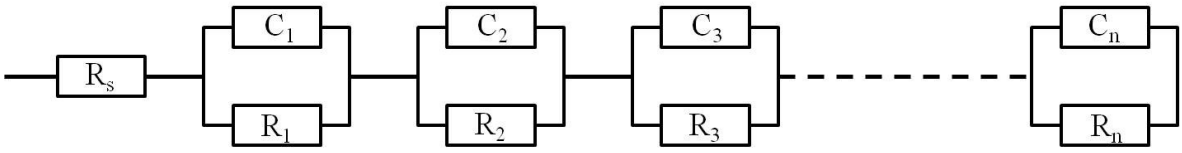

Figure 4.1: Circuit proposed by Agarwal *et al*.[140] to model experimental data to test the Kramers-Kronig compliance of the data. C represents a capacitor, R represents a resistor, R_s represents the solution resistance, and n is the number of Voight elements which, by definition, is less than or equal to the number of experimental data points being modeled.

Agarwal[140–142] suggests that although it is possible to determine the Kramers-Kronig compliance using either a measurement model (such as the one shown in Figure

4.1) or a process model (an EEC, in which each circuit element relates directly to a physical process that occurs in the system under study, Section 2.4.3), the use of a measurement model is beneficial as it eliminates any wrongful rejection of data that may occur due to a poor EEC choice. Specifically, if a poor fit is obtained using the Voight measurement model, it can only be attributed to the non-compliance of the experimental data. In contrast, when a poor fit is obtained using an EEC, it could be attributed to either the non-compliance of the experimental data or to the fact that the EEC does not adequately model the processes that are occurring in the system under study. It is optimal, then, to first prove the Kramers-Kronig compliance of the data using a measurement model, and subsequently fit the data with process models (EECs) such that any disagreement between the EEC and the experimental data can be attributed only to the inadequacy of the model and not to the non-compliance of the data.

For the data presented in this thesis, experimental frequency limits of 500 kHz to 100 mHz were used for all EIS experiments. As this frequency range is not sufficient to allow the direct integration of the Kramers-Kronig relations, the Voight measurement model method[140–142] will be used to determine the Kramers-Kronig compliance of the data presented in this thesis. Additionally, the frequency range within which the data is Kramers-Kronig compliant will be determined, such that this frequency range can be used for equivalent circuit fitting in subsequent chapters. This chapter will show a sample Kramers-Kronig analysis, and the results from the analysis of each set of experiments presented in this thesis.

4.2 Process for Determining Kramers-Kronig Compliance Illustrated Using Blank Data

As will be discussed in Chapter 5, it was necessary to perform Blank experiments in PBS and characterize this system, before complicating the system by the addition of protein molecules. Four replicate experiments were conducted during which impedance spectra were collected over 20 hours. Before the data can be modeled using the EEC method, it must be proven to be Kramers-Kronig compliant. The method of determining Kramer-Kronig compliance will be demonstrated with this data set.

While all the collected data points are relevant, only those which are Kramers-Kronig compliant can be used when modeling the EIS data with and EEC. Therefore, it is important to determine the largest frequency range for which all experiments of one type (all Blank experiments, in this case), are compliant. To do this, first the data which fall above zero on the imaginary impedance axis are removed from the analysis, as they typically result from the inductance of the wires connecting the electrodes to the potentiostat,[143,144] and therefore do not provide useful physical information about the protein/metal system. Second, the remaining data are modeled using the measurement model with 12 Voight elements (as this is the maximum number available in the EC-Lab software used for analysis), and the residual error for both the real and imaginary components of impedance (σ_{real} and σ_{im}) is calculated using Equations 4.3 and 4.4. In equations 4.3 and 4.4, $Z_{real,expt}$ and $Z_{im,expt}$ are the real and imaginary impedances measured from the experimental results, respectively; $Z_{real,fit}$ and $Z_{im,fit}$ are the real and imaginary impedances calculated from the fit from each circuit.

$$\sigma_{real} = \left(\frac{Z_{real,expt} - Z_{real,fit}}{Z_{real,expt}}\right) \times 100\% \tag{4.3}$$

$$\sigma_{im} = \left(\frac{Z_{im,expt} - Z_{im,fit}}{Z_{im,expt}}\right) \times 100\% \quad (4.4)$$

Table 4.1 contains the relative error values calculated for one blank experiment. Note that points 1 to 8 are removed as their imaginary impedance values fall below zero. Before proceeding with the analysis, it is necessary to determine the error range that is deemed acceptable for the points to be considered Kramers-Kronig compliant. While there is no value which is widely considered to be the maximum relative error to deem the data Kramers-Kronig compliant, values in the literature range from 5%[133] to 3%[134,140] to less than 1%[134]. Given the literature precedent, relative error values of less than 3% will be considered to indicate the Kramers-Kronig compliance of the data in this chapter.

As many of the error values tabulated in Table 4.1 (points 9 to 37) fall above the 3% limit set for the compliance of the data, the frequency window must be further truncated until all error values are less than 3%. Low frequencies are typically modeled by a Warburg impedance, W, which gives information about the diffusion of molecules to the surface, as opposed to physical processes occurring on the electrode surface.[114] For protein adsorption studies, then, the lowest frequency points generate the least valuable information when fit with an EEC. Accordingly, the frequency window was truncated by removing the lowest frequency point first (beginning with point 37). The remaining data are re-modeled using the measurement model and the relative errors are recalculated. Importantly, the removal of even one data point results in a slightly different fit and different relative error values (Table 4.1, points 9 to 36). This process of fitting the data to the measurement model and removing the lowest frequency point is repeated several times (iteratively), until all error values fall within 3%. The final points and corresponding residual errors are shown in Table 4.1, points 9 to 25. The remaining data

points for the blank experiments have a frequency range of 5879 Hz (point number 9) to 11.052 Hz (point number 25). The total number of data points remaining is 17. Since the number of Voight elements (n=12) is less than the number of data points (m=17), and the error values obtained are less than 3%, it can be concluded that the blank data, in the given frequency range (11.052 – 5879 Hz), is Kramers-Kronig compliant.

The fitting process outlined here for one blank EIS replicate was repeated for four identical experiments. For each experiment, the data were compliant in a slightly different frequency range. For the three replicate blank experiments conducted in addition to that already discussed, the point ranges determined to be Kramers-Kronig compliant are 9 to 34, 9 to 33, and 9 to 36, respectively. For EEC fitting, the frequency range in which all replicates are Kramers-Kronig compliant is used. Therefore, for the blank experiments, all EEC fitting used the 11.052-5879 Hz (point 9 to 25) range for every replicate.

Table 4.1: Calculated relative error values for a Pt electrode in (*ca*. 0.09 cm^2) in 0.2 M PBS with 3 mM ferri/ferrocyanide redox couple. Values are obtained by fitting the experimental data to the measurement model using 12 Voight elements, and calculating the relative error between the experimental data and the fit using Equations 4.3 and 4.4. Points 1 to 8 have been removed as they have imaginary impedance values below zero.

Point Number	Frequency /Hz	$\lvert\sigma_{real}\rvert$/% (points 9 to 37)	$\lvert\sigma_{im}\rvert$/% (points 9 to 37)	$\lvert\sigma_{real}\rvert$/% (points 9 to 36)	$\lvert\sigma_{im}\rvert$/% (points 9 to 36)	$\lvert\sigma_{real}\rvert$/% (points 9 to 25)	$\lvert\sigma_{im}\rvert$/% (points 9 to 25)
9	5879	9.98	88.53	0.24	10.48	0.33	0.68
10	3691	1.93	10.89	0.26	4.02	0.65	0.64
11	2679	4.51	0.68	0.67	2.00	0.19	0.53
12	1808	7.51	2.84	0.04	0.38	0.53	0.50
13	1222	6.28	7.40	0.98	0.26	0.31	0.58
14	826.322	2.56	8.82	0.83	1.35	0.44	0.79
15	558.036	0.29	5.22	0.21	1.86	0.32	1.01
16	377.537	0.58	0.07	0.88	0.11	0.49	0.37
17	254.105	0.62	2.61	0.38	2.15	0.15	0.84
18	172.037	1.38	2.93	0.93	1.75	0.19	0.13
19	116.378	2.05	2.59	1.13	0.67	0.03	0.09
20	78.518	2.90	1.15	0.29	2.00	0.19	0.24
21	53.179	2.62	2.17	0.11	1.48	0.09	0.08
22	35.79	1.77	4.86	0.59	1.07	0.20	0.08
23	24.172	0.97	5.15	0.19	0.49	0.39	0.15
24	16.367	2.19	1.16	0.03	1.50	0.06	0.46
25	11.05	1.20	3.32	0.62	0.92	0.04	0.48
26	7.469	1.17	3.75	0.79	0.25	-	-
27	5.034	3.10	0.30	0.10	1.15	-	-
28	3.409	2.03	3.15	0.22	2.00	-	-
29	2.309	0.88	3.84	0.67	1.61	-	-
30	1.559	2.29	0.40	1.31	0.29	-	-
31	1.05	0.60	2.99	0.86	1.10	-	-
32	0.711521	1.72	3.21	1.13	0.07	-	-
33	0.479589	2.41	0.73	2.07	2.10	-	-
34	0.323901	0.83	4.27	0.37	2.67	-	-
35	0.219452	1.67	3.19	0.86	0.44	-	-
36	0.148279	1.44	1.02	1.91	3.26	-	-
37	0.100206	3.09	3.63	-	-	-	-

4.3 Kramers-Kronig Compliance of BSA Experiments

Several types of BSA EIS experiments are presented in this thesis; the method summarized in the previous section was applied to each experiment (and the replicates), and the Kramers-Kronig compliant frequency range was determined. In each case, the total number of points determined to be Kramers-Kronig compliant was greater than the number of Voight elements used to model the data (n=12). A summary of the Kramers-Kronig compliant frequency ranges for each type of experiment modeled using in EEC in this thesis is presented in Table 4.2.

Table 4.2: Summary of frequency ranges obtained to be Kramers-Kronig compliant for each type of experiment presented in the thesis.

Experiment	Relevant Conditions	Sections of Thesis	Points Determined to be Kramers-Kronig Compliant	Frequency Range Determined to be Kramers-Kronig Compliant
BSA Incubation	1 g L^{-1}; ferricyanide present in incubation solution; no Initial EIS; incubation performed at open-circuit potential (E_{oc}); dc potential applied during incubation	Section 5.4 Sections 6.2, 6.3 Section 8.3	7 to 29	12852 Hz to 2.3087 Hz
BSA Incubation	1 g L^{-1}; ferricyanide present in incubation solution; Initial EIS; dc E_{oc} applied during incubation	Section 6.2	7 to 30	12852 Hz to 1.5588 Hz
BSA Incubation	1 g L^{-1}; no ferricyanide present in incubation solution; no Initial EIS; dc E_{oc} applied during incubation	Section 6.3	8 to 27	8685 Hz to 5.0338 Hz
BSA Incubation	1 g L^{-1}; ferricyanide present in incubation solution; no Initial EIS; dc E_{eq} (equilibrium potential of the redox couple, 0.171 V) applied during incubation	Section 6.4, 6.5	7 to 28	12852 Hz to 3.4086 Hz
BSA Incubation	1 g L^{-1}; ferricyanide present in incubation solution; no Initial EIS; ac E_{eq} applied during incubation	Section 6.5	7 to 27	12852 Hz to 5.0338 Hz
BSA Injection	BSA injected above electrolyte solution; total cell concentration 1 g L^{-1}	Section 6.6	8 to 26	8685 Hz to 7.4689 Hz
BSA Injection	BSA injected into electrolyte solution; total cell concentration 1 g L^{-1}	Section 6.6	7 to 25	12852 Hz to 11.0502 Hz
BSA In Cell	1 g L^{-1} BSA in PBS in electrochemical cell	Section 6.6 Section 8.4	7 to 27	12852 Hz to 5.0338 Hz
BSA Injection	Initial EIS; 17 °C; injection into solution; total cell concentration 1 g L^{-1}	Section 6.7	7 to 28	12852 Hz to 3.4086 Hz
BSA Injection	Initial EIS; 22 °C; injection into solution; total cell concentration 1 g L^{-1}	Section 6.7	7 to 26	12852 Hz to 7.4689 Hz
BSA Injection	Initial EIS; 27 °C; injection into solution; total cell concentration 1 g L^{-1}	Section 6.7	7 to 24	12852 Hz to 16.3670 Hz
BSA Incubation and Subsequent Addition	1 g L^{-1} incubation followed by addition of 1 g L^{-1} BSA to the electrochemical cell	Section 8.5	8 to 29	8685 Hz to 2.3087 Hz
BSA Incubation	10 g L^{-1}; ferricyanide present in incubation solution; no Initial EIS; dc E_{oc} applied during incubation	Section 8.6	7 to 28	12852 Hz to 3.4086 Hz
BSA Incubation	20 g L^{-1}; ferricyanide present in incubation solution; no Initial EIS; dc E_{oc} applied during incubation	Section 8.6	8 to 29	8685 Hz to 2.3087 Hz

4.4 Conclusions

The Kramers-Kronig relations are critical in the evaluation of EIS data for causality, linearity, and stability. It is necessary to prove the compliance of experimental data to the Kramers-Kronig relations before proceeding to analyze data using the EEC method, so that any difference between the experimental data and the fit based on an EEC can be attributed only to the failure of the EEC to adequately model the data, and not to the non-compliance of the data with the Kramers-Kronig relations. Although many methods have been developed to extrapolate experimental data such that the Kramers-Kronig relations can be evaluated directly, the simplest and most efficient method to test for the compliance of the data is the measurement model method, proposed by Agarwal *et al.*.[140–142]

The measurement model method was used to determine the frequency ranges in which the data for each type of experiment that will be presented in this thesis are Kramers-Kronig compliant. For the Blank experiments, the data are compliant between the frequencies of 5879 - 11.0502 Hz. For BSA data, the data are compliant in the ranges specified in Table 4.2.

The compliant data will be modeled using EECs through this thesis. Given that the modeled data are Kramers-Kronig compliant, any variation between the experimental and fit data can be attributed to EEC choice, as opposed to non-compliance of the data.

Chapter 5 METHOD FOR EQUIVALENT CIRCUIT DETERMINATION FOR ELECTROCHEMICAL IMPEDANCE SPECTROSCOPY DATA OF PROTEIN ADSORPTION ON SOLID SURFACES

The main body of work in this chapter has been accepted as a paper entitled *"Method for equivalent circuit determination for electrochemical impedance spectroscopy data of protein adsorption on solid surfaces", Michelle A. MacDonald and Heather A. Andreas, Electrochimica Acta,* February 13, 2014. I was responsible for the data collection, analysis, and a large part of the writing and editing of this paper. This chapter is different from the paper as the data from all fits are presented and the discussion is expanded.

5.1 Introduction

As mentioned previously, with protein adsorption, EIS data are generally fit to an Equivalent Electrical Circuit (EEC) to extract quantitative information about the processes occurring at the electrode surface.[106,145] Typically, researchers examine the fit between the circuit and the Nyquist (or Bode) plot to determine whether or not the circuit is a good model for the system.[10,27,106] In this chapter, a more thorough method of circuit choice is developed, based on relative residual errors between the experimental data and fit data, generated circuit parameter values relating to known physical parameters, and standard deviations based on replicate experiments. The method eliminates possible incorrect EEC assignment based purely on Nyquist plot fitting, and provides for more

confidence in the choice of an EEC, and by extension more understanding of what occurs in the protein/surface environment.

Many EECs have been used in the literature to model protein adsorption at a metal electrode surface, however, the most common is the modified Randles circuit,[30,35,60,64,78,95,102,146–148] shown in Figure 5.1a. In this circuit there is a solution resistance (R_s) that models the migration of charge through the electrolyte solution, a double-layer capacitance (C_{dl}) to model double-layer formation at the electrode surface, a charge-transfer resistance (R_{ct}) which models the charge-transfer reaction at the electrode surface, and finally a Warburg impedance (W) which models linear diffusion toward the electrode surface.

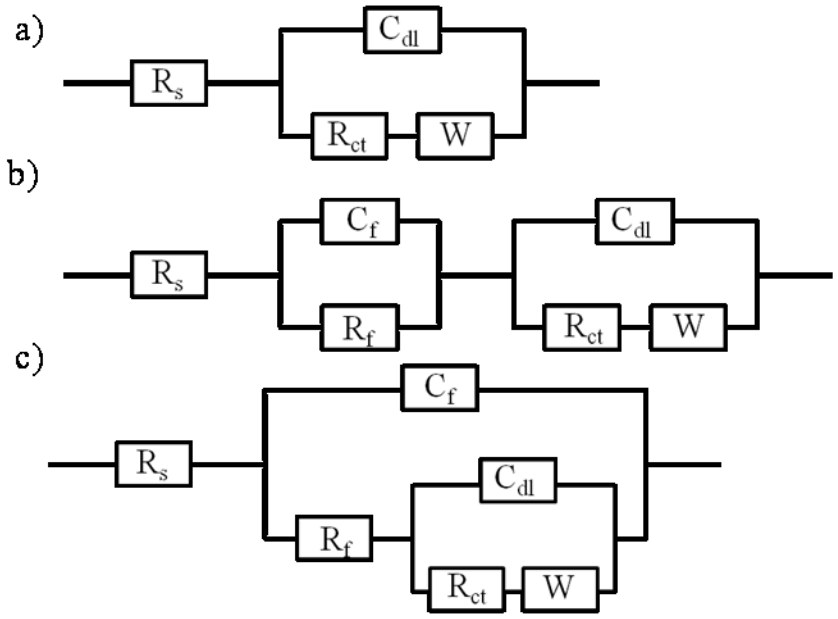

Figure 5.1: Examples of EECs used in the literature to model BSA adsorption at a metal electrode surface, in the presence of a redox couple.

In addition to the Randles circuit, other EECs have also been used to model protein adsorption. Xie *et al.*[27] add an additional time constant (resistor and capacitor in parallel) to the modified Randles circuit (Figure 5.1b) suggesting that the additional

resistor and capacitor model the resistance and capacitance of the adsorbed protein film on the electrode surface, R_f and C_f respectively in Figure 5.1b. Diniz *et al.* [10] also add a second time constant to the modified Randles circuit, but change slightly the location of the new resistor and capacitor, as shown in Figure 5.1c. Diniz *et al.* [10] suggest that the added resistor and capacitor are associated with an insulating layer on the surface of the electrode. Given that all three of the circuits presented in Figure 5.1 are used to model protein adsorption on a solid surface, the question arises of how to determine which circuit best represents the physical system.

This chapter presents a systematic method for the determination of the EEC that best represents EIS data collected in protein adsorption experiments. To demonstrate the method, the literature equivalent circuits described above are applied to a model system of BSA adsorption on a platinum electrode.

5.2 Choosing a Library of Circuits

Before proceeding to model the data with any one circuit, it is necessary to create a library of circuits that may provide an adequate model for the system under study. As mentioned in the introduction, the modified Randles circuit, shown in Figure 5.1a, is the most common circuit in the literature used to model protein adsorption at a metal electrode surface. This circuit has four important elements: R_s, the solution resistance, C_{dl}, the double-layer capacitance, R_{ct}, the charge-transfer resistance, and W, the Warburg impedance.

The Randles circuit can be modified to incorporate a Constant Phase Element (CPE) in place of the C_{dl} element. The CPE accounts for inhomogeneity at the surface of

the electrode.[24,149] To be thorough, the experimental data must be modeled with and without the CPE to determine which circuit provides a better fit of the data. The Randles-type circuits described here will be denoted as circuit A1 (with C_{dl}) and A2 (with CPE). Figure 5.2 provides a legend of all circuits studied and their corresponding notation.

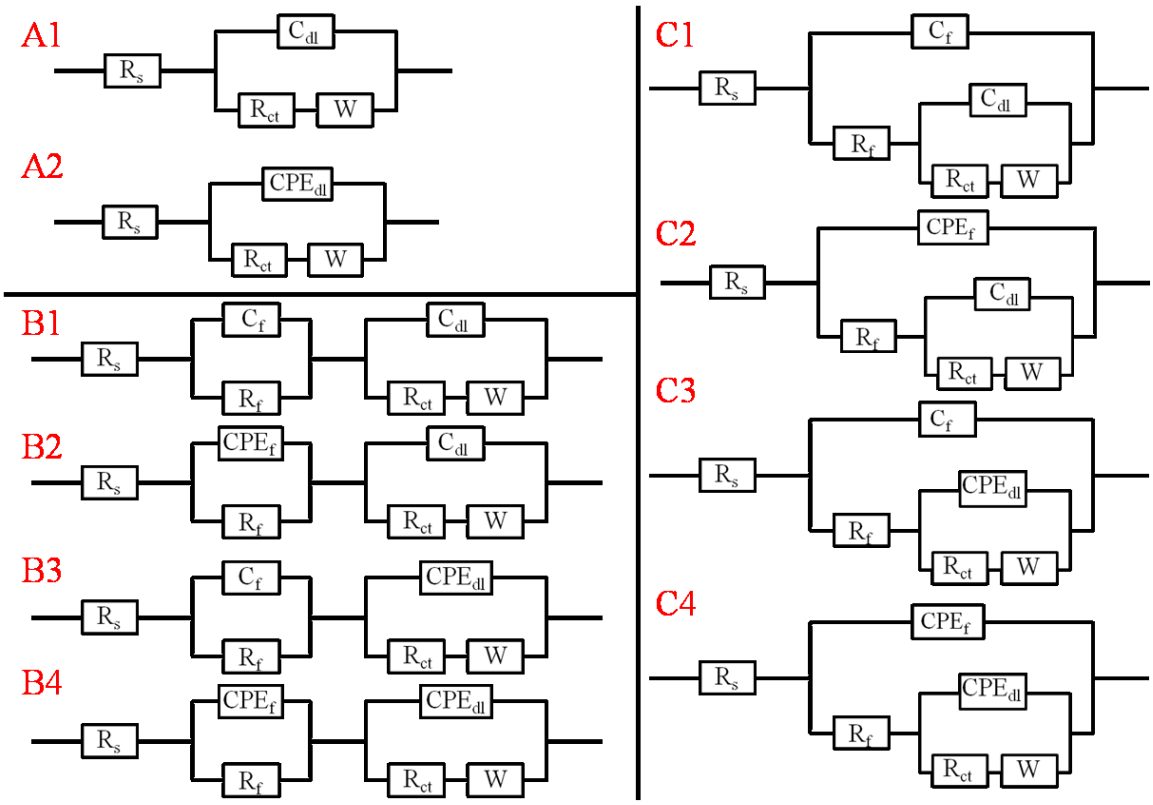

Figure 5.2: Diagram of all circuits used to model experimental data obtained for BSA adsorption on a platinum wire electrode in PBS solution

While the A-type (Randles-type) circuits may provide an adequate model for the system, they do not take into account the resistance and capacitance of the film itself. A second time constant can be added to the circuit to model the film,[22,27] as is the case for the circuits presented in Figure 5.1b and c (also labelled type B1 and C1 in Figure 5.2). Although these circuits have the same elements, their physical significance is slightly different.

In the case of the circuit labelled B1 in Figure 5.2, the second time constant (composed of C_f and R_f) represents a conductive film[150] – as charge must move through the film before accessing the surface (represented by the Randles part of the circuit). In the case of the circuit labelled C1 in Figure 5.2, the second time constant represents either a porous, insulating film[10] (as charge flowing through the circuit is either used to charge the film or travel through the pores of the film to reach the surface) or a conductive film with a high resistance.

Each of the capacitors in the circuits in the B1 and C1 circuits can be replaced by a CPE, to account for a lack of homogeneity in the surface or the film. The families of circuits created by doing this will be called the B-type circuits and C-type circuits, respectively, and are displayed in Figure 5.2.

5.3 EEC Choice for Blank Data

Prior to modelling the protein (BSA) adsorption data using the library of EECs suggested above, it is necessary to first determine the circuit which best models the blank (BSA-free) system. By understanding which circuit best fits the system in which a platinum electrode is immersed in PBS solution, one can gain insight into the differences that occur in the BSA-containing system which may help elucidate the "correct" circuit for that system.

Figure 5.3 shows the Nyquist plot for a Pt wire electrode in 0.2 M PBS solution containing 3 mM $K_3Fe(CN)_6$, after 20 hours of EIS. The experimental data are compared with the fits of each of the circuits shown in Figure 5.2. While no film formation is expected in this case, comparing the data with circuits that model bare electrode surfaces

(A-type) and those modelling film formation on the electrode surface (B-type or C-type) may provide insight into unidentified processes that may occur in the electrochemical system. Note that a total of four replicate blank experiments were completed, and plots for the fit of each replicate to each circuit are presented in the Appendix, Figures A1, A2, and A3.

The plots in Figure 5.3 show a similar quality of fit for each of the modeled circuits. The data illustrate the need for a more thorough method of circuit determination as each of the presented circuits generates what would be considered a "good" fit in the literature. Initially, circuit B3 (Figure 5.3e) appears to have the worst fit and the best fit is indistinguishable between circuits C1 and C4 (Figure 5.3g and j, respectively). The similarity of fits of the Nyquist plot suggest that more than one possible circuit adequately models the experimental data; however, these circuits model very different physical situations at the surface *(i.e.* no film, conducting film, insulating film). Thus, a simple comparison of the Nyquist plot is not sufficient to elucidate the best model for the system. For this reason, further analysis must be completed to determine the best circuit for the system.

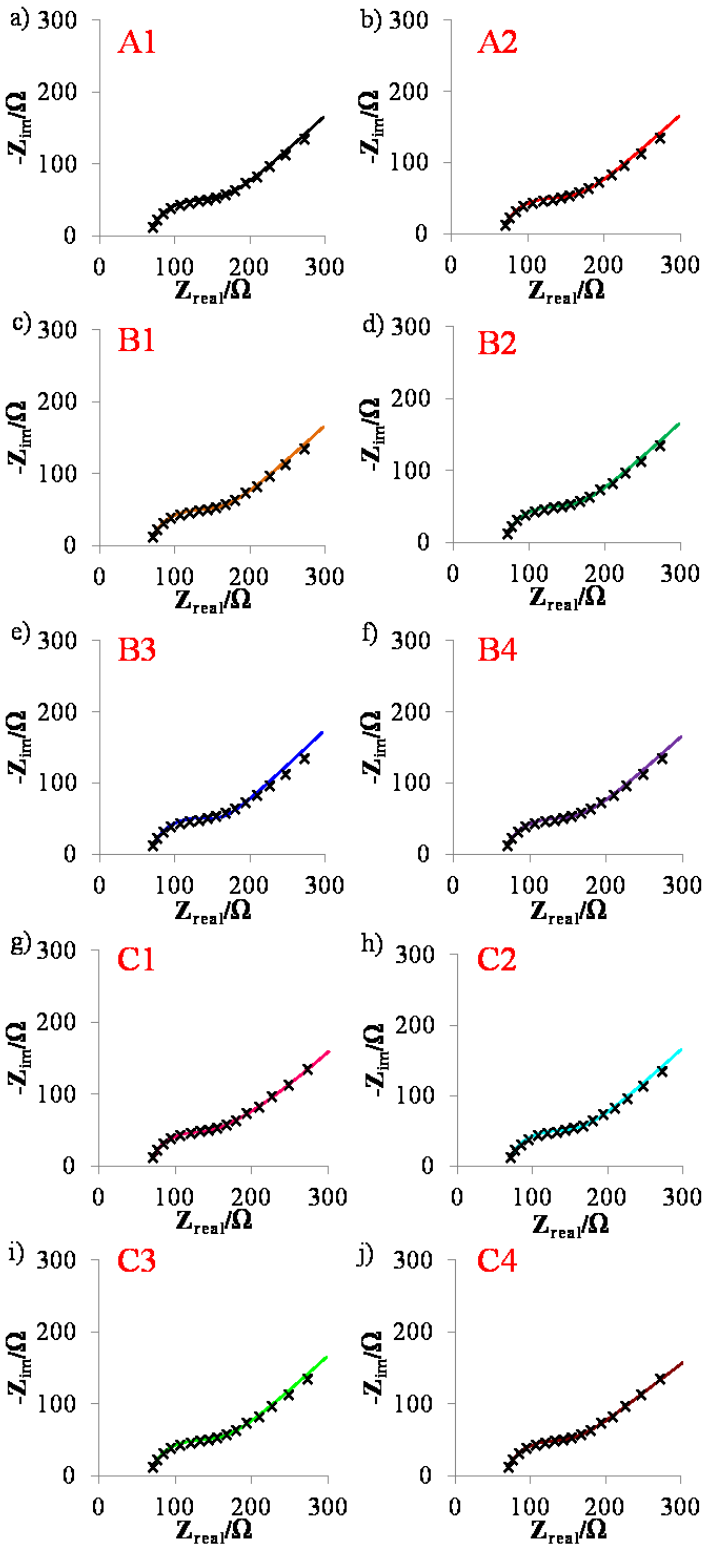

Figure 5.3: Nyquist plots for a Pt electrode in 0.2 M PBS with 3 mM ferri/ferrocyanide (20 h), with fit data generated from fitting experimental data to each circuit in Figure 5.2. (x) indicate experimental data and solid lines indicate fit.

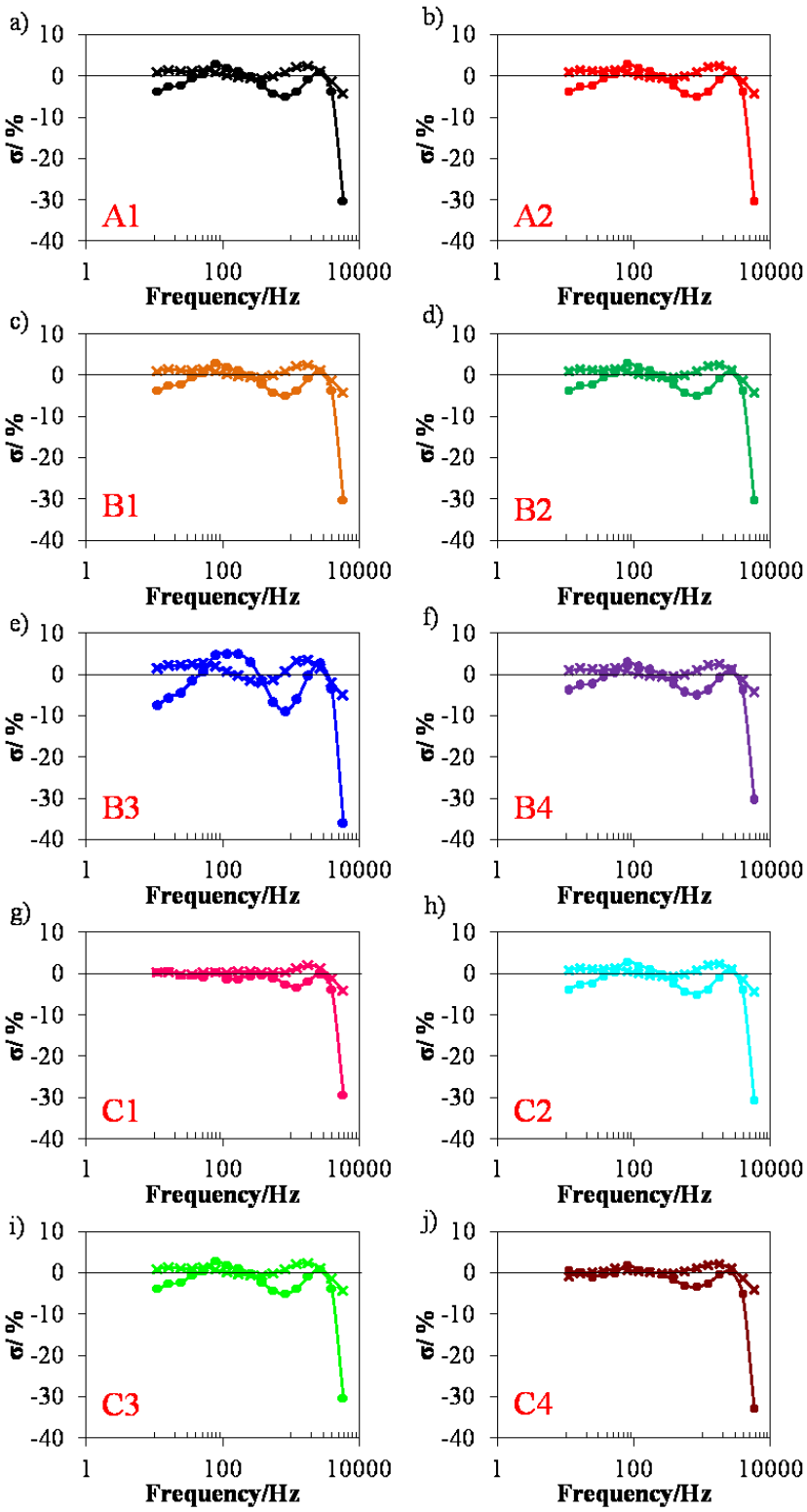

Figure 5.4: Relative residual errors resulting from the fit of circuits in Figure 5.2 to the 20 h data (Figure 5.3) for a Pt wire electrode in 0.2 M PBS solution with 3 mM ferri/ferrocyanide. Crosses represent σ_{real} and circles represent σ_{im}, discussed in Chapter 4.

After the data is fit to a circuit, the relative residual errors for the real and imaginary components of the impedance (σ_{real} and σ_{im}) can be calculated using Equations 4.3 and 4.4, respectively. The residual errors provide a means for understanding the quality of the fit obtained. Since the data are Kramers-Kronig compliant, discrepancies between the modeled and experimental data can be related to the lack of fit of the EEC[141] – in other words, that the particular EEC is an inadequate model for the system being studied. Residual error plots for the blank (BSA-free) experiments are presented in Figure 5.4.

Figure 5.4 shows the relative residual errors obtained when the data collected after 20 h of Pt in PBS solution is fit to each of the circuits in Figure 5.2. Similar plots for replicate experiments can be found in the Appendix, Figures A4, A5, and A6. Residual errors are most frequently used to determine the quality of fit when determining the Kramers-Kronig compliance of the EIS data using the measurement model method[140] – in which cases error values of 5 % and less have been shown to indicate compliance (a good fit) of the data. Many of the circuit fits result in error values of less than 5 %, with the exception of the highest frequency data point, which is consistently higher in error. Consistent with the data presented in Figure 5.3, B3 has the worst fit as it results in the highest residual errors, and circuits C1 and C3 have the best fit. As was the case with the Nyquist plots, however, the residual errors alone are not sufficient to select the circuit that best models the data as they do not provide information about the extracted parameter values which must be consistent with the physical processes they describe, as discussed below.

It is important to be able to separate these circuits since the models examined describe a range of very different physical processes/environments on the electrode surface, and more analysis is needed in order to choose the best model for the physical system. The Nyquist plots and the residual errors are commonly used to choose a circuit,[10,22,23,27,113] however, it is clear from the data presented here that these plots alone are not sufficient. The extracted circuit parameters (R_s, C_{dl}, etc.) must be analyzed and compared to the known values from literature or non-EIS experiments to determine if the each circuit is providing reasonable values and thus, adequately describing the real system. Additionally, replicate experiments will provide a measure for how reproducible an extracted circuit parameter is for a particular system and circuit.

Table 5.1 summarizes the values for the circuit parameters and their standard deviations obtained for four replicate experiments in which a Pt wire was exposed to PBS solution and EIS was run for 20 hours such that steady-state was reached (discussed in detail in Chapter 8). For each replicate experiment, the data obtained after 20 hours was modeled with each of the circuits in Figure 5.2. Note that the standard deviations are those among replicates, not standard deviations of the fit. The standard deviations between replicates are used to highlight circuits which show large variations in the parameters. When variation is not expected between the replicates (*e.g.* in blank experiments where the same parameter values are expected for each experimental run), large standard deviations can indicate that the circuit is not fitting the data appropriately.

The values indicated in bold in Table 5.1 are values for which the standard deviation among the four replicate experiments is greater than the average value, suggesting that either the four replicate experiments produced largely different results, or

that the circuit used to model the data is not an appropriate model. As each of the experiments was performed in exactly the same way using an electrode of the same surface area, and PBS solution from the same batch, it is very unlikely that the surface/electrolyte interactions and processes (modeled by the circuits) would be significantly different. Thus, in this case, the values obtained are good indicators that the EECs which exhibit the high standard deviations in the circuit parameters are not good models for the system under study. As there is at least one of these values for each of circuits B1, B2, B3, B4, C2, C3, and C4, this type of data analysis indicates that these EECs are not adequate models for the system. Again, these findings highlight the importance of replicate experiments for choosing appropriate EECs, since each of these circuits appeared to model the data well when only one replicate and the residual error analysis (above) was used, whereas the use of replicates showed that these EECs were not modelling the system appropriately.

Table 5.1: Summary of parameters obtained by fitting four EIS experiments on a Pt wire electrode in 0.2 M PBS solution with 3 mM ferri/ferrocyanide. The standard deviations presented are for the four replicates, not for the fit. Numbers in bold indicate values for which the standard deviation is greater than the average value.

	Parameters									
Circuit	**Rs /Ω**	**C_f /μF**	**CPE_f /μF $s^{(n-1)}$**	**n**	**R_f /Ω**	**C_{dl} /μF**	**CPE_{dl} /μF $s^{(n-1)}$**	**n**	**R_{ct} /Ω**	**W /Ω $s^{-0.5}$**
A1	61 ± 11	--	--	--	--	1.5 ± 0.3	--	--	77 ± 13	1500 ± 170
A2	61 ± 11	--	--	--	--	--	1.5 ± 0.3	1.0 ± 0.0	77 ± 13	1500 ± 170
B1	60 ± 11	**3.0 x 10^{-7} ± 5.1 x 10^{-7}**	--	--	0.24 ± 0.20	1.5 ± 0.3	--	--	77 ± 13	1500 ± 170
B2	51 ± 13	--	**5.5 x 10^{-6} ± 6.6 x 10^{-6}**	0.48 ± 0.35	**10 ± 12**	1.5 ± 0.3	--	--	77 ± 13	1500 ± 170
B3	51 ± 19	**1.2 ± 1.4**	--	--	35 ± 27	--	**2.5 ± 3.2**	0.99 ± 0.02	54 ± 41	1500 ± 170
B4	61 ± 11	--	**4.1 x 10^{31} ± 8.1 x 10^{31}**	**0.50 ± 0.58**	**3.6 x 10^{-13} ± 5.0 x 10^{-13}**	--	1.5 ± 0.3	1.0 ± 0.0	77 ± 13	1500 ± 170
C1	61 ± 12	1.5 ± 0.3	--	-	91 ± 14	9.3 ± 2.3	--	--	**39** ± 14	1400 ± 200
C2	50 ± 12	--	**0.05 ± 0.06**	0.77 ± 0.25	**11 ± 14**	1.5 ± 0.3	--	--	77 ± 13	1500 ±170
C3	61 ± 11	1.5 ± 0.3	--	--	**1.7 ± 3.1**	--	**58 ± 110**	0.68 ± 0.43	75 ± 14	1500 ± 160
C4	61 ± 11	--	1.5 ± 0.3	1.0 ± 0.0	**19 ± 39**	--	**72 ± 140**	**0.51 ± 0.56**	58 ± 41	1500 ± 150

The numerical value for each circuit parameter must also be examined and compared to expected values in order to verify a circuit's applicability to a system. As discussed in detail in Section 3.1.5, approximate parameter values were obtained from a combination of similar, literature experiments, and non-EIS electrochemical experiments. In particular, R_s was determined using a constant current charge-discharge experiment, presented in Figure 5.5. In this experiment, a positive 0.05 mA current was applied to the electrode surface (and the potential was recorded) and switched to a negative 0.05 mA

current. The instantaneous drop in voltage when the current is switched is related to the solution resistance, as depicted in Figure 5.5. In the example shown in Figure 5.5, the voltage drop is 0.0059 V, resulting in a solution resistance of 59 Ω (since I = 0.00005 A). Estimates of R_{ct} were determined by extrapolating the semi-circle of the Nyquist plots to the x-axis and using the x-intercept as an initial estimate of R_{ct}. Estimates of W were obtained by fitting only the linear region of the curve with a single W element. All other parameter values were estimated based on previously reported literature values (see Section 3.1.5).

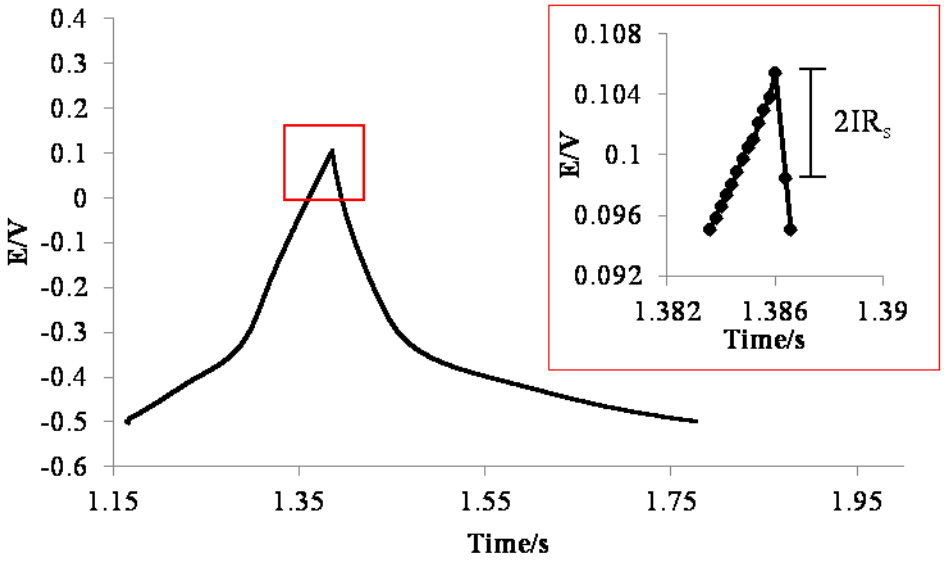

Figure 5.5: Constant current charge-discharge experiment for a Pt electrode in 0.2 M PBS. R_s is determined by measuring the instantaneous drop when the applied current is switched directions.

As mentioned in the experimental section (Section 3.2.2), literature suggests that the value of C_{dl} for a metal in solution should be in the range of 10 to 40 μF cm^{-2}.[99] The surface area of the electrode used in these experiments is *ca.* 0.08 cm^2, suggesting that C_{dl} obtained for this experiment should be in the range of 0.8 to 2.3 μF. Circuits C1, C3, and C4 extract CPE or C_{dl} values which far exceed the upper limit of the expected

capacitance values, confirming that the C-type circuits do not provide a good model for the blank (BSA-free) system. It is relevant to note that circuits C1 and C3 provided the smallest residual errors, confirming that residual errors alone are not sufficient to choose a circuit.

The B-type circuits, however, extract reasonable values for C_{dl} or the corresponding CPE. Since the experiment here contains no BSA, and therefore no BSA film is expected, it is unclear what film may be modeled by this circuit. Possibly it is a film formed by other adsorbed species (ions) from solution. In any case, these circuits will be used to model the BSA film (in Section 5.4), so for completeness their fitting is examined here. Although it is not possible to know the expected value for C_f or R_f parameters given that the nature of the film is unknown, a comparison of extracted circuit parameter values shows that for circuits B1, B2, and B4, average values obtained for the C_f or CPE_f are 10^{-7} μF, 10^{-6} μF, and 10^{31} μF, respectively. As these parameters model the same physical process for the same data sets, it is expected that they would be approximately the same value. Nonetheless, capacitances as small as 10^{-7} μF or as large as 10^{31} μF are unreasonable and have no physical significance in this system. The examination of the numerical values for the circuit parameters are a good indication the B-type circuits are not adequate models for the data presented in this paper.

Through examination of the standard deviation of the replicates and the numerical values for the parameters, most of the circuits examined can be eliminated as possibilities for this system. The two remaining circuits, Circuits A1 and A2, are both Randles-type circuits with the only difference between them being that circuit A2 has a CPE in place of the C_{dl}. The n-value associated with the CPE is an indication of CPE's deviation from an

ideal capacitor. An n-value of 1, as is obtained when the data is modeled with circuit A2, indicates that the CPE is, in fact, acting as a capacitor. Thus, in this case there is no need for the CPE in the circuit and the CPE is only an unnecessary complexity; therefore circuit A2 is not the best model for the data and therefore can be eliminated.

As the above analysis of these data show, there are a number of possible circuits which all appear to fit the Nyquist plots adequately, suggesting that if only the Nyquist plots are used to choose a circuit, the wrong circuit could easily be chosen. Additionally, while the comparison of residual errors is important, it also may not be sufficient to eliminate inappropriate circuits. Ultimately, as the data presented here show, a broader, more thorough approach is required to correctly elucidate which circuit best models the EIS data and the electrochemical system under study. A step-wise procedure which evaluates the Nyquist plots, residual errors of the circuit fits, standard deviations, and values of circuit parameters, allows for the elimination of circuits which do not adequately model the data or that provide unnecessary complexity to the system. In the case presented for the blank (BSA-free) system, the use of this method results in the emergence of circuit A1 as the best EEC to model the system under study. Circuit A1 is the Randles circuit which models the solution resistance, double-layer capacitance, charge-transfer resistance, and the Warburg impedance. Circuit A1 provides a good fit of the experimental data, small relative residual errors, and parameter values which agree with both those determined from other experimental methods (R_s, see Section 3.2.2) and literature (C_{dl}). Based on this information, Circuit A1 can confidently be chosen as an excellent model for the electrochemical system.

5.4 EEC Choice for BSA Data

As mentioned previously, one very common use of EIS is to study protein adsorption for the purpose of biosensor development.[32,66,101,106] Therefore, it is important that the previously presented method for determination of the best EEC to model a system be applied to a system in which protein adsorption occurs. To study this, a Pt electrode was incubated in a 1 g L^{-1} BSA in PBS solution for 30 minutes. Past studies of BSA adsorption suggest that 30 minutes is a sufficient incubation time to form a BSA film on the electrode surface.[13,23] After the BSA film was formed, the electrode was immersed in PBS solution (no BSA in solution) and EIS was recorded over a 20 hour period to ensure that the protein film on the surface reached constant coverage before the analysis was undertaken. The experiment was repeated three times and the electrode was cleaned between each replicate experiment.

The first step in the analysis is to fit each of the circuits presented in Figure 5.2 to the experimental data. Figure 5.6 shows the experimental data and fit of each circuit to one of the three replicates; similar plots for the other two replicates are presented in Figures A7 and A8 in the Appendix. Often in the literature the Nyquist plot fit of only one circuit is used to show that the circuit appropriately models the surface. However, the Nyquist plots in Figure 5.6 show that more than one possible circuit results in an adequate fit – the fits of the circuits are actually indistinguishable with the exception of A1, which deviates to a greater extent in the Warburg (linear, low frequency) region. These findings highlight two points: when fitting EIS data all possible EECs must be included in the comparison since circuit A1 would have appeared to be an adequate fit if not compared to the others, and the Nyquist plots alone are not sufficient to determine

which circuit best models the data. Once again, this highlights the importance of completing the full and thorough analysis in order to determine which circuit best models the system.

Figure 5.7 shows the relative residual error plots for the circuits fit to the experimental data presented in Figure 5.6. Again, similar plots for the other two replicates can be found in the Appendix (Figures A9 and A10). A1 has a higher residual error than each of the other circuits (*ca.* ± 6 % as compared with ± 2 % for A2, B1-B4, and C1-C4), consistent with the fit presented in Figure 5.6. The larger residual error of A1 indicates that it is not a good model for the electrochemical system. In this case, the residual errors appear to be able to begin to eliminate possible circuits, but a more in-depth analysis of the parameter values and standard deviations obtained from all three replicate experiments is needed before any circuits can be eliminated confidently.

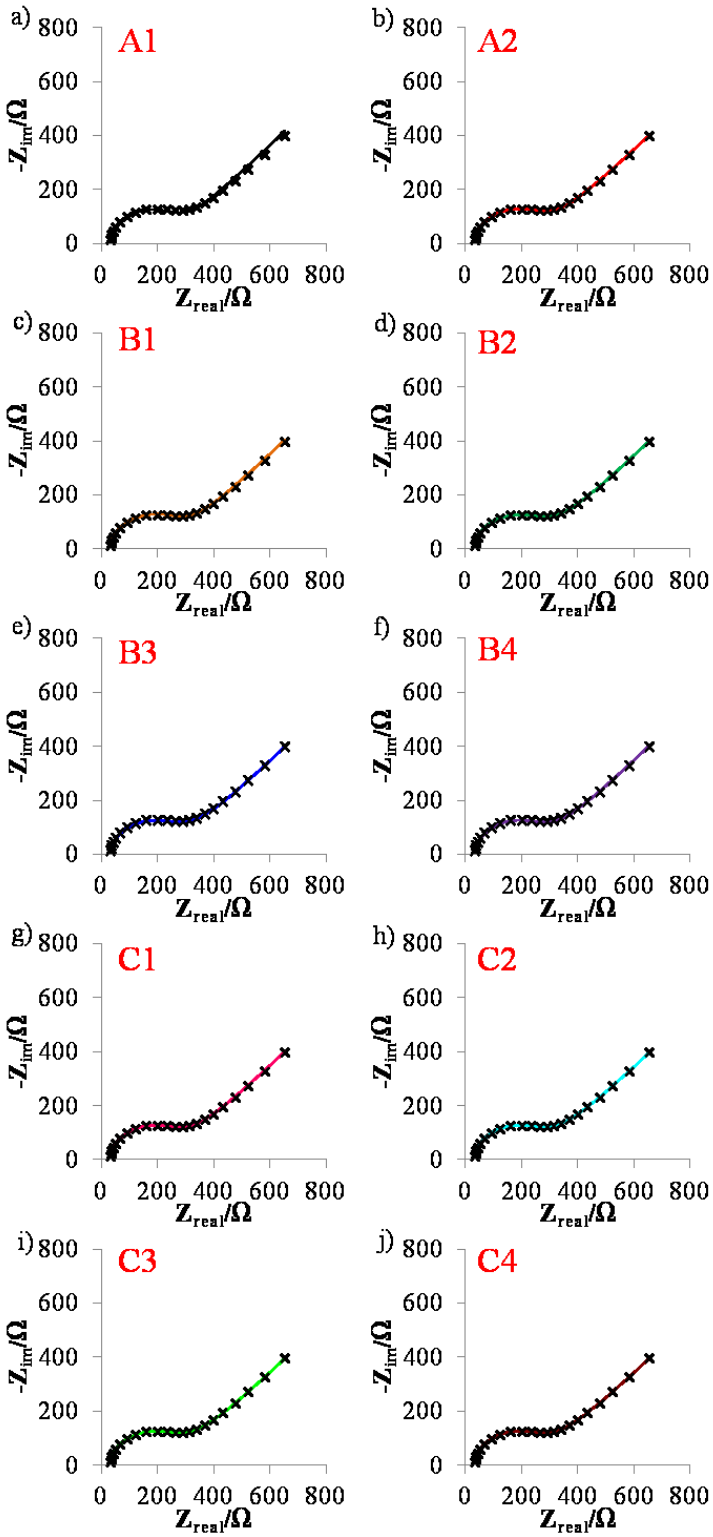

Figure 5.6: Nyquist plots for a Pt wire electrode incubated in 1 g L^{-1} BSA for 30 minutes, followed by EIS in a 0.2 M PBS solution with 3 mM ferri/ferrocyanide (20 h), with fit data generated from fitting experimental data (Figure 5.6) to circuits presented in Figure 5.2.

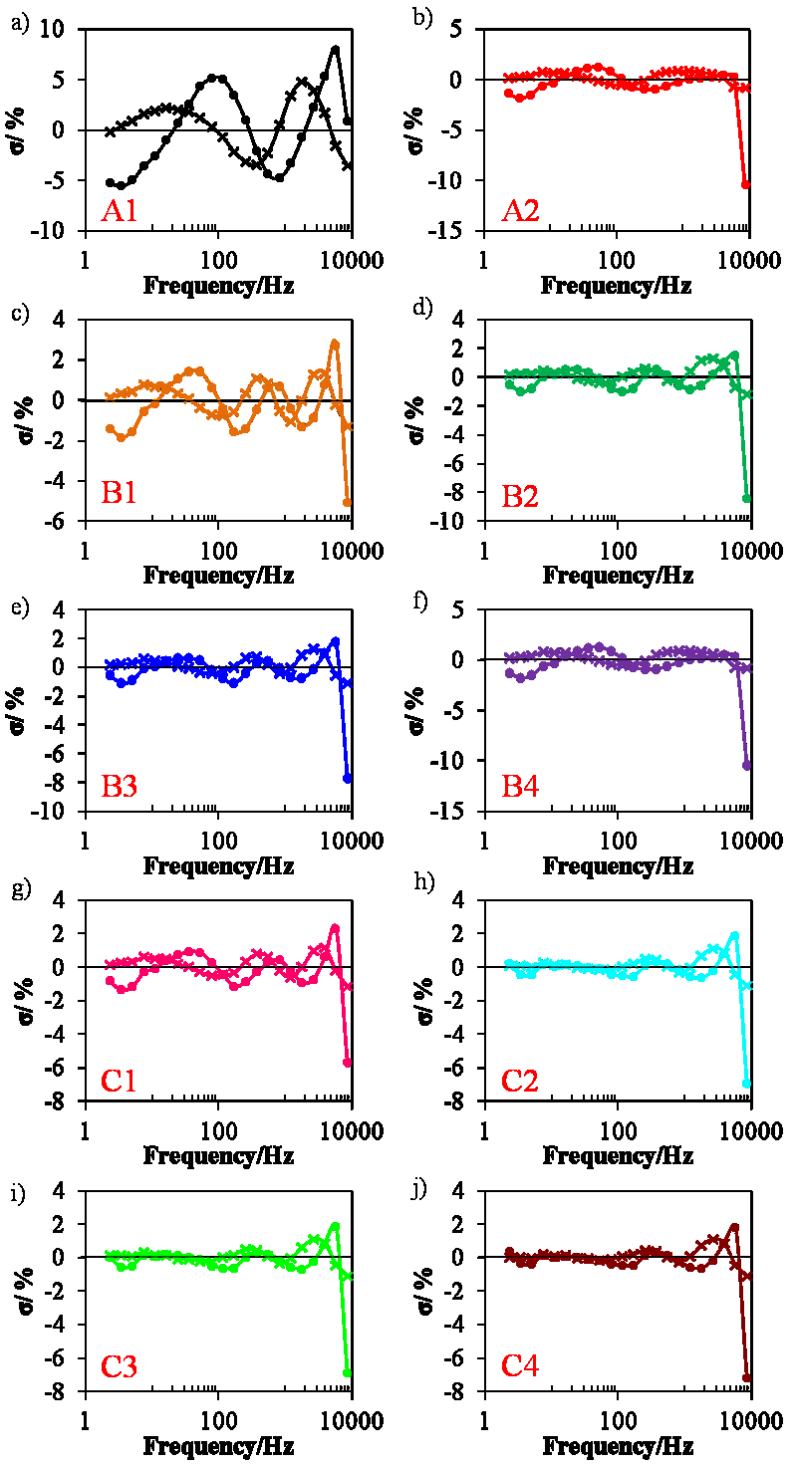

Figure 5.7: Relative residual errors resulting from the fit of circuits in Figure 5.2 to the data shown in shown in Figure 5.6 for a Pt wire electrode incubated in 1 g L^{-1} BSA for 30 minutes, followed by EIS in 0.2 M PBS with 3 mM ferri/ferrocyanide (20 h). Crosses represent σ_{real} and circles represent σ_{im}.

Table **5.2** summarizes the parameter values extracted from the fits of each of the circuits in Figure 5.2 to the three replicate experiments. Note that the standard deviations given are those for the replicate experiments, not for the fits. In the case where a protein film is formed on the electrode surface, adsorption of BSA molecules to the electrode surface is predicted to result in less available surface for charge-transfer reactions (when a redox couple is present) and therefore an increase in the charge-transfer resistance, R_{ct}.[7,22,23,151] This increase is expected to be reflected in the extracted R_{ct} values – an increase in R_{ct} should be observed after protein adsorption. Indeed, for most of the circuits modeled, there is an obvious increase in the R_{ct} when BSA is adsorbed on the electrode surface (

Table **5.2**), as compared to the 77 Ω value found when no BSA is present (Circuit A1, Table 5.1). However, the R_{ct} value for circuit C1 is smaller than that for the blank experiments (62 Ω as compared with 77 Ω), eliminating C1 as an appropriate model for the electrochemical system. All other circuits extract reasonable R_{ct} values.

A comparison of the R_s in Table 5.1 and

Table **5.2** shows a difference between the solution resistance with and without BSA. This result does not reflect a true change in the R_s, but is rather an artifact of the fitting procedure. As can be observed from the residual error plots, higher residuals are seen in the high frequency region – particularly for the first two points, and this increases the error associated with the R_s value. Additionally, the fitting of a semi-circular model to the blank data, where the semi-circle is less well defined adds a small bias to the R_s extracted. Thus, the differences in R_s between Tables 1 and 2 can be ignored.

As BSA adsorbs on the electrode surface and surface area is reduced, a decrease in C_{dl} is expected.[23] A relatively small decrease in C_{dl} is expected, as capacitance is proportional to the dielectric of the material (ε, Equation 2.1) and, since BSA is able to balance some of the charge on the electrode surface in the double-layer, the dielectric is not expected to greatly change. In the previous section, it was shown that the circuit that best models the BSA-free system is circuit A1. This circuit extracts a parameter value of 1.5 μF for C_{dl} (see Table 5.1). Therefore, in order for a circuit to adequately fit the BSA experiments, it must extract a C_{dl} value of less than 1.5 μF. For circuits in which a CPE replaces C_{dl}, the C_{dl} value can be calculated using the equation presented by Hsu *et al.*[152] (Equation 5.1), where ω_{max} is the frequency value at which Z_{im} reaches a maximum in the semi-circle.

$$C = CPE(\omega_{max})^{n-1} \tag{5.1}$$

Table **5.3** summarizes the C_{dl} values resulting from the fits of all circuits to the experimental data, and by the calculation of C_{dl} from the CPE, where necessary. Immediately, circuits B1 and B3 can be removed from consideration as they result in C_{dl} values which are higher than that resulting from the blank experiments. Circuit C1 also results in a higher C_{dl} value, but has been previously removed based on R_{ct} considerations.

Table 5.2: Summary of parameters obtained by fitting three experiments on a Pt wire electrode which was incubated in 1 g L^{-1} BSA for 30 minutes, and EIS was run in a 0.2 M PBS solution with 3 mM ferri/ferrocyanide. Note that the standard deviations presented are those for the three replicate experiments, not for the fit.

	Parameters									
Circuit	**R_s /Ω**	**C_f /μF**	**CPE_f /μF $s^{(n-1)}$**	**n**	**R_f /Ω**	**C_{dl} /μF**	**CPE_{dl} /μF $s^{(n-1)}$**	**n**	**R_{ct} /Ω**	**W /Ω $s^{-0.5}$**
A1	43 ± 9	--	--	--	--	1.4 ± 0.04	--	--	223 ± 12	1600 ± 100
A2	40 ± 9	--	--	--	--	--	2.2 ± 0.1	0.94 ± 0.01	248 ± 9	1500 ± 100
B1	42 ± 9	3.0 ± 0.5	--	--	62 ± 25	2.4 ± 0.5	--	--	188 ± 10	1500 ± 100
B2	31 ± 9	--	26 ± 24	0.80 ± 0.02	67 ± 31	1.6 ± 0.2	--	--	186 ± 48	1500 ± 63
B3	41 ± 10	3.7 ± 1.2	--	--	67 ± 25	--	3.4 ± 0.7	0.96 ± 0.04	191 ± 15	1500 ± 100
B4	38 ± 12	--	0.6 ± 1.2	0.80 ± 0.12	2.3 ± 3.9	--	2.2 ± 0.1	0.94 ± 0.01	248 ± 9	1500 ± 100
C1	42 ± 9	1.3 ± 0.05	--	--	201 ± 21	3.4 ± 1.2	--	--	62 ± 4	1500 ± 100
C2	38 ± 7	--	36 ± 19	0.44 ± 0.08	4 ± 4	1.2 ± 0.05	--	--	284 ± 20	1600 ± 100
C3	41 ± 9	1.2 ± 0.5	--	--	39 ± 58	--	49 ± 16	0.4 ± 0.1	250 ± 68	1600 ± 100
C4	41 ± 9	--	1.3 ± 0.04	1.0 ± 0.0	2.8 ± 2.6	--	46 ± 20	0.4 ± 0.1	284 ± 19	1600 ± 100

Table 5.3: Summary of C_{dl} values obtained by fitting three experiments in which a Pt wire electrode was incubated in 1 g L^{-1} BSA for 30 minutes, followed by EIS in a 0.2 M PBS solution with 3 mM ferri/ferrocyanide. C_{dl} values obtained by converting CPE values to C_{dl} values, where necessary.

Circuit	**A1**	**A2**	**B1**	**B2**	**B3**	**B4**	**C1**	**C2**	**C3**	**C4**
C_{dl}/μF	1.4 ± 0.0	1.4 ± 0.0	2.4 ± 0.5	1.6 ± 0.2	2.4 ± 0.5	1.4 ± 0.0	3.4 ± 1.2	1.2 ± 0.0	0.3 ± 0.3	0.1 ± 0.0

As was the case for the experiments without BSA, some of the remaining circuits can be eliminated simply due to the unreasonableness of the numbers which are obtained from their fit. Circuits B2 and C3 result in an R_f values of 67 ± 31 Ω and 39 ± 58 Ω,

respectively – values much greater than the predicted value for R_f (3 to 7 Ω, see Section 3.2.2). Based on this, circuits B2 and C3 can be eliminated. Circuit C4 results in a C_{dl} value of 0.07 μF – less than 10% of the expected minimum C_{dl} value for the electrode used in these experiments (see Section 3.2.2), eliminating C4 as an appropriate model for the system.

The circuits that remain are A1, A2, B4, and C2. Each of these circuits extracts reasonable parameter values for each parameter; therefore, we can return to the residual error values to determine which circuit best models the data. Circuit A1, as mentioned previously, has residual error values much greater than the other circuits; circuit A1 can be eliminated. Of the remaining circuits, circuit C2 results in the smallest residual error – with the highest frequency point having an error of 7 % and all other points having errors of less than 2 %. C2 is the best model for the data. Circuit C2 models a porous, insulating film, as is consistent with previous literature of BSA on metal surfaces which suggest that a 30 minute incubation time is sufficient to promote significant BSA adsorption on the electrode surface.[12,23]

Circuit C2 provides a good fit of the experimental data, small relative residual errors, and parameter values which agree with both those determined from other experimental methods (R_s) and literature. Based on this information, circuit C2 can confidently be chosen as an excellent model for a BSA film adsorbed on a platinum electrode. In the case of circuit C2, the two time constants are associated with ferri/ferrocyanide moving through the pores of the film to subsequently react at the electrode surface, or charge storage at the surface of the film itself. The CPE in place of C_f further accounts for inhomogeneities in the adsorbed BSA film. Circuit C2 models a

porous, insulating film on the electrode surface, indicating that the BSA film on the surface is not a homogenous monolayer.

5.5 Conclusions

This chapter outlines a novel method which should be used to determine the circuit which best models the physical processes occurring in a protein/surface system being studied by EIS. First, a library of circuits which express the possible physical processes in the system must be created and each circuit is used to model the experimental data. The goodness of fit of the Nyquist plot may be used to eliminate some of the proposed circuits, but as is shown in this chapter, is typically not sufficiently sensitive to differentiate convincingly between most of the circuits, and a more thorough analysis must be completed. The method discussed here uses a process of elimination to determine which circuit best models the data based on: high residual errors, which suggest a discrepancy between the model and the experimental data; unreasonable parameter values as compared with literature or non-EIS electrochemical results; and inconsistency among replicates. The method is applied to model systems. It was determined that the Randles circuit (denoted as A1) best models the system in which a Pt wire electrode is exposed to PBS solution for 20 hours (no BSA present). In the presence of a BSA film on the electrode, the system is best described by a circuit in which a CPE is used in place of the C_{dl}, and an additional time constant is added to model the charge interaction with the film (circuit C2 in Figure 5.2). The circuit models a porous, insulating film on the electrode surface – suggesting that charge is stored at the

film/electrolyte boundary on the film covered portions, but may also move through the pores of the film to reach the electrode surface.

Use of the method outlined in this chapter can not only provide researchers with greater knowledge of the system under study, but can also generate greater confidence in the results obtained from fitting an EEC to EIS data.

Chapter 6 FACTORS INFLUENCING BSA ADSORPTION

Most of the work presented in this chapter was submitted as *"Examination of Electrochemical Impedance Spectroscopy Factors and Impact on Bovine Serum Albumin Film Adsorption", Michelle A. MacDonald and Heather A. Andreas,* to *Electrochimica Acta* on January 28, 2014 . I was responsible for the data collection, analysis, and a large part of the writing and editing of this paper. This chapter is different from the paper as Sections 6.3.1 and 6.3.2, focusing on method of protein introduction and temperature, were not part of the publication.

6.1 Introduction

As mentioned previously, BSA is commonly used as a blocking molecule to reduce non-specific adsorption in electrochemical biosensors. To behave as a blocking molecule, BSA must not only provide good surface coverage of the electrode surface, but must also form a stable film such that analyte signal is not convoluted by changes in the BSA film.

EIS is used extensively[27,30,32,57,95,106,153] in protein adsorption and biosensor studies as it is a useful tool for understanding the processes that occur at the metal/electrolyte boundary, before, during, and after protein adsorption on an electrode surface. While many researchers use EIS, each uses it in a slightly different way (with different applied potentials, perturbations, *etc.*) making it difficult to confidently compare

literature results. Since EIS is often used to study BSA films, it is crucial to understand the influence of EIS measurements on the protein film.

As discussed in Section 2.2, there are many factors which are known to influence BSA film formation including, but not limited to, potential,[12,23,28] pH,[87,89,154] temperature,[58,77] and concentration.[96] There are additional considerations, however, that have not to the best of our knowledge been addressed thoroughly in the literature such as performing initial measurements in phosphate buffered saline (PBS) solution before BSA adsorption, ferricyanide presence, changes in potential after film formation, the method by which protein is introduced into the electrolyte, and small fluctuations in room temperature; such considerations are the focus of this Chapter. Insight into the factors that impact BSA adsorption is necessary to lead to greater consistency in the literature and a better understanding both of BSA as a blocking molecule and of EIS as a tool to study protein adsorption.

The BSA data presented in this Chapter are modeled with the circuit presented in Figure 6.1. This circuit was determined in Chapter 5 to best model BSA films, and is reproduced here for the convenience of the reader. Additionally, in this Chapter, R_{ct} values will be used to compare EIS spectra. The choice to use R_{ct} comes from two factors: 1) when a redox couple is present in solution (such as the ferri/ferrocyanide redox couple used here), R_{ct} provides a means for detecting change at the electrode surface,[106] and 2) R_{ct} is commonly used in EIS protein studies,[7,20,22,23,30,35,84,107] thus, using R_{ct} provides the best means for comparison with the literature.

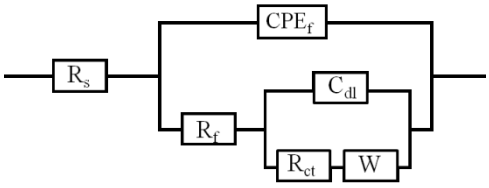

Figure 6.1: EEC used to model BSA adsorption on platinum electrode surfaces. Also labelled C2 in Figure 5.2.

6.2 Influence of Initial Bare Pt EIS Experiments Prior to BSA Film Formation

For electrochemical biosensors, it is common to collect "initial EIS" spectra on the bare electrode in the electrolyte before adsorbing the protein to the electrode surface.[23,24,95,107,155] These spectra provide a means for comparison "before" and "after" protein film formation; however, the impact of these initial spectra on the electrode surface and subsequent BSA film formation is unknown. Thus, the EIS spectrum of a BSA film formed on a pristine surface is compared to that formed on an electrode which had undergone an "initial EIS" experiment (Figure 6.2). For simplicity, only one replicate of each experiment is presented, but two additional replicates were collected and are presented in Figure A11. Note that the differences in x-intercept (modeled by R_s) occur due to slight differences in the positioning of the electrode in the three-compartment cell and do not reflect changes in the BSA film. The Nyquist plots in Figure 6.2 show large differences in the shape and in the size of the semi-circular portion; the R_{ct} values extracted from the fitting procedure were 83 ± 77 Ω and 376 ± 53 Ω for experiments with and without the initial EIS, respectively. A simple t-test results in a t-value of 3.84 which is greater than the critical t-value of 2.776 (v=4, p=0.05), confirming that the two sets of data are significantly different from one another. Clearly, performing the initial EIS

experiment in PBS changes the surface, possibly due to adsorption of chloride[156] and phosphates.[156,157] The adsorption of these anions results in a less positive surface and reduces the electrostatic attraction between the BSA molecules and the surface, leading to less BSA adsorption (as shown by the lower R_{ct} value). Alternatively, performing initial EIS could result in the formation of a platinum oxide film, which subsequently blocks BSA adsorption. Platinum oxide film formation is expected to occur above *ca.* 0.2 V, and since the EIS is run close to this potential, platinum oxide film formation is a possibility. The surface change that occurs due to EIS performed in PBS (no BSA present) will be further explored in Chapter 8.

While it is important to collect initial EIS to serve as a blank against which the protein film is compared, the results presented in this section show that it is vital to clean the electrode between the initial EIS and the BSA incubation as exposing a clean electrode to the protein solution achieves maximum adsorption (Figure 6.2). Literature procedures are inconsistent regarding whether the electrode is cleaned after initial exposure to buffer; some researchers polish the electrode after the initial EIS,[23] some do not clean,[107] and others do not specify if a cleaning process is used.[95] We achieve clean platinum surfaces by electrochemical cleaning in 1 M H_2SO_4 (as described in section 3.2.1), but other methods, such as electrode polishing, are equally useful. Clearly, knowledge of whether a cleaning procedure is used is important when trying to compare literature results, since, when the electrode is not sufficiently cleaned there can be ~4x less adsorption, as compared to when a clean electrode is exposed to BSA. For situations where BSA is used as a blocking protein, this is a significant result as running the blank experiment can result in a less complete or poorer BSA blocking layer.

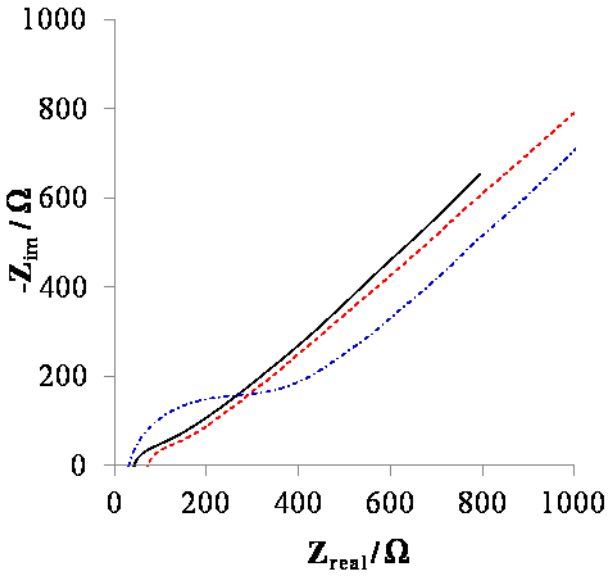

Figure 6.2: EIS spectra for a Pt wire in 0.2 M PBS with 3 mM ferri/ferrocyanide with no exposure to protein (black, solid), after initial EIS and incubation (red, dashed), and after incubation without prior initial EIS (blue, dot-dash). Incubation was performed in 1 g L^{-1} BSA for 30 minutes.

6.3 Factors Influencing Data Reproducibility

6.3.1 Temperature

As BSA films on platinum electrodes were examined using EIS, irreproducibility became apparent among replicates. Initially, it was thought that the inconsistency between trials may be caused by changes in temperature, as all experiments were completed at room temperature, which fluctuates slightly each day. A survey of the literature showed that previous work by Rouhana *et al.*[58] focused on understanding the effects of temperature on BSA adsorption on platinum electrode surfaces, and found that a plateau in BSA surface coverage occurs between the temperatures of 26 to 50 °C, suggesting that temperature does not affect BSA adsorption in this range.

The experiments presented in this thesis, however, were completed at room temperature: 22 ± 3 °C. To determine whether irreproducibility occurs due to small

fluctuations in room temperature, 1 g L^{-1} BSA in cell experiments were completed in a water bath at 17 °C, 22 °C, and 27 °C. It was hypothesized that if temperature was affecting reproducibility, then the replicates within one temperature would be very reproducible and there would be significant differences among the different temperatures.

Figure 6.3 shows the Nyquist plots for two replicate experiments at each temperature, recorded 20 hours after the incubation for each of the experiments. Fitting the experimental data yields R_{ct} values of 402 Ω and 130 Ω for experiments completed at 17 °C (266 ± 192 Ω), 176 Ω and 609 Ω for experiments completed at 22 °C (392 ± 306 Ω), and 326 Ω and 283 Ω for experiments completed at 27 °C (304 ± 30 Ω). It is immediately apparent that the replicates are not reproducible at any of the temperatures studied, suggesting that controlling the temperature of the experiments does not result in more reproducible data.

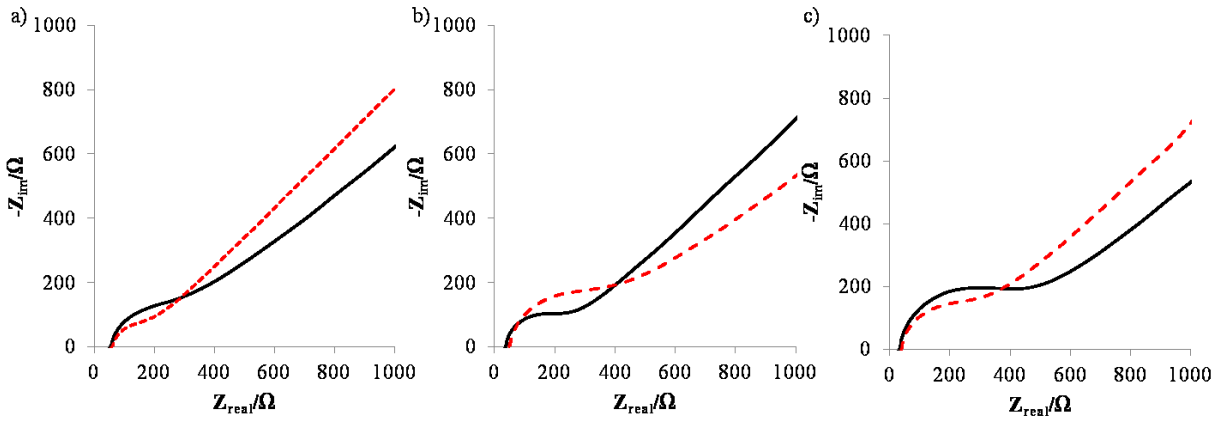

Figure 6.3: EIS spectra for a Pt wire electrode in 0.2 M PBS with 3 mM ferri/ferrocyanide 20 hours after injection of BSA into solution for a total BSA concentration of 1 g L^{-1} at a) 17 °C, b) 22 °C, and c) 27 °C. Two replicates are shown for each temperature (black solid and red dashed lines).

6.3.2 Method of Protein Introduction

A second possible cause of irreproducibility was identified. When preparing experiments in which BSA is present in the electrolyte, there are two methods by which BSA can be introduced into solution: either by injection into the electrochemical cell (above the solution or directly into solution) or by filling the whole electrochemical cell with electrolyte which already contains BSA. Three experiments were completed to determine if the method of protein introduction affects the reproducibility of the BSA experiments. Figure 6.4 shows Nyquist plots for experiments in which BSA was injected above the PBS solution (Figure 6.4a), into the PBS solution (Figure 6.4b), and when the three-compartment cell was filled with PBS containing 1 g L^{-1} BSA (Figure 6.4c).

The R_{ct} values that result from the fitting of the experimental data are 232 ± 242 Ω, 360 ± 34 Ω, and 577 ± 30 Ω, respectively. It is immediately apparent that the greatest irreproducibility occurs when the BSA in injected above the electrolyte (Figure 6.4a). In contrast, when no injection takes place, the spectra are very reproducible (with a relative standard deviation of 5 % as compared with 104 % for the injection above solution and 9 % for the injection into solution). Injection of BSA, therefore, was identified as a cause of irreproducibility in the experiments. The reason for the irreproducibility is thought to be poor mixing of BSA into the solution, creating a layer of BSA on top solution and decreasing the expected BSA concentration in solution. Mixing is again expected to be the cause of irreproducibility in the experiments where BSA was injected directly into the PBS solution, because there was no mechanical mixing of the solution and dispersal of BSA relied on diffusion (Figure 6.4b). These results also

suggest that solution concentration has a significant impact on BSA adsorption, which will be discussed in greater detail in Chapter 8.

Overall, it is concluded that the irreproducibility observed is due to the method of protein introduction to the electrolyte (and not temperature or other factors) and that BSA should be well-mixed into solution (injection methods should be avoided) to ensure maximum reproducibility among replicates. All EIS experiments presented in Chapters 4, 5, 6 (other than Section 6.3), and 8 were completed with well-mixed (injection-free) BSA solutions.

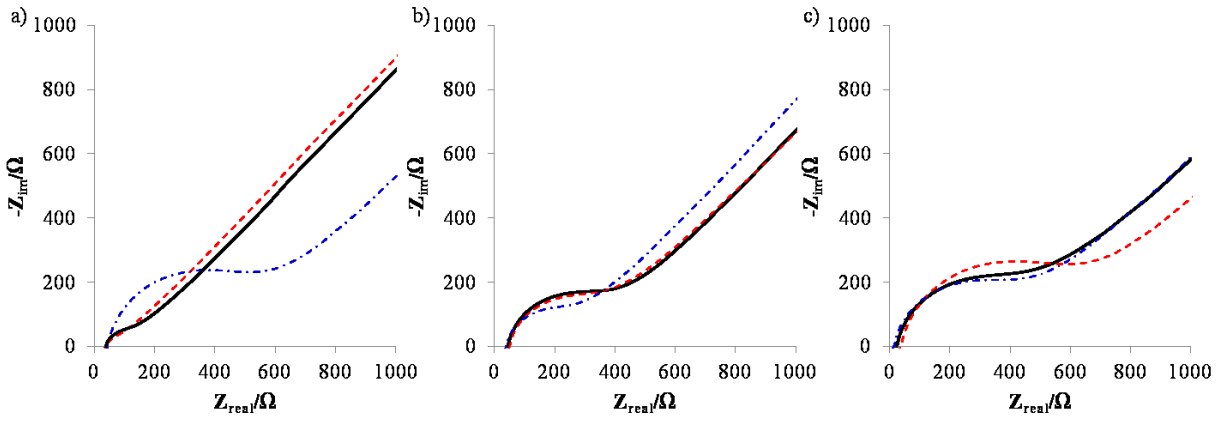

Figure 6.4: EIS spectra for a Pt wire electrode in 0.2 M PBS with 3 mM ferri/ferrocyanide containing *ca.* 1 g L^{-1} BSA introduced by injection above solution (a, three replicates), injection into solution (b, three replicates), and by filling the three-compartment cell with PBS containing 1 g L^{-1} BSA (c, three replicates).

6.4 Influence of Ferricyanide Presence on BSA Adsorption

Many EIS biosensor studies use ferricyanide in the electrolyte solution to provide a charge-transfer reaction and R_{ct} by which protein adsorption can be measured.[23,27,33,57,65,95,108] However, it is not yet established whether ferricyanide may

compete with the adsorbed BSA, either during adsorption or after the BSA film is formed. Comparing EIS spectra with and without a redox probe is not possible, since the redox processes, R_{ct} values, and shapes of the Nyquist spectra will be very different from one another and the differences will be unrelated to the protein film. Instead, ferricyanide effects can be examined by adding ferricyanide to the incubation solution. The four consecutive spectra recorded immediately after incubation with and without ferricyanide in the incubation solution are presented in Figure 6.5. For the experiment in which ferricyanide was present in the incubation solution, three replicates were completed and are presented in Figure A11b of the Appendix.

The data were modeled using the circuit determined in Chapter 5 to best model the BSA-Pt system and a larger R_{ct} value of 514 Ω was extracted for the ferricyanide-free incubation experiment (0 min, Figure 6.5a), indicating increased BSA adsorption in the absence of ferricyanide than when ferricyanide is present (376 ± 53 Ω, 0 min, Figure 6.5b). These results suggest that ferricyanide may therefore interfere with the EIS results of the BSA film.

Further evidence supporting ferricyanide interference with BSA is observed by examining four consecutive EIS spectra recorded after incubation. For the BSA film formed in the absence of ferricyanide (Figure 6.5a), a significant drop in R_{ct} occurs upon exposure to the ferricyanide-containing EIS solution. Importantly, by 10 minutes post-incubation, the Nyquist plots of the two films become very similar (9 min, Figure 6.5a and 9 min, Figure 6.5b), with R_{ct} values of 328 Ω and 326 ± 10 Ω for the ferricyanide-free and ferricyanide-containing incubations, respectively. This result suggests that at equilibrium a similar amount of BSA is present on the surface for both experiments.

Thus, when present in the incubation solution the competition between BSA and ferricyanide for adsorption on the electrode surface results in less BSA adsorption (Figure 6.5a), and for already formed films the subsequent introduction of ferricyanide causes the desorption of BSA from the electrode surface.

The interference of ferricyanide with BSA adsorption suggests that results that are most descriptive of the true BSA film (in the absence of any competition from other solution species) may be obtained from experiments in which no ferricyanide is present; however, the removal of a redox probe from solution requires that changes at the electrode surface be tracked by capacitance as opposed to resistance.[23,106] Removal of a redox probe offers the advantage that EIS can be performed at any potential, but special care must then be taken when reporting and comparing results, as BSA adsorption varies with applied potential.[12,23,26,28] To maintain the ability to track protein adsorption through both R_{ct} and C_{dl}, and to be able to best compare with previous literature results, incubation procedures can be completed with ferricyanide present and the film be allowed to equilibrate during EIS before further analytes are introduced to the electrochemical system.

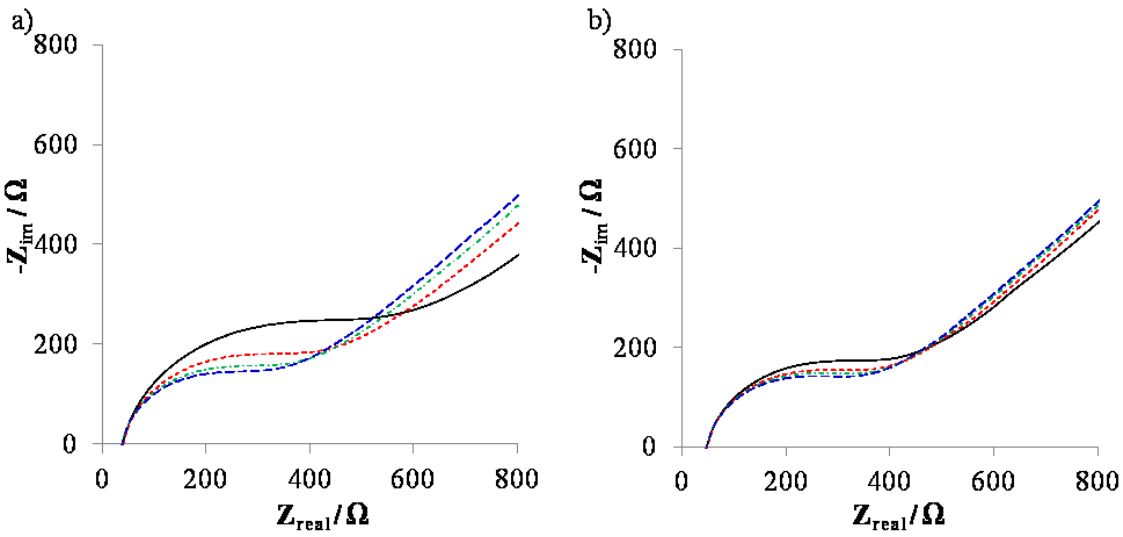

Figure 6.5: EIS spectra for a Pt wire in 0.2 M PBS with 3 mM ferri/ferrocyanide after incubation in 1 g L^{-1} BSA for 30 minutes without (a) and with (b) 3 mM $K_3Fe(CN)_6$ in the incubation solution. Time after incubation: 0 min (black, solid), 3 min (red, short dash), 6 min (green, dot-dash), and 9 min (blue, long dash).

6.5 Influence of Applied Potential on BSA Film Formation

It is well established in the literature that BSA adsorbs on Pt surfaces by electrostatic interaction with the surface,[12,23,26,28] and that the potential applied to the working electrode during incubation affects the amount of protein adsorption that occurs on the electrode surface.[23] It remains common in biosensor studies, however, that an electrode be incubated in a solution of BSA (with no applied potential) to create a blocking layer on the electrode surface, and then the subsequent electrochemical measurements are performed at a different potential than the incubation,[7,11,12] typically the equilibrium potential of the redox probe (for example, ferricyanide at 0.171 mV). The impact of this change in potential from incubation to EIS, on an already formed BSA film, is unknown.

The impact of potential is examined using open-circuit potential (E_{oc}, *ca*. 0.350 V) and 0.171 V (the equilibrium potential of the redox couple, E_{eq}, which is the same potential at which the subsequent EIS is performed). Changing the potential at which the EIS is conducted makes comparison of EIS spectra difficult since as the potential moves away from the E_{eq} of the redox couple, the potential-current relationship (and therefore the shape and size of the Nyquist plot) changes. Thus, an EIS recorded at E_{eq} and E_{oc} cannot be easily compared. For this reason the best method to probe the impact of potential is to alter the incubation potential and continue to record EIS at the E_{eq}.

Figure 6.6a shows a comparison of results obtained from incubation at E_{eq} and E_{oc}, as well as a blank (no incubation) experiment. Both incubation experiments show an increase in semi-circle size as compared with the blank spectrum, confirming BSA adsorption occurs at both potentials. Comparison of the two incubation experiments, however, shows a smaller semi-circle portion of the Nyquist plot for those incubation experiments performed at E_{eq} vs. those performed at E_{oc}, with R_{ct} values of 154 ± 59 Ω and 376 ± 53 Ω, respectively. The standard deviation values are calculated from three replicates of each experiment; two additional replicates of each are presented in Figure A12 of the Appendix (0 h). A simple t-test confirms that the two data sets are significantly different (t-value 3.43, critical value 2.775 using ν =4,p=0.05). The larger R_{ct} value for E_{oc} confirms a larger degree of BSA adsorption at more positive potential (E_{oc}), as is consistent with previous literature.[23] BSA adsorption, then, increases with increasing potential. For biosensor applications using BSA as a blocking molecule, these results suggest that a more complete blocking layer will result from the application of a more positive potential.

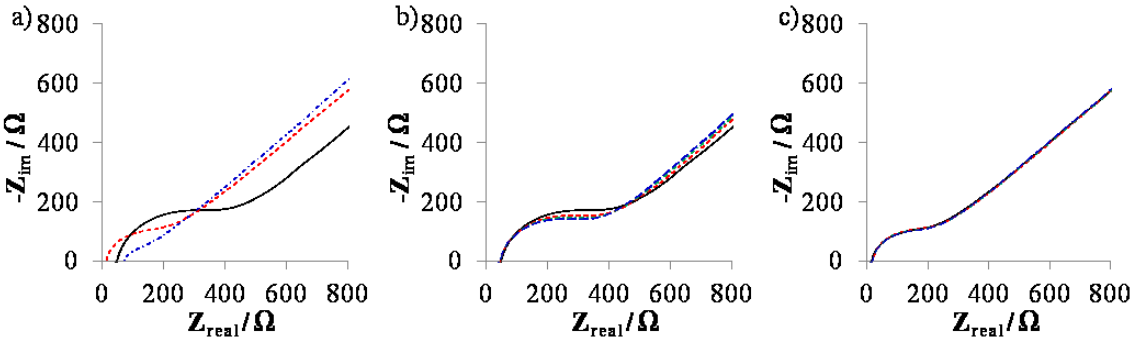

Figure 6.6: EIS spectra for a Pt wire electrode in 0.2 M PBS with 3 mM ferri/ferrocyanide. a) no exposure to BSA (blue, dot-dash), and immediately after incubation in 1 g L-1 BSA for 30 minutes at Eoc (black, solid), Eeq (red, short dash). b) and c) four consecutive spectra recorded after incubation at Eoc and Eeq, respectively; Time after incubation: 0 min (black, solid), 3 min (red, short dash), 6 min (green, dot-dash), and 9 min (blue, long dash).

Examination of the four consecutive EIS spectra collected after incubation shows that when the potential for incubation was different from the potential of subsequent EIS testing, a decrease in the Nyquist semi-circle (R_{ct}) is observed over time (Figure 6.6b). No similar change in the Nyquist plot was seen for films when the incubation and EIS potential were the same (E_{eq}, Figure 6.6c). Again, replicates are presented in Figure A12 of the Appendix. The decrease in semi-circle size in Figure 6.6b indicates that the change in potential from E_{oc} to E_{eq} (0.350 V to 0.171 V) results in a decrease in adsorbed protein at the electrode surface immediately after incubation. The decrease in potential from 0.350 V to 0.171 V results in a less overall positive charge on the electrode surface, which reduces the electrostatic attraction between the BSA molecules and the surface. Ultimately, this causes some of the adsorbed BSA to leave the surface. It is important to note, however, that after 10 minutes of EIS, the two films remain different, with R_{ct}

values of 125 ± 49 Ω (Incubation at E_{eq}) and 326 ± 10 Ω (Incubation at E_{oc}). Therefore, although some BSA is lost from the surface after incubation at E_{oc}, a greater amount of BSA remains on the surface than when the incubation is completed at E_{eq} and no subsequent loss is observed.

The change in BSA layer due to the applied EIS potential clearly indicates that care should be taken when choosing potentials at which to form the BSA film and to perform the EIS analysis. In biosensor applications that use BSA as a blocking molecule, changes due to alterations of the blocking layer could easily convolute the analyte signal, particularly in the first 6 minutes of measurement where the most significant changes to the BSA film are seen. When using the ferricyanide redox couple, incubation should be performed at E_{eq}, to avoid changes in the film after incubation. While this approach may lead to lower surface coverage, previous studies report that only 35 % surface coverage can lead to 90-100% blocking efficiency.[92] In this case, then, it is more important to form a stable, unchanging film to avoid signal convolution. If, on the other hand, a redox couple is not used, as is the approach taken by some researchers,[23,85] a greater range of potentials may be probed to find the optimal conditions for that system. In any case, both incubation potential and EIS potential need to be considered carefully and reported explicitly when studying protein adsorption by EIS to allow for comparisons to be made with other literature sources.

6.6 Influence of ac vs. dc Potential on BSA Film Formation

The results presented in the previous section indicate that the change in potential from E_{oc} to E_{eq} after incubation results in a loss in protein film from the electrode surface.

To ensure that, in addition to the change in potential, the change from dc to ac applied potential does not impact the formation of the film, the incubation experiment at 0.171 mV (Figure 6.6c) was repeated with an additional ac perturbation on the potential applied during the 30 minute incubation period (Figure 6.7). The four EIS spectra recorded after incubation are presented in Figure 6.7. Replicate spectra are presented in Figure A13 of the Appendix. The spectra are similar to those observed for the dc 171 mV incubation potential (Figure 6.6c) in that they do not change over time; BSA is not lost from the electrode surface after the incubation process.

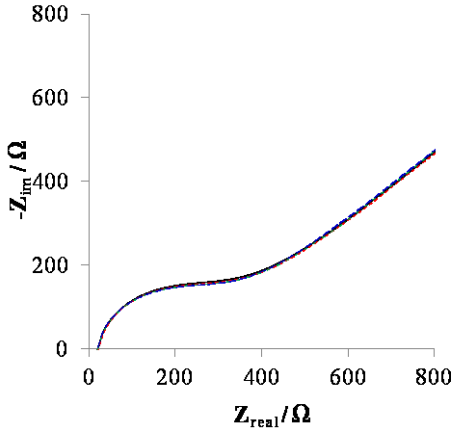

Figure 6.7: EIS spectra for a Pt wire in 0.2 M PBS with 3 mM ferri/ferrocyanide after incubation in 1 g L^{-1} BSA at 0.171 mV with an ac perturbation of 10 mV for 30 minutes. Time after incubation: 0 min (black, solid), 3 min (red, short dash), 6 min (green, dot-dash), and 9 min (blue, long dash).

While the trend in spectra is the same for both the ac and dc incubations, the magnitude of R_{ct} is not. The R_{ct} values extracted for the three ac 0.171 V replicates (presented in Figure 6.7 and Figure A13) are 368 ± 196 Ω, as compared to 154 ± 59 Ω extracted for the dc 0.171 V incubation experiments. The observed R_{ct} values are, in fact, more similar to those extracted for the E_{oc} incubation experiments (376 ± 53 Ω). The ac incubation is not, to the best of my knowledge, an incubation method used in the

literature. It was attempted in this section to determine if the desorption of BSA from the electrode surface is the result of the change from dc to ac applied potential in addition to a change in the value of applied potential; the results presented in Figure 6.7 show that the application of ac potential is not a contributing factor in the desorption of BSA from the electrode surface.

It follows from the observed R_{ct} values, however, that incubation at ac 0.171 V could be advantageous as it results in surface coverage similar to that resulting from incubation at higher potentials (E_{oc}), but forms a more stable film as potential is not changed between incubation and EIS measurements. Also important, however, is that the standard deviation on the ac 0.171 V incubation experiments is much greater than that observed for either dc incubation experiments (E_{oc} or E_{eq}). It is relevant to note, however, that the relative standard deviation of the ac 0.171 V replicates is much greater than that for the dc incubation experiments (53% as compared to 14% for the E_{oc} incubation and 38% for the dc 0.171 V incubation). Therefore, the ac 0.171 V incubation should be used with caution, as it may be more difficult to obtain reproducible results.

6.7 Conclusions

This Chapter first examined various EIS factors which can influence BSA adsorption on Pt electrode surfaces. The impact of these factors on the BSA film, from greatest to least impact is:

1. performing initial EIS in PBS solution before introducing the electrode surface to BSA, where this initial EIS spectrum results in less overall BSA adsorption – likely due to interference from pre-adsorbed chloride and phosphate anions;

2. the potential applied during incubation and EIS experiments, with greater BSA adsorption occurring at more positive potentials;
3. a change in potential between incubation and EIS measurements, where changes in the BSA film are observed after incubation, particularly in the first 6 minutes of EIS measurement, when the incubation is performed at a different potential than the EIS;
4. ferricyanide when used as an EIS redox couple influences BSA adsorption on the electrode surface, resulting in less overall BSA adsorption;
5. the application of an ac potential during incubation (as opposed to a dc potential) does not result in the desorption of BSA from the electrode surface after incubation.

In addition, the method of protein introduction to the electrolyte impacts BSA adsorption with the greatest reproducibility resulting when no injection of BSA is made, and instead the BSA is mixed directly into the PBS electrolyte before filling the electrochemical cell. Small fluctuations in room temperature (17 °C to 27 °C) are not the cause of irreproducibility among replicates.

For applications in which BSA is used as a blocking molecule, changes in signal could convolute the analyte signal, so researchers are cautioned to examine all of these factors carefully during experimental design and report on these variables when publishing EIS examinations of BSA films adsorbed on Pt electrodes.

Chapter 7 Surface-Enhanced Raman Spectroscopic Studies of Serum Albumin Adsorption on the Surface of Gold Sphere Segment Void Substrates

The research presented in this chapter was completed at the University of Southampton in Southampton, England, in the Bartlett Research Group, supported by a Michael Smith Foreign Study Supplement.

7.1 Introduction

Surface-Enhanced Raman Spectroscopy (SERS) is a well-known spectroscopic technique, commonly used to study interactions between biomolecules and surfaces.[42–46,121,122] In particular, protein detection by SERS has become increasingly popular due to its increased sensitivity over traditional fluorescence-based methods and its small sample size thereby making more efficient use of biological samples.[45]

There are two common methods by which proteins can be studied using SERS: unlabelled protein detection and Raman dye-labelled protein detection. When unlabelled proteins adsorb on a substrate surface, the Raman signal is generated from the vibration of the individual Raman-active amino acids that constitute the protein. In contrast, proteins can be labelled with a Raman-active dye molecule such that, when the protein adsorbs on the electrode surface, signal is generated from the dye molecules that are attached to the protein. While the unlabelled method may be able to provide more insight into the makeup of the protein itself, both methods can provide valuable information on the adsorption properties of the protein being studied.

As discussed in Section 2.5, a considerable amount of research over the past two decades has focused on producing SERS substrates that show large and reproducible enhancements. The Bartlett Group at the University of Southampton has developed one of the most commonly-used substrates in the field called gold sphere segment void substrates (SSV). These substrates produce enhancements that are at least 10 times greater than those observed for roughened gold surfaces.[131] Additionally, gold SSV substrates show only a 10 % standard deviation in enhancement across the surface – a significant improvement over roughened surfaces for which the signal varies by about a factor of 10 from place to place across the substrate.[131]

The research presented in this chapter focuses on using electrochemical-SERS to elucidate the effects of potential on BSA adsorption on gold substrate surfaces. Two-protein adsorption studies of HSA and Immunoglobulin G (IgG) are also presented. The research in this chapter is included in the thesis as it provides an example of the attempt to use a second (non-EIS) technique to elucidate serum albumin adsorption properties.

7.2 Scanning Electron Microscopy (SEM) Imaging of SSV Substrates

Gold SSV substrates were prepared using the method developed by Abdelsalem *et al.*[131] in the Bartlett Group at the University of Southampton, as described in the Section 3.2.3. The substrates were imaged using Scanning Electron Microscopy at each step during the fabrication process. Figure 7.1a shows an SEM image of the bare gold-coated microscope slide, prior to immobilization of the polystyrene spheres. The image is featureless, indicating a clean and flat gold surface. Figure 7.1b shows an SEM image of the polystyrene spheres immobilized on the gold-coated slide. The black circles

superimposed on the image outline individual spheres. Finally, Figure 7.1c and Figure 7.1d show the final SSV substrate after gold electrodeposition and dissolution of the polymer spheres. The regular pattern of troughs and planar gold surface is evident from these images.

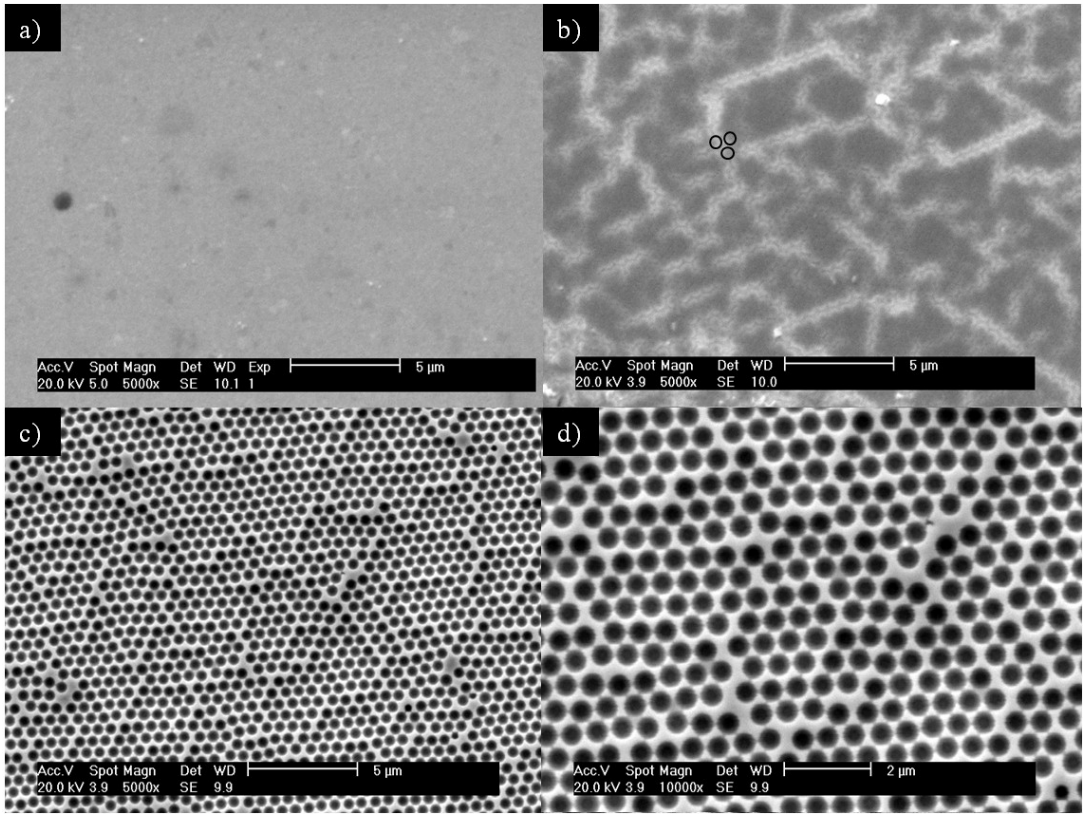

Figure 7.1: SEM images of SSV surfaces during preparation. a) gold-coated microscope slide prior to polystyrene sphere immobilization, 5000x magnification. b) After polystyrene sphere immobilization, 5000x magnification. Black circles are superimposed to aid in visualization of spheres. c) After gold electrodeposition and dissolution of the polystyrene spheres, 5000x magnification. d) After gold electrodeposition and dissolution of the polystyrene spheres, 10000x magnification.

7.3 SERS Studies of Bovine Serum Albumin

Prior to electrochemical experiments, it is important to determine whether or not a reproducible SERS signal for BSA on the gold SSV substrates can be obtained. A SERS

spectrum was collected for the bare gold surface, in the absence of BSA and is presented in Figure 7.2; this spectrum provides a background against which BSA spectra can be compared.

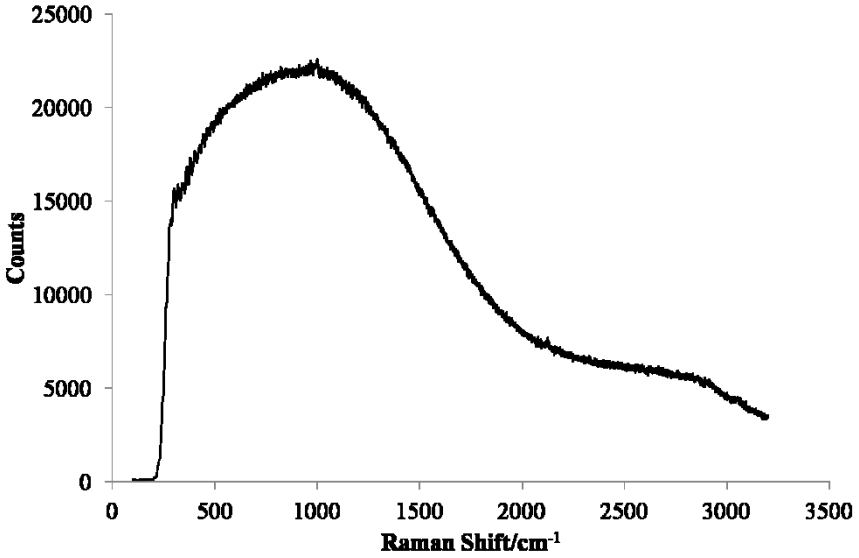

Figure 7.2: SERS spectrum of a bare gold SSV substrate.

BSA was adsorbed on the gold substrate surface by dropping a *ca.* 0.25 g L^{-1} solution of BSA (in PBS) on the surface and allowing it to dry. The SERS spectra recorded for BSA dried on the gold surfaces shows no obvious spectral features above the background in this spectrum (Figure 7.3). While SERS spectra for BSA have been reported in the literature,[44,120,121,125,127,128] many attempts to collect SERS spectra for unlabelled BSA on the gold SSV substrates were unsuccessful. Modifications were made to increase the spot size and accumulation time, both of which were unsuccessful. Previous reports have used 830 nm,[121,128] 633 nm (as is used here),[44,125] and 515 nm[120] lasers, BSA concentrations from 0.5 g L^{-1},[121,128] to greater than 60 g L^{-1},[125] and a variety

of surfaces. As such, it is not well-understood why a BSA spectrum could not be obtained on the gold SSV surfaces.

It may have been possible to obtain the BSA spectra by increasing the accumulation time to greater than 100 seconds, but the information would not be relevant as this amount of irradiation would denature the protein. As the goal of this project was to understand the adsorption properties of BSA in its globular form, denaturing the protein would not provide any new information. Due to time constraints, an alternative method to generate the same information was developed.

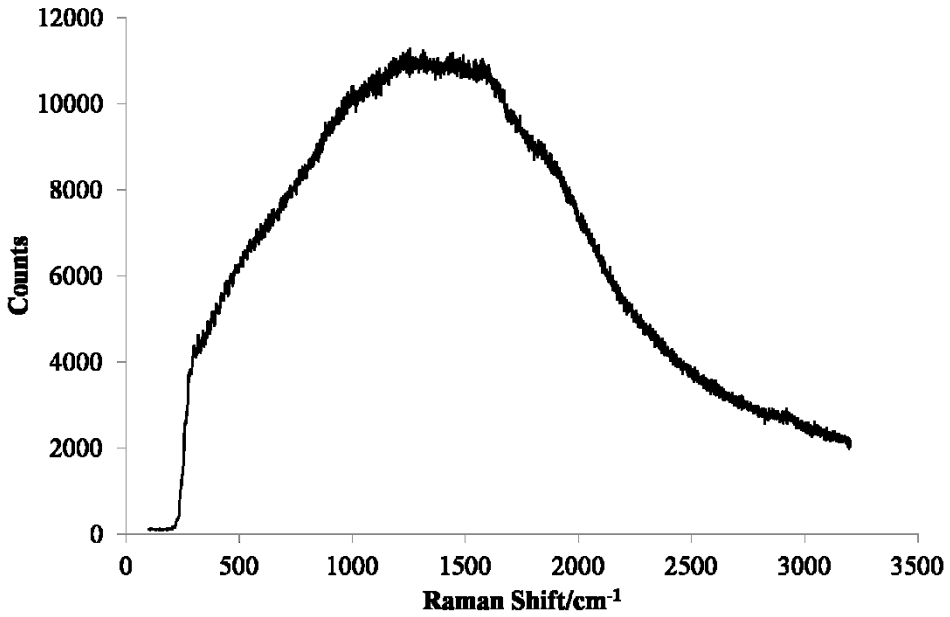

Figure 7.3: SERS spectrum of BSA on gold SSV substrate. (No BSA peaks are visible).

In the absence of a strong protein signal, it is possible to tag biomolecules with a Raman-active dye molecule such that, when the protein is adsorbed on the substrate, a signal can be generated from the dye as opposed to the protein itself.[46,122] Commercially available dye-labelled BSA was not available for purchase at the time of these

experiments; for this reason, the remaining results presented in this chapter will report on the adsorption behaviour of Human Serum Albumin (HSA), which can be purchased pre-tagged with the Raman dye Rhodamine 6G (Rh6G). It is expected that, given the similarities in structure and function of the two serum variants (see Section 2.2), HSA adsorption is analogous with BSA adsorption.

7.4 SERS Spectra of HSA

Figure 7.4 shows the SERS spectrum for rhodamine-labelled HSA molecules adsorbed on the gold SSV substrate *in situ* (in the spectroelectrochemical cell), recorded from 1200 cm^{-1} to 1750 cm^{-1}. Rh6G has characteristic peaks at: 1312 cm^{-1}, 1363 cm^{-1}, 1507 cm^{-1}, 1575 cm^{-1}, 1601 cm^{-1}, 1650 cm^{-1}.[158–160] Figure 7.4 has peaks at *ca.* 1350 cm^{-1}, 1500 cm^{-1}, 1525 cm^{-1}, and 1650 cm^{-1}; these peaks correlate well with those expected for Rh6G and are significantly greater than the baseline suggesting that Rh6G-HSA is an excellent option for the study of HSA adsorption on the gold surface.

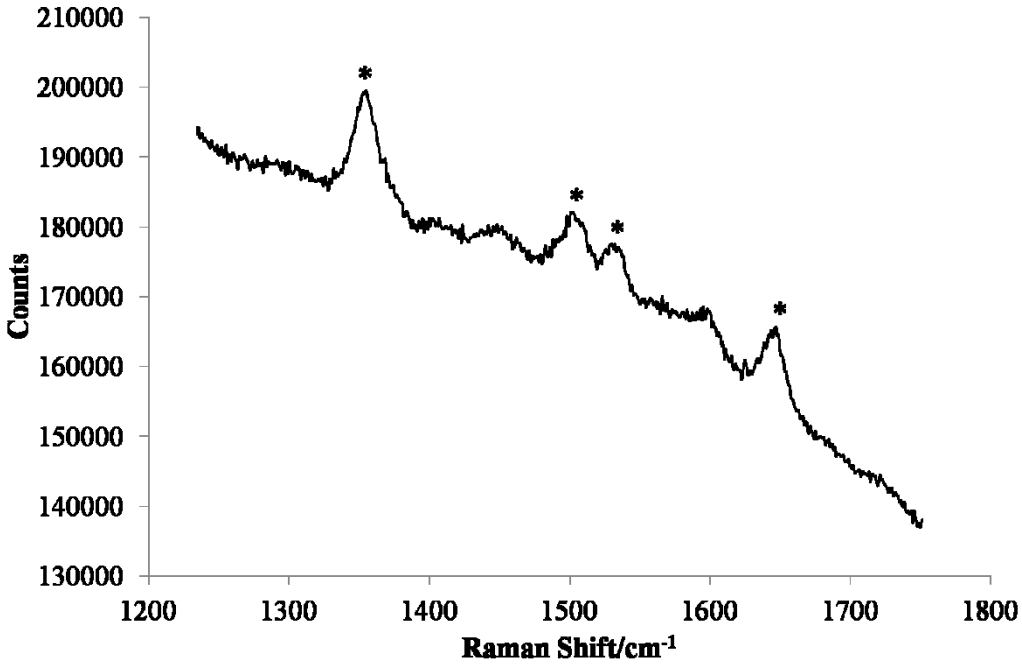

Figure 7.4: SERS spectrum of a gold SSV substrate coated with Rh6G-HSA and in a spectroelectrochemical cell containing PBS electrolyte. Asterisks note peaks which are expected for Rh6G.

7.5 Effects of Potential on HSA Adsorption on Gold SSV Substrates

As mentioned previously (Section 2.2), the pI of HSA is 4.7. As the pH of the PBS electrolyte used for these experiments is 7, HSA is expected to carry a net negative charge. It is therefore hypothesized that if the interaction between HSA and the electrode surface is electrostatic in nature – as is suggested in the literature[12,23,26,28] – HSA will adsorb more strongly (and a greater quantity of HSA will adsorb) at positive potentials than at negative potentials.

Figure 7.5 shows the SERS spectra obtained for a gold substrate in 0.25 g L^{-1} BSA in PBS in the spectroelectrochemical cell, during a potentiostatic hold at -300 mV (a) or 900 mV (b). SERS spectra were recorded using a 30 second accumulation time

such that four spectra were recorded during each 120 second hold time. Each spectrum was recorded at a different spot on the substrate surface, to avoid denaturation of the protein. Figure 7.5 shows Rh6G peaks at 1363, 1507, 1575, and 1650 cm^{-1}, suggesting that HSA is adsorbed to the electrode surface. The unchanging peak heights – both within one potential hold and between the two potentials – however, suggest that potential does not impact the amount of adsorption.

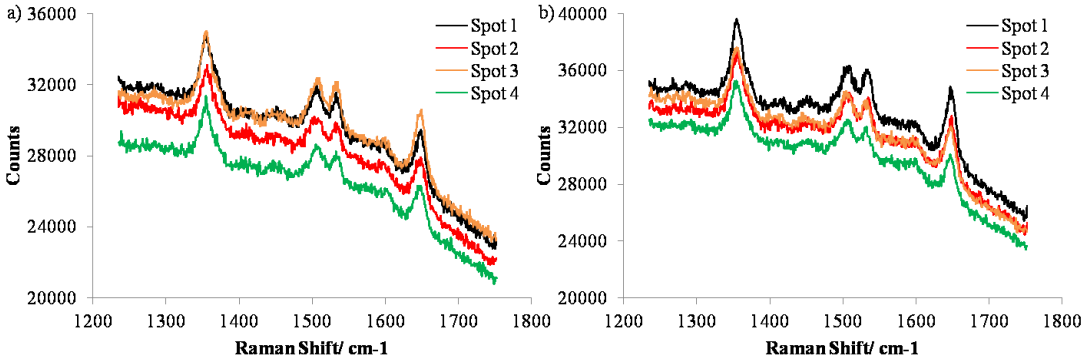

Figure 7.5: SERS spectra of a gold SSV substrate in PBS containing 0.25 g L^{-1} Rh6G-HSA during a 120 second potential hold at a) -300 mV and b) 900 mV.

This result that potential does not affect HSA adsorption is unexpected given that previous research leads to an electrostatic adsorption mechanism.[12,23,26,28] Although it was initially thought that the desorption (or adsorption, depending on applied potential) would occur very quickly (certainly within the 120 second timeframe used here), later research conducted using EIS with protein in the electrolyte (Section 8.4) suggests that longer periods of time are required to detect changes in serum albumin films. It is possible, then, that the potential applied to the SERS substrates does impact the film, but that the changes are not detectable in the 120 seconds used for these experiments.

While the conclusive reason for no change in signal with the application of potential is not known, the results are such that the effects of potential on the adsorption of HSA molecule on the electrode surface cannot be studied using the method attempted here. Therefore, given the time constraints of this project, it was necessary to use a different method to understand HSA adsorption at the gold substrate surfaces.

7.6 Two-Protein Studies

BSA is a commonly-used blocking molecule in electrochemical biosensors platforms.[11–17] The blocking efficiency of albumin proteins can be studied using SERS by first adsorbing the albumin on an electrode surface, and then attempt to desorb it by introducing other molecules to the surface.

Immunoglobulin-G (IgG) is a commonly studied serum protein because of its applications to biosensors.[21,23,65,92,161] IgG is commercially available tagged with the Raman-active dye molecule Cy3, which has characteristic peaks at: 1400 cm^{-1}, 1450 cm^{-1}, 1550 cm^{-1} and 1600 cm^{-1}.[122,162]

Figure 7.6 shows the SERS spectra of Rh6G-HSA (Figure 7.6a) and Cy3-IgG (Figure 7.6b). The background was subtracted using a simple multipoint subtraction method, to easily compare with literature precedent. In each spectrum, expected peak locations for Rh6G and Cy3 are indicated in blue and green, respectively. For the Rh6GHSA spectrum, the peaks at 1363, 1507, 1601, and 1650 cm^{-1} correlate very well to those expected for Rh6G. For the Cy3-IgG spectrum, the peaks at 1450, 1550, and 1600 cm^{-1} correlate well with those expected for Cy3. It is important that the peaks observed for Cy3 and Rh6G do not overlap with one another such that when both dyes

(proteins) are present, it is possible to differentiate between them. The only shift for which both dyes have peaks is *ca*. 1600 cm^{-1}; this peak will not be used to indicate the adsorption of either protein.

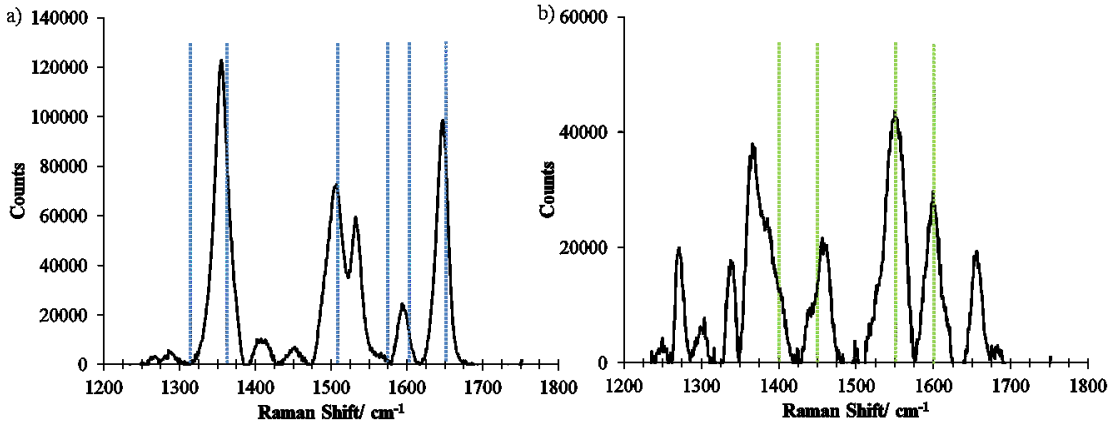

Figure 7.6: SERS spectra of a gold SSV substrate after adsorption of a) rhodamine-labelled HSA and b) Cy3-labelled IgG. Blue and green lines indicated expected peak locations for Rh6G and Cy3, respectively.

Figure 7.7 shows the SERS spectra collected at four different locations on the substrate on which Rh6G-HSA was first adsorbed, followed by Cy3-IgG (a) and vice versa (b). The peaks in the spectra presented in Figure 7.7 at 1363, 1507, and 1650 cm^{-1} strongly suggest the presence of Rh6G and therefore HSA on the substrate. The peaks at 1400 and 1450 cm^{-1} suggest the presence of IgG on the substrate surface. Initially, it was thought that the incubation method used here (0.25 g L^{-1} for 30 minutes) would result in a complete monolayer of HSA at the surface (because serum albumin is commonly used as a blocking molecule and 30 minute incubation times are typically used to achieve film formation[13,23]) and, therefore, the presence of IgG would be indicative of IgG's ability to push HSA off of the surface (for the substrate first exposed to HSA). Later research,

however, has indicated that the conditions used (particularly the 0.25 g L^{-1} concentration) are not sufficient to achieve complete coverage of the electrode surface (Chapter 8). Therefore, it is likely that the presence of both IgG and HSA peaks in Figure 7.7 is the result of both proteins finding adequate space to adsorb on the electrode surface.

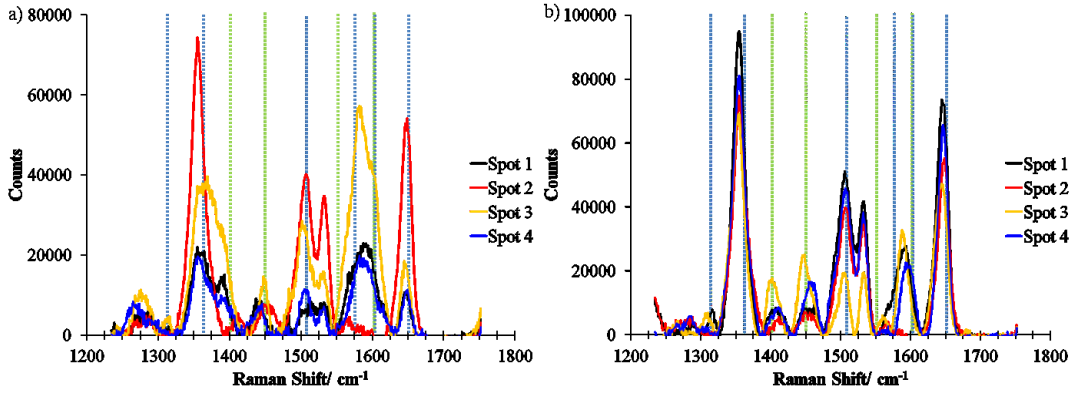

Figure 7.7: SERS spectra at four different spots on a gold SSV substrate which was a) exposed to Rh6G-HSA before exposure to Cy3-IgG b) exposed to Cy3-IgG before exposure to Rh6G-HAS. Blue and green lines indicate expected peak locations for Rh6G and Cy3, respectively.

To further investigate the ability of HSA to adsorb on the substrate surface in the presence of other molecules, a similar experiment to that previously discussed was conducted with HSA and DNA. The Bartlett Group has expertise in the chemisorption of Cy3-DNA to the gold SSV substrate surfaces. Figure 7.8a shows the spectrum obtained by attaching the DNA molecules to the gold surface. Figure 7.8b shows the spectra obtained after introduction of Rh6G-HSA. Note that the green lines indicate expected peak locations for Cy3 and the blue lines indicate expected peak locations for Rh6G.

The spectrum presented in Figure 7.8a confirms the attachment of the Cy3-DNA molecules to the electrode surface as all four expected peaks for Cy3 are present. The

spectra presented in Figure 7.8b, shows both Cy3 peaks and Rh6G peaks, suggesting the presence of both DNA and HSA on the substrate surface. Since DNA is expected to chemisorb to the electrode surface,[47,130] the results suggest that the DNA does not form a complete monolayer as HSA is still able to access the substrate surface.

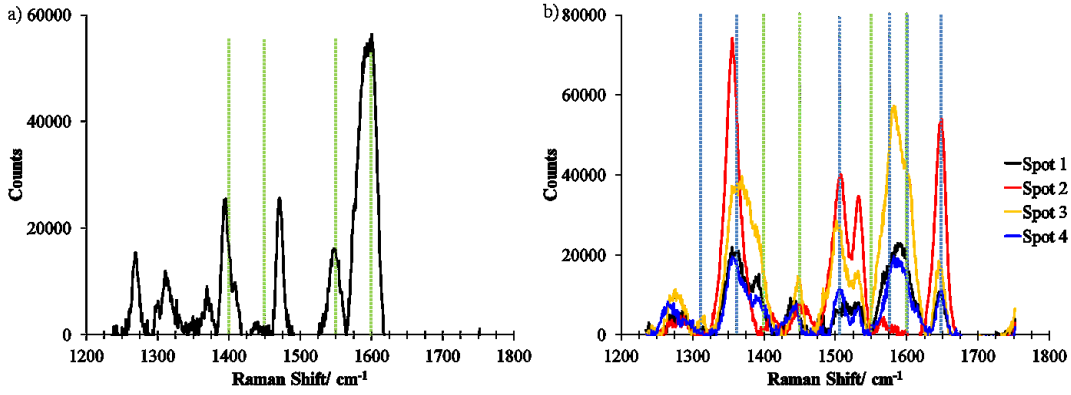

Figure 7.8: SERS spectra of a gold SSV substrate after adsorption of a) Cy3-labelled DNA b) Cy3-labelled DNA followed by Rh6G-labelled HSA. Blue and green lines indicated expected peak locations for Rh6G and Cy3, respectively.

7.7 Conclusions

The work presented in this chapter was conducted over a limited time period and as such primarily presented preliminary results for HSA adsorption studies. A BSA signal was not able to be obtained from BSA adsorbed on the gold substrate surfaces. Rh6G-labelled HSA was used in lieu of BSA as it was more readily available and is expected to have analogous adsorption properties to BSA.

A strong Rh6G-HSA signal was obtained for HSA adsorption on gold SSV substrate surfaces. The application of positive or negative potential did not affect the SERS spectra, suggesting that the amount of HSA adsorption was not impacted by the

electrode potential. Since the HSA-gold interaction is reported to be electrostatic,[12,23,26,28] it is concluded that the apparent lack of response to electrode potential is due to the lack of ability to detect the change in signal as opposed to the lack of change in the adsorption/desorption of HSA.

Studies involving two proteins suggest that the incubation in 0.25 g L^{-1} Rh6G-HSA or Cy3-IgG is not sufficient to achieve complete coverage of the substrate surface. As such, introduction of a second protein results in the co-adsorption of both proteins on the electrode surface. DNA also does not form a complete monolayer under the conditions used, as HSA is able to access substrate surface area after DNA chemisorptions has occurred.

Chapter 8 Studies of Bovine Serum Albumin Adsorption on Platinum Electrode Surfaces Over Time

8.1 Introduction

This thesis has presented a method by which proteins can be reproducibly studied at electrode surfaces using EIS. This chapter will present an application of the developed method to examine how BSA films change over time. Time becomes an important factor in biosensor design as many biosensors require a prolonged shelf-life,[163,164] or are implanted in the body for extended periods of time[79] (*in vivo* biosensors). Therefore, understanding how a protein film changes at the electrode surface over time can be crucial to the optimization of biosensor platforms. Previous research examined incubation times of up to 12 hours;[7,11,13,65,67,100,165] however no potential was applied to the electrode during this time, since the focus was on determining the optimal time to form a BSA film not to study film changes over time. Applying potential to the electrode over a longer period of time (20 hours is used in this Chapter) is advantageous as it enables monitoring of the changes in the film over the entire time period (as opposed to at the beginning and end only) and also sheds light on how the application of potential for *in vivo* monitoring applications may impact the film.

This chapter examines changes in BSA films over a 20 hour time period, in the presence of an applied, alternating potential (EIS); to our knowledge, there are no longer, similar experiments presented in the literature. Additionally, the effects of protein concentration in the electrolyte on the film will be briefly discussed.

8.2 EIS of Pt in PBS over time

Before examining the trend in EIS over time when a BSA film is present on the electrode surface, blank (BSA-free) experiments are performed to provide a background against which BSA experiments can be compared. Figure 8.1 shows Nyquist plots for a Pt electrode in PBS over 20 hours. Replicate experiments are presented in the Appendix, Figure A14.

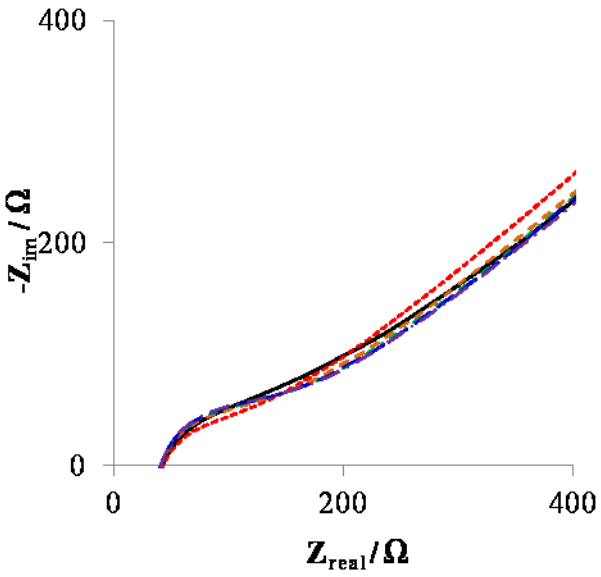

Figure 8.1: Nyquists plots for a Pt electrode in 0.2 M PBS solution with 3 mM ferri/ferrocyanide. 0 h (black, solid), 1 h (red, dotted), 5 h (orange, short dash), 10 h (green, dot dash), 15 h (blue, long dash), 20 h (purple, long dash dot).

While the spectra are similar, they are not identical, indicating a change at the surface of the electrode over time. The spectra were fit to the Randles' circuit (determined in Chapter 5 to best model the BSA-free data) and the resulting R_{ct} values are presented in Table 8.1. The Randles' circuit has been presented previously, but is presented again in Figure 8.2a for the convenience of the reader; the circuit presented in Figure 8.2b is used to model the BSA data in subsequent sections. The quality of the fits

of the data to the Randles' circuit is very good, with a maximum error (other than the highest frequency point) of 10 % for Trial 1 (shown in Figure 8.3, discussed later in this section) and 5 % for Trials 2, 3, and 4.

In this Chapter (as was discussed in Chapter 6), changes in R_{ct} will be used to identify changes at the electrode surface. The R_{ct} values (Table 8.1) for each replicate blank experiment indicate a decrease in R_{ct} over the first hour of the experiment, followed by a subsequent increase in R_{ct} over the remaining 19 hours. The question arises, however, as to whether or not the changes in R_{ct} are due to physical changes at the electrode surface, or due to errors in the fitting procedure. An examination of R_s values can help to answer this question.

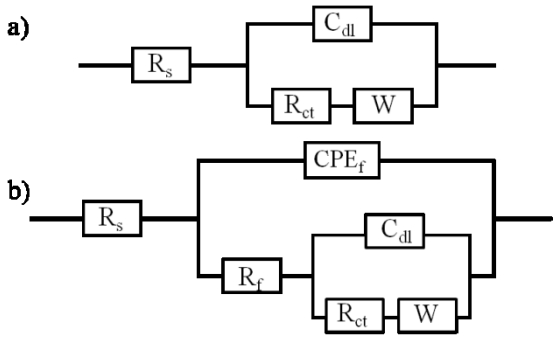

Figure 8.2: a) Randles circuit used to model blank data. b) EEC used to model BSA data (circuit C2 in Chapter 5).

Table 8.1: Summary of R_{ct} values obtained by fitting four experiments on a Pt wire in 0.2 M PBS solution with 3 mM ferri/ferrocyanide.

Time	Trial 1			Trial 2			Trial 3			Trial 4		
	R_{ct} /Ω	ΔR_{ct} /%	Change	R_{ct} /Ω	ΔR_{ct} /%	Change	R_{ct} /Ω	ΔR_{ct} /%	Change	R_{ct} /Ω	ΔR_{ct} /%	Change
0 h	83	-	-	61	-	-	44	-	-	45	-	-
1 h	66	-21	↓	36	-41	↓	27	-37	↓	25	-44	↓
5 h	82	25	↑	51	41	↑	36	30	↑	52	107	↑
10 h	90	9	↑	63	24	↑	47	32	↑	64	24	↑
15 h	92	3	↑	69	9	↑	56	19	↑	72	13	↑
20 h	95	3	↑	73	6	↑	76	36	↑	76	6	↑

R_s is dependent only on the position of the electrode in the electrochemical cell, and the conductivity of the electrolyte solution and therefore is not expected to change throughout the 20 hour experiment, as the electrode is not moved and the applied potential should not change the conductivity of the electrolyte solution. The change in R_s that occurs, then, is expected to be due to error in the fitting procedure, as opposed to a physical change in R_s. The amount of change in R_s, can therefore be used as an estimate of fitting error. The R_s values obtained for each trial are presented in Table 8.2. For the four replicate blank experiments, the relative standard deviations on R_s (over the 20 hour experiment) are 2 %, 4 %, 1 %, and 2 % for trials 1 through 4, respectively. These values can be used to determine whether changes in R_{ct} are significant. For example, for Trial 1, the change in R_{ct} must be greater than 2 % to be considered significant.

Table 8.2: Summary of R_s values obtained by fitting four experiments on a Pt wire in 0.2 M PBS solution with 3 mM ferri/ferrocyanide.

	R_s/Ω			
Time	**Trial 1**	**Trial 2**	**Trial 3**	**Trial 4**
0 h	48	76	69	59
1 h	48	74	72	60
5 h	46	70	69	58
10 h	46	70	68	58
15 h	45	70	69	58
20 h	45	70	68	59
Average	46	72	69	59
Standard Deviation	1	3	1	1
Relative Standard Deviation	2 %	4 %	1 %	2 %

The incremental changes (*i.e.* from 0 h to 1 h, 1 h to 5 h, *etc.*, presented in Table 8.1) in R_{ct} for each of the replicates are greater than the required change to be considered significant (2 %, 4 %, 1 % or 2 % for each trial). Therefore, changes in R_{ct} for the blank experiments are indicative of changes at the electrode surface (as opposed to error in the fitting procedure). Note that the ΔR_{ct} values were calculated prior to rounding the R_{ct} values. In the first hour of the experiment, a decrease in R_{ct} is observed for all replicates (Table 8.1). It is believed that the large R_{ct} value observed for the 0 h experiment may be the product of trying to impose a semi-circle on a plot in which a semi-circle is not present, as the Randles' circuit predicts a semi-circular Nyquist plot and the 0 h spectrum does not have this feature (Figure 8.3). As such, the decrease in the first hour of EIS may be an artifact of the fitting procedure as opposed to a true decrease in R_{ct}.

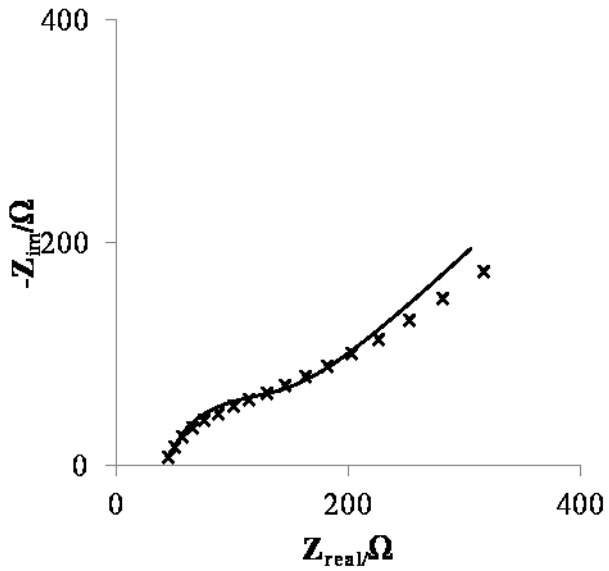

Figure 8.3: 0 h Nyquist plot for a Pt electrode in 0.2 M PBS with 3 mM ferri/ferrocyanide, with fit data generated from fitting experimental data to the Randles circuit presented in Figure 5.1a. (x) indicate experimental data and solid lines indicate fit.

Between hours 1 and 20 of EIS, an increase in R_{ct} is observed. It is hypothesized that the increase in R_{ct} observed from 1 h to 20 h may be the result of the adsorption of solution species on to the electrode surface; literature precedent suggests that chloride[156] and phosphate[156,157,166] anions adsorb on platinum electrode surfaces. As discussed previously (Section 2.3.3), R_{ct} is impacted by the energy-barrier associated with transport of the redox species to the electrode surface.[66] The adsorption of chloride and phosphate anions on the electrode surface results in a decrease in the net surface charge and, consequently, a decrease in the electrostatic attraction between the negatively-charged ferri/ferrocyanide molecules and the surface. Therefore, as anions adsorb on the electrode surface, there is less impetus for the ferri/ferrocyanide molecules to reach the surface and

an increase in the impedance, resulting in an increase in R_{ct}. Additionally, the adsorption of chloride and phosphate also creates a larger distance between the ferri/ferrocyanide redox species and the surface, increasing the difficulty of transferring an electron from the redox molecules to the surface (and vice versa). Finally, the increase in R_{ct} from 1 h to 20 h could also be the result of platinum oxide film formation (as discussed in Chapter 6). An increase in R_{ct} in buffer has been previous reported by other research groups: Bogomolova *et al*. reported an increase in R_{ct} with repeated measurements on the same electrode[7] and Moulton *et al*. reported an increase in R_{ct} upon exposure of a gold electrode to PBS.[23]

The spectra presented in Figure 8.1, along with the parameter values presented in Table 8.1 serve as a background against which BSA results can be compared.

8.3 Changes in BSA Film Over Time In BSA-Free Electrolyte

As mentioned previously, the most common method by which to adsorb a BSA film on the surface of a metal electrode is by incubation of the electrode in a BSA-containing solution. EIS is then measured in a BSA-free solution. Figure 8.4 shows Nyquist plots recorded over 20 hours after incubation in a 1 g L^{-1} BSA solution; replicates are presented in Figure A15 of the Appendix. The initial decrease in the semi-circular portion of the Nyquist plots is observed during the first hour post-incubation. A decrease immediately after incubation is expected, as a decrease in potential (from E_{oc} during incubation to E_{eq} during EIS) was shown in Chapter 6 to result in desorption of BSA from the electrode surface. The R_s and R_{ct} values resulting from the fit of the data to the EEC presented in Figure 8.4 are tabulated in Table 8.3 and 8.4, respectively. R_s

values indicate that changes in R_{ct} smaller than 7 %, 3 %, and 8 % (for Trials 1, 2, and 3, respectively) cannot be attributed to physical changes at the electrode surface.

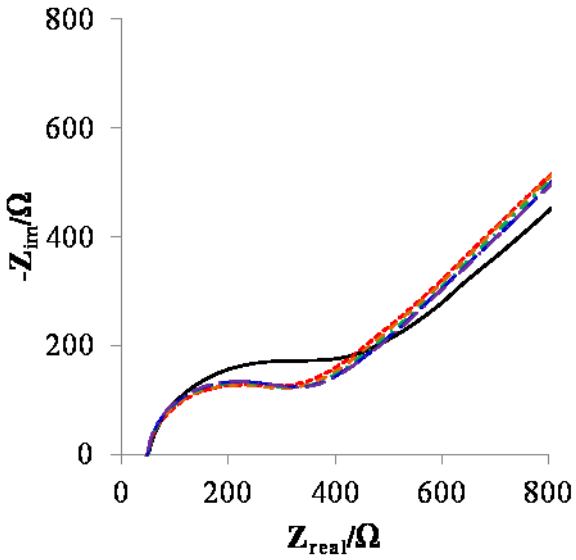

Figure 8.4: Nyquist plots a Pt wire electrode in 0.2 M PBS solution with 3 mM ferri/ferrocyanide, after incubation in 1 g L^{-1} BSA for 30 minutes. Time after incubation: 0 h (black, solid), 1 h (red, dotted), 5 h (orange, short dash), 10 h (green, dot dash), 15 h (blue, long dash), 20 h (purple, long dash dot).

Table 8.3: Summary of R_s values obtained by fitting three experiments on a Pt wire electrode in 0.2 M PBS solution with 3 mM ferri/ferrocyanide, after incubation in 1 g L^{-1} BSA for 30 minutes.

	R_s/Ω		
Time	**Trial 1**	**Trial 2**	**Trial 3**
0 h	49	33	31
1 h	46	32	38
5 h	51	31	37
10 h	44	31	37
15 h	44	34	37
20 h	43	30	39
Average	46	32	36
Standard Deviation	3	1	3
Relative Standard Deviation	7 %	3 %	8 %

Examination of the extracted R_{ct} values (Table 8.4) confirms the expected decrease in R_{ct} during the first hour post-incubation, for all replicates, showing desorption of BSA from the electrode surface (Chapter 6) due to the change from E_{oc} to E_{eq}. Between 1 h and 20 h, the incremental changes in R_{ct} are smaller than the estimated fitting error (relative standard deviation of R_s, Table 8.3) and therefore cannot be attributed changes in the BSA film. The data suggest that, when no BSA is present in the electrolyte, steady-state is reached within one hour post-incubation. This result is important for biosensor applications as it suggests that, when a BSA blocking film is applied by incubation, performing measurements within one hour of blocking film formation could results in convolution of analyte signal by changes in the BSA film.

Instead, the films formed by incubation should be allowed to equilibrate for at least one hour prior to analyte measurements.

Table 8.4: Summary of R_{ct} values obtained by fitting three experiments on a Pt wire in 0.2 M PBS solution with 3 mM ferri/ferrocyanide, after incubation in 1 g L^{-1} BSA for 30 minutes.

Time	Trial 1			Trial 2			Trial 3		
	R_{ct}/Ω	ΔR_{ct}/%	Change	R_{ct}/Ω	ΔR_{ct}/%	Change	R_{ct}/Ω	ΔR_{ct}/%	Change
0 h	360	-	-	332	-	-	435	-	-
1 h	299	-17	↓	290	-13	↓	272	-37	↓
5 h	293	-2	no change	283	-2	no change	276	2	no change
10 h	300	2	no change	278	-2	no change	294	7	no change
15 h	303	1	no change	276	-1	no change	289	-2	no change
20 h	304	0	no change	264	-4	↓	285	-1	no change

8.4 Changes in BSA Film Over Time In BSA-Containing Electrolyte

Serum albumin is present at a high concentration in the electrolyte solution of any blood-sampling electrochemical biosensors; for this reason, it is essential to understand how BSA films on surfaces change over time when BSA is present in the electrolyte solution. Changes in BSA adsorption over time with BSA present in the electrolyte were examined by performing similar experiments to those presented in Section 8.3, with 1 g L^{-1} BSA in the electrolyte solution. Nyquist plots are presented in Figure 8.5 (replicates in Figure A16 of the Appendix). The Nyquist plots show a decrease in the semi-circular region of the plots over the first *ca*. 5 hours, followed by a stabilization,

suggesting that BSA desorbs from the electrode surface over the first 5 hours of EIS. The extracted R_s and R_{ct} values are presented in Tables 8.5 and 8.6, respectively. R_s values indicate that changes in R_{ct} smaller than 19 %, 6 %, and 20 % (for Trials 1, 2, and 3, respectively) cannot be attributed to physical changes at the electrode surface.

Examination of R_{ct} values (Table 8.6) shows that, for Trial 1, incremental changes in R_{ct} are significant in the first five hours of EIS (*ie*. from 0 h to 1 h and 1 h to 5 h), and over this time there is a decrease in R_{ct}, suggesting desorption of BSA from the electrode surface. Trial 2 shows a similar decrease in R_{ct}, but the incremental change from 5 h to 10 h is also significant in this trial. Finally, Trial 3 shows no significant incremental changes in R_{ct}. In the case of Trial 3, an analysis of the R_{ct} and Nyquist plot (Table 8.6 and Figure A16b) suggest that a decrease in R_{ct} is observed in the first 5 hours of EIS; this decrease is not able to be detected, however, due to the high relative standard deviation of the R_s values for Trial 3. A second look at the R_s values (Table 8.5) shows that the values are much lower than any other R_s values presented in this thesis. Accordingly, although the standard deviation is similar to others, the relative standard deviation gets magnified by the small average R_s values. In short, it is believed that there is a decrease in R_{ct} for Trial 3, but it is masked by the large relative standard deviation value obtained due to the uncommonly small R_s values.

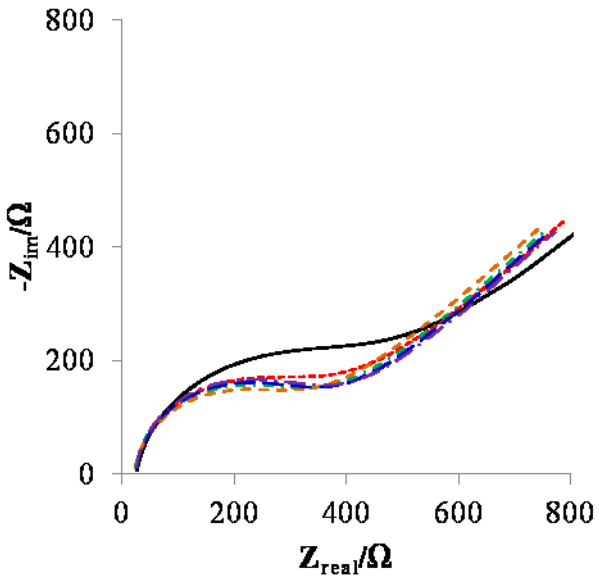

Figure 8.5: Nyquist plots a Pt wire electrode in 0.2 M PBS solution with 3 mM ferri/ferrocyanide and 1 g L^{-1} BSA, after 30 minutes at E_{oc}. Time after 30 minute rest at E_{oc}: 0 h (black, solid), 1 h (red, dotted), 5 h (orange, short dash), 10 h (green, dot dash), 15 h (blue, long dash), 20 h (purple, long dash dot).

Table 8.5: Summary of R_s values obtained by fitting three experiments on a Pt wire electrode in 0.2 M PBS solution with 3 mM ferri/ferrocyanide and 1 g L^{-1} BSA, after 30 minutes at E_{oc}.

	R_s/Ω		
Time	**Trial 1**	**Trial 2**	**Trial 3**
0 h	22	39	14
1 h	17	37	11
5 h	15	35	10
10 h	15	35	9
15 h	14	34	9
20 h	14	34	8
Average	16	36	10
Standard Deviation	3	2	2
Relative Standard Deviation	19 %	6 %	20 %

Table 8.6: Summary of R_{ct} values obtained by fitting three experiments on a Pt wire in 0.2 M PBS solution with 3 mM ferri/ferrocyanide and 1 g L^{-1} BSA, after 30 minutes at E_{oc}.

Time	Trial 1			Trial 2			Trial 3		
	R_{ct}/Ω	ΔR_{ct}/%	Change	R_{ct}/Ω	ΔR_{ct}/%	Change	R_{ct}/Ω	ΔR_{ct}/%	Change
0 h	591	-	-	597	-	-	543	-	-
1 h	471	-20	↓	560	-6	↓	495	-9	no change
5 h	376	-20	↓	444	-21	↓	440	-11	no change
10 h	390	4	no change	412	-7	↓	451	3	no change
15 h	395	1	no change	403	-2	no change	466	3	no change
20 h	408	3	no change	403	0	no change	485	4	no change

A comparison between the experiments presented without (Section 8.3) and with (Section 8.4) BSA in the electrolyte shows that a greater period of time is required to reach steady-state when BSA is present in the electrolyte. It is believed that while the desorption of BSA is driven by the change in potential from E_{oc} to E_{eq}, the kinetics are governed by the chemical potential gradient between the surface and the solution. When BSA is present in the electrolyte, longer desorption times (slower desorption kinetics) are observed, suggesting a smaller gradient between the surface and the solution. In contrast, when BSA is not present in solution, the desorption time is shorter - suggesting faster desorption kinetics due to a larger chemical potential gradient.

8.5 BSA Incubation; Subsequent Addition of BSA to Electrochemical Cell

The results from Section 8.4 and 8.5 suggest that the BSA film desorption occurs at different rates when BSA is and is not present in the electrochemical cell. To further probe the changes in the BSA film, a typical incubation experiment was performed (no BSA in electrolyte) but after 8 hours of EIS, BSA was injected into the electrolyte to a total concentration of 1 g L^{-1}. The results from this "Incubation and Subsequent Addition" experiment are presented in Figure 8.6 and the corresponding R_{ct} values are presented in Table 8.7. The error in R_s for this experiment is 10 %; therefore, changes in other parameters must be greater than 10 % to be attributed to BSA film changes.

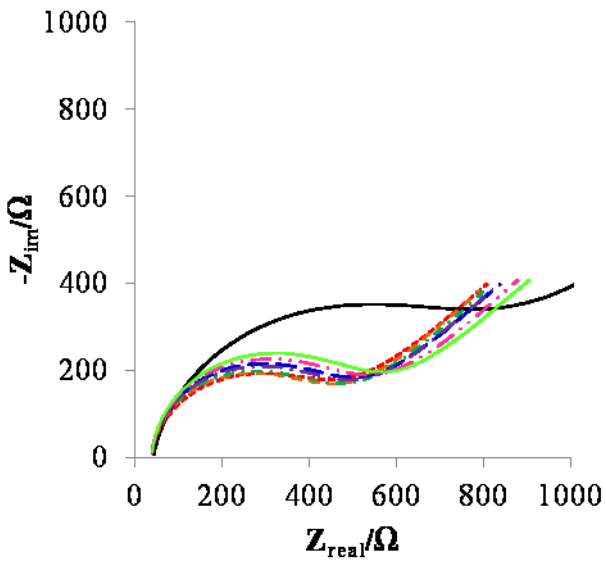

Figure 8.6: Nyquist plots for a Pt wire electrode (*ca*. 0.08 cm^2) incubated in 1 g L^{-1} BSA for 30 minutes, and then moved to 0.2 M PBS solution with 3 mM ferri/ferrocyanide and EIS recorded for *ca*. 8 hours before injection of BSA to the electrolyte for a concentration of 1 g L^{-1} and then EIS recorded for 10 hours. Time: 0 h post-incubation (black, solid), 1 h post-incubation (red, dotted), 5 h post-incubation (orange, short dash), immediately before injection (green, dot dash), immediately after injection (blue, long dash), 1 h post-injection (purple, long dash dot), 5 h post-injection (pink, dot-dot-dash), 10 h post-injection (lime, solid).

The results show a large decrease in R_{ct} (41 %) within the first hour post-incubation – consistent with that observed for previous incubation experiments (Section 8.3). The R_{ct} does not change between 1 h and 5 h post-incubation; again, this is consistent with the previous observations for incubation (no BSA in electrolyte, Section 8.3). Upon addition of BSA to the electrolyte, no incremental changes (greater than 10 %) in R_{ct} are observed; an 18 % increase in R_{ct} is observed over 10 hours post-incubation. It is hypothesized that the subsequent addition of BSA to the electrolyte solution results in a total concentration of BSA higher than that examined previously, as the injected BSA (700 μL of 10 g L^{-1} BSA) is added to that which desorbed from the surface in the first five hours. Since BSA adsorption is dependent on bulk concentration (described in Section 2.2.2 and further explored in Section 8.6), the higher BSA concentration results in more BSA adsorption on the electrode surface and, consequently, higher R_{ct} values. The slow increase in R_{ct} (over 10 hours) as compared to when a bare electrode is incubated in BSA (30 minutes) may be attributed to the different chemical potential gradients between the surface and the bulk solution. When a bare electrode is incubated in 1 g L^{-1} BSA, the gradient between the surface (no BSA) and the bulk solution is much steeper than that between a BSA film-coated electrode and the bulk solution. The smaller chemical potential gradient that exists when a BSA film is already formed on the electrode surface causes slower adsorption of BSA to the electrode surface. The results also suggest that the incubation procedure does not saturate the electrode surface with BSA, as, upon addition of BSA to solution, more adsorption occurs. For biosensor applications in which BSA is present in the analyte matrix (*i.e.* blood-sampling

biosensors), this result is significant as it suggests that, over time, the analyte signal could be convoluted by additional BSA adsorption to the electrode surface.

Table 8.7: Summary of R_{ct} values obtained by fitting one experiment on a Pt wire in 0.2 M PBS solution with 3 mM ferri/ferrocyanide after 30 minute incubation in 1 g L^{-1} BSA. 700 µL of 10 g L^{-1} BSA was injected into the electrolyte after 8 hours of EIS, as noted.

Time	R_{ct}/Ω	ΔR_{ct}/%	Change
0 h post-incubation	817	-	
1 h post-incubation	481	-41	↓
5 h post-incubation	457	-5	no change
Immediately before injections of BSA into electrolyte	467	2	no change
Immediately after injections of BSA into electrolyte	478	2	no change
1 h post-incubation	498	4	no change
5 h post-incubation	521	5	no change
10 h post-incubation	549	5	no change

8.5.1 Removal of BSA From Solution

Based on the results from the incubation and subsequent addition experiment – where the addition resulted in a gradual change in the BSA film, experiments were attempted that would strip the BSA from solution – such that BSA could be removed from the electrolyte and changes in the BSA film could be observed. It was not possible to simply dilute the electrolyte solution by removing a small quantity and replacing it PBS, because this method would result in stirring of the solution, which may disrupt the BSA film. Instead, past research by Urano and co-workers[88,167,168] found that BSA

adsorbs well to Al_2O_3; it was hypothesized, then, that Al_2O_3 may be used to extract BSA from solution.

The fluorescence emission spectra of a 1 g L^{-1} BSA solution before and after the addition of Al_2O_3 are compared in Figure 8.7. A small decrease in peak height is observed each time Al_2O_3 is added to the BSA solution, suggesting that the BSA is being stripped from solution by the Al_2O_3. However, at the point at which 0.35 g of Al_2O_3 was added to the cuvette, the cuvette was *ca*. 40 % filled with the white solid and a peak height reduction of < 30 % was observed. If this method was used to extract BSA from the electrolyte solution, the large mass of Al_2O_3 required to change the BSA concentration would physically interfere with the electrode which sits near the bottom of the electrochemical cell. Therefore, although Al_2O_3 is able to strip the BSA from solution, it appears that the concentration of BSA in solution is too high for the Al_2O_3 to be able to remove all of the BSA from solution. Therefore, this method was not successful and EIS experiments in which BSA is stripped from solution could not be completed.

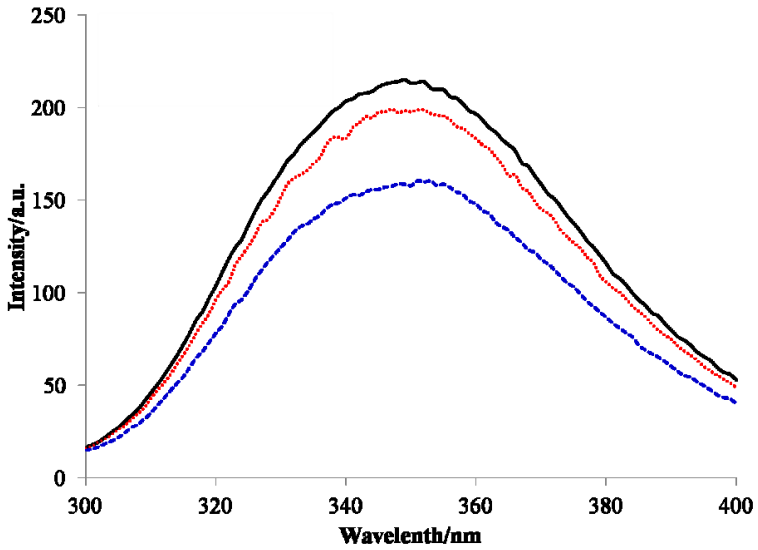

Figure 8.7: Fluorescence emission spectra for 1 g L^{-1} BSA (black, solid) with 0.1 g added Al_2O_3 (red, dotted) and 0.35 g added Al_2O_3 (blue, dashed). Excitation λ = 290 nm.

8.6 Concentration Studies

As mentioned in Section 8.5, preliminary results from the addition of BSA to solution suggest that the surface of the electrode is not being saturated by BSA. Since BSA is commonly used as a blocking molecule for electrochemical biosensors,[11–17] it is important that the electrode surface be well-covered such that the blocking efficiency of BSA is as high as possible. It is well-known in the literature that protein adsorption is dependent on the concentration of protein in the bulk solution;[96] therefore, experiments were completed to determine if saturation of the Pt electrode surface is possible, and, if so, what R_{ct} value can be associated with surface saturation.

Nyquist plots for 10 g L^{-1} and 20 g L^{-1} incubation experiments are presented in Figure 8.8a and b, respectively, and their corresponding R_{ct} values in Table 8.8. R_s values for the 10 g L^{-1} BSA incubation had a relative standard deviation of 2 %, and R_s values for the 20 g L^{-1} BSA incubation had a relative standard deviation of 11 %.

The results of the 10 g L^{-1} show a significant decrease in R_{ct} over the first 5 hours of the experiment followed by a stabilization in R_{ct}. Importantly, the final R_{ct} value for the 10 g L^{-1} experiment is 493 Ω as compared with 284 Ω ± 20 Ω for the 1 g L^{-1} experiments of the same type, confirming that the surface was not saturated with BSA in the 1 g L^{-1} case as a greater R_{ct} value suggests greater surface coverage is achieved with the 10 g L^{-1} incubation.

Results of the 20 g L^{-1} incubation show a significant decrease in R_{ct} over the first 10 hours of the experiment, followed by a stabilization. The 0 h R_{ct} value of *ca*. 9000 Ω is greater than any R_{ct} value previously observed, and suggests that a much larger quantity

of BSA is able to adsorb on the electrode surface. The final R_{ct} value is 1933 Ω - again, much larger than any R_{ct} value previously observed.

Globular proteins are expected to form monolayers on a solid surface, as there is insufficient protein-protein attraction to form a multilayer.[96] At very high concentrations, however, some proteins have been found to form multilayers as the conformation of the protein changes with crowding to enhance the protein-protein interactions.[97,98] It is possible, then, that the R_{ct} values observed for the 20 g L^{-1} concentration could result either from greater surface coverage by a monolayer of BSA (due to conformational changes of the BSA allowing for greater adsorption), or from the development of a multilayer of BSA. A multilayer is expected to cause an increase in R_{ct} because a thicker film would result in greater difficulty for the redox molecules to reach the electrode surface.

The concentration of serum albumin in human serum is 35 to 50 g L^{-1};[169,170] therefore, forming a BSA blocking layer using a 1 g L^{-1} solution and then subsequently introducing the electrode (biosensor) to a higher concentration of albumin (*ie.* in blood) will result in changes in the BSA film as the bulk concentration of serum albumin will increase the concentration of adsorbed albumin. This is demonstrated to a small extent in the "Incubation and Subsequent Addition" experiments presented in Section 8.5, as well as the concentration experiments in this section that suggest that 1 g L^{-1} incubation does not result in complete surface coverage. This concentration is commonly used for BSA blocking purposes.[14,23,92,93] As biosensors are developed, researchers should be aware of the changes in BSA blocking films that will occur when the electrode is introduced to different concentrations of albumin – pre-dilution of analyte matrices or formation of

BSA blocking films using higher concentration may be required to avoid convolution of analyte signal due to changes in the BSA film.

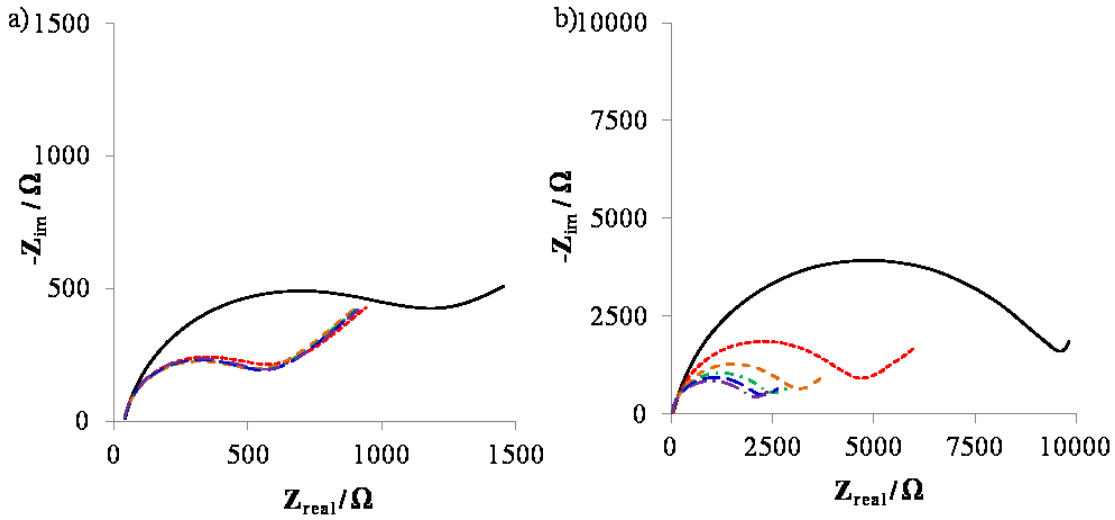

Figure 8.8: Nyquist plots a Pt wire electrode in 0.2 M PBS solution with 3 mM ferri/ferrocyanide after incubation for 30 mintues in a) 10 g L^{-1} BSA and b) 20 g L^{-1} BSA. Time after incubation: 0 h (black, solid), 1 h (red, dotted), 5 h (orange, short dash), 10 h (green, dot dash), 15 h (blue, long dash), 20 h (purple, long dash dot).

Table 8.8: R_{ct} values for a Pt wire electrode in 0.2 M PBS solution with 3 mM ferri/ferrocyanide after incubation for 30 mintues in 10 g L^{-1} BSA or 20 g L^{-1} BSA.

Time	10 g L^{-1}			20 g L^{-1}		
	R_{ct}/Ω	ΔR_{ct}/%	Change	R_{ct}/Ω	ΔR_{ct}/%	Change
0 h	1081	-	-	9122	-	-
1 h	523	-52	↓	4363	-52	↓
5 h	483	-8	↓	2943	-33	↓
10 h	486	1	no change	2372	-19	↓
15 h	488	0	no change	2116	-11	no change
20 h	493	1	no change	1933	-9	no change

It is interesting to compare the desorption of BSA in the 10 and 20 g L^{-1} incubation experiments to the 1 g L^{-1} incubation experiment. Firstly, greater BSA desorption occurs in the first hour post-incubation for the two higher concentration experiments (52 %) as compared to the 1 g L^{-1} experiment (17 %, 13 %, 37 % for Trials 1 to 3, respectively). It is expected that the greater desorption in the higher concentration experiment occurs due to a greater chemical potential gradient between the BSA adsorbed on the electrode surface and the bulk solution, as compared to the 1 g L^{-1} experiment. Also relevant is the length of time required for the system to reach steady-state: 10 h for the 20 g L^{-1} incubation, 5 h for the 10 g L^{-1} incubation, and 1 h for the 1 g L^{-1} incubation. The differences in the time required to reach steady-state are likely related to the amount of BSA lost from the surface; a much greater amount of BSA is lost in the 20 g L^{-1} case, resulting in a longer period of time required to reach steady-state.

8.7 Conclusions

The results presented in this chapter examine the changes that occur in the 20 hours post-BSA film formation, with and without the presence of BSA in the electrolyte solution. First, background experiments conducted in PBS (no BSA) over time show a small increase in R_{ct} over the 20 hour time period of the experiment – likely due to the adsorption of phosphate and chloride anions from solution onto the electrode surface. The 1 g L^{-1} incubation experiments (no BSA in electrolyte) show that steady-state is reached within the first hour post-film formation and that the film does not change significantly from 1 h to 20 h. Similar 1 g L^{-1} experiments with BSA in the electrolyte also result in a steady-state, although a greater amount of time (5-10 h) was required for it to be achieved. The differences in time required to reach steady-state are attributed to

differences in the chemical potentials gradients between the electrode and the bulk solution. When BSA was injected into the electrolyte after steady-state was reached, no significant incremental changes in R_{ct} were observed, but a significant total increase in R_{ct} was observed in the 10 hours post-injection. This increase is attributed to a small increase in concentration (1 g L^{-1} injected plus an unknown concentration of BSA that desorbed from the surface after incubation).

The concentration of the incubation solution has an impact on the amount of BSA which is initially adsorbed at the electrode surface, with higher concentrations resulting in higher amounts of adsorbed protein. After a 10 g L^{-1} incubation, steady-state is reached within the first 5 hours; steady-state is reached within 10 hours after the electrode is incubated in a 20 g L^{-1} solution of BSA. Importantly, the 20 hour R_{ct} value for the 10 g L^{-1} incubation (493 Ω) is similar to those observed for the 1 g L^{-1} incubations while that for the 20 g L^{-1} incubations is much higher (1933 Ω), suggesting possible multilayer surface coverage after incubation at 20 g L^{-1}.

The results presented in this chapter should caution researchers to choose incubation solution and electrolyte concentrations carefully, as variations in each can impact BSA films over time. Additionally, care must be taken to ensure steady-state for the BSA film has been reached before proceeding with analyte measurements, to ensure that changes in the BSA film do not convolute analyte signal. Results from this chapter suggest that, for BSA films formed at 1 g L^{-1} concentrations, waiting 10 hours after film formation will ensure steady-state has been reached.

Chapter 9 CONCLUSIONS AND FUTURE WORK

9.1 Conclusions

In this thesis, a method has been presented for studying protein adsorption on solid surfaces by EIS, using a model system of BSA on platinum electrode surfaces. EIS is a commonly used analytical technique for electrochemical biosensors, particularly useful because of the ability to model the electrochemical data with EECs and extract meaningful quantitative values for physical processes that are occurring in the electrochemical system. Use of the methodology presented in this thesis will allow researchers to have greater confidence in EEC choice, greater reproducibility of results, and will enable easier comparison between literature values. In turn, use of the developed method will lead to better understanding of protein films on solid surfaces.

Kramers-Kronig compliance of data from both blank and BSA adsorption experiments was tested using the Measurement Model method developed by Agarwal *et al.*[140] Kramers-Kronig compliant frequency ranges were determined for each set of data, and were subsequently used in all modeling throughout the thesis. Choosing Kramers-Kronig compliant data is crucial because it ensures that the data used in further analysis meets the requirements of stability, causality, and linearity. Knowledge that a data set is Kramers-Kronig compliant provides confidence that any difference between the experimental data and the fit when the data is modeled with an EEC is due to improper EEC choice, as opposed to the non-compliance of the data set.

EEC choice is a crucial part of EIS analysis; it is common in electrochemical biosensor and protein adsorption studies for an EEC to be chosen based on an estimate of

the physical system and subsequently to be justified by comparing the experimental and fit data. The research presented in this thesis, however, shows that this is not an adequate method to properly choose an EEC. The results show that for the same data several circuits can provide an adequate fit. A more thorough, comprehensive method of EEC choice was proposed herein and tested using a model system of BSA adsorbed on platinum electrode surfaces. The selection process begins by creating a library of circuits, based on literature precedent and knowledge of the electrochemical system. Next, the experimental data is fit to each circuit in the library. A process of elimination based on residual errors, parameter values, and standard deviations based on replicate measurements is used to select the circuit which best models the electrochemical system. For the two systems presented in this thesis (platinum in PBS with and without a BSA film), it is found that when no BSA is present, the Randles circuit best models the data, and an additional time constant (resistor and constant phase element in parallel), modeling a porous, insulating film, is needed when a BSA film is formed on the surface. It is suggested that researchers using EECs to model protein adsorption data use the developed method to avoid errors in circuit choice.

Continuing with the theme of improving and understanding EIS with respect to protein films, the influence of a number of factors related to experimental set-up and EIS conditions on BSA adsorption were examined. Performing EIS in BSA-free PBS solution before exposure to BSA results in a significant drop in protein adsorption, proposed to be due to the adsorption of chloride and phosphate ions on the electrode surface, reducing the affinity of BSA for the surface. Initial EIS is important as it allows for comparison "before" and "after" protein film formation, and therefore this thesis suggests that to

avoid issues resulting from Initial EIS, researchers should ensure that the electrode is cleaned between the initial EIS and exposure to protein. Results conclude that small fluctuations in temperature do not impact the reproducibility of replicate experiments, but that injection of BSA into the electrolyte solution causes high irreproducibility. This irreproducibility is attributed to the poor mixing of BSA into solution; this thesis suggests that protein-containing solutions be well-mixed before EIS measurements are completed. Ferricyanide influences with BSA for adsorption and results in less overall BSA adsorption. Researchers are cautioned that the presence of ferricyanide may complicate the analysis of protein films by changing the EIS signal. Applied potential also impacts BSA adsorption; while greater BSA adsorption occurs at higher potentials, the change from a high to low potential results in desorption of BSA from the electrode surface and therefore poorer film stability post-incubation. Change in potential is common in EIS studies, as electrodes are typically incubated at E_{oc} before EIS is measured at E_{eq}; it is suggested, then, that both the incubation and EIS potentials be considered carefully when studying protein adsorption by EIS. The application of ac vs. dc potential does not affect the BSA film, giving researchers confidence that this experimental variable is not changing the protein film under study.

Surface-Enhanced Raman Spectroscopy (SERS) studies showed that, under the experimental conditions used, a SERS spectrum of unlabelled BSA on gold SSV substrates could not be obtained. Further, changes in rhodamine-labelled HSA adsorption with potential could not be detected. Experiments involving two proteins showed neither HSA, IgG, nor DNA form complete monolayers upon incubation in 0.25 g L^{-1} protein for 30 minutes.

Studies of BSA film changes over time showed that less time is required for BSA films to reach steady-state when BSA is not present in the electrolyte. The differences are attributed to differences in the chemical potential gradient between the surface and the bulk solution, with smaller chemical potential gradients leading to slower desorption of BSA from the surface. These results are relevant to the development of biosensors that use BSA, as convolution of analyte signal due to BSA desorption may occur if the film is not allowed to reach steady-state before analyte measurement. When the BSA film was allowed to reach steady-state and, subsequently, more BSA was added to the electrolyte, a slow increase in R_{ct} (and therefore quantity of adsorbed film) was observed. Again, this slower adsorption (as compared to when a bare electrode is incubated in BSA) is attributed to a smaller concentration gradient. Researchers who use BSA as a blocking molecule for biosensors should be aware that gradual changes in the blocking layer may occur when BSA is present in the analyte matrix. Studies of BSA incubation in 10 g L^{-1} and 20 g L^{-1} solutions showed that greater BSA adsorption occurs with greater concentration. The high magnitude of R_{ct} observed for the 20 g L^{-1} BSA incubation (as compared with 10 g L^{-1} and 1 g L^{-1} incubations) suggests possible multilayer formation. These results suggest that incubations in 1 g L^{-1} BSA or 10 g L^{-1} BSA do not form a complete and compact monolayer on the electrode surface, impacting the ability of BSA to be used as a blocking molecule in electrochemical biosensor applications.

9.2 Future Work

The work presented in this thesis provides a comprehensive method for EEC selection for protein adsorption data. Future work in this area would test the current

method on a wide variety of proteins on different solid surfaces. It would be of interest to determine whether the identified circuit for BSA adsorption on platinum also applied to non-platinum electrodes (gold, polymer, or metal oxide, for example), or if the circuit (and therefore BSA film) is strongly impacted by electrode material. Identifying the circuit(s) which best model BSA films on a variety of surfaces may lead to a greater understanding of the interactions that govern BSA adsorption.

The method could also be modified to encompass a broader range of systems; for example, the method could be used to study systems in which an antibody is chemisorbed on the electrode surface. Alternatively, the method could be extended to study proteins that have multiple adsorption motifs. For example, EIS could be used to identify film changes as proteins are denatured with temperature - because the denaturation of the protein would result in a change in the BSA film which would subsequently change the EEC which best models the data. The effects of pH, convection (studied by mixing or bubbling the electrolyte during EIS), or sheer (as *in vivo* biosensors will have solution flowing past the biosensor at all times) could also be studied in this way.

As mentioned previously, the ferri/ferrocyanide redox couple typically used for EIS protein adsorption experiments influences BSA adsorption (Chapter 6). It would be extremely interesting to study a wide variety of redox couples and determine which one, if any, do not compete for adsorption. Using different redox couples would also allow for performing EIS at different potentials such that the effect of potential on the BSA film could be studied in more detail. Further, it would be advantageous to be able to perform EIS without a redox couple. Experiments could be performed in this way and the method

developed for EEC choice could be used to gain a thorough understanding of physical processes occurring when no redox couple is present.

The ability to quantify surface concentration of BSA using EIS remains a challenge. Future work in this area would build on the current method and knowledge of BSA adsorption to develop a method by which the concentration of proteins on solid surfaces can be quantified. To begin, values of R_f and CPE_f could be studied closely – something which is rarely undertaken in the literature. Step-wise concentration experiments could be used to build a calibration curve between R_{ct} (or R_f or CPE_f) and bulk concentration of BSA. The results could be compared with surface coverage results obtained by other methods (*i.e.* cyclic voltammetry or EQCM).[83,171] Quantification of surface concentration of BSA could also provide information about the orientation of adsorbed BSA, since more BSA could adsorb on the electrode surface in the end-on position than the side-on position.

It would also be of interest to work on the experiments in which BSA is present in the electrolyte in more detail. Concentration and kinetic studies could be conducted to elucidate more information about the BSA film and how it is impacted by the presence of BSA in solution. Varying the solution concentration of BSA carefully until little BSA desorption occurs could help elucidate the surface concentration of BSA by identifying the point at which there is no concentration gradient from surface to solution. Additionally, the effects of time (greater than 20 hours) could be studied. One can imagine that these studies would be of particular interest in the field of *in vivo* electrochemical biosensors, where biosensor surfaces are surrounded by many different types of proteins for prolonged periods of time.

The use of other analytical techniques to further confirm the results presented in this thesis would be valuable. For example, ellipsometry is often used to study protein adsorption and may be able to be used before and after EIS studies to confirm (for example), that BSA is desorbing from the electrode surface. Ellipsometry can also give information about the thickness of protein films, which may be nicely compared to R_f values to determine whether these values can independently provide information about the structure of the BSA film (for example, multilayer development).

Weingarth *et al.*[172] have recently developed a method to perform *in situ* electrochemical X-ray Photoelectron Spectroscopy (XPS) using a three-electrode setup. Again, XPS can provide information about the film thickness. *In situ* XPS and EIS could therefore be very useful as XPS could track the film thickness and orientation while EIS monitors the surface coverage (through R_{ct}).

Ultimately, knowledge gained in the field of protein adsorption for a single protein must be applied to mixtures of several proteins. A combined spectroelectrochemical technique would be best suited for this study: a spectroscopic technique can identity which protein(s) is(are) present on the electrode surface, and EIS can provide information about surface coverage, orientation, and changes with environmental factors. For electrochemical biosensor systems, the knowledge gained by developing such a technique would be unparalleled.

REFERENCES

(1) Nakanishi, K.; Sakiyama, T.; Imamura, K. *J. Biosci. Bioeng.* **2001**, *91*, 233–244.

(2) Déjardin, P. *Proteins at Solid-Liquid Interfaces*; Schreck, S., Ed.; Springer Berlin Heidelberg, 2006.

(3) Thévenot, D.; Toth, K.; Durst, R.; Wilson, G. *Pure Appl. Chem.* **1999**, *71*, 2333–2348.

(4) Wang, J. *Biosens. Bioelectron.* **2006**, *21*, 1887–1892.

(5) Gamby, J.; Abid, J.-P.; Girault, H. H. *J. Am. Chem. Soc.* **2005**, *127*, 13300–13304.

(6) Sung, D.; Park, S.; Jon, S. *Langmuir* **2009**, *25*, 11289–11294.

(7) Bogomolova, A; Komarova, E.; Reber, K.; Gerasimov, T.; Yavuz, O.; Bhatt, S.; Aldissi, M. *Anal. Chem.* **2009**, *81*, 3944–3949.

(8) Berggren, C.; Johansson, G. *Anal. Chem.* **1997**, *69*, 3651–3657.

(9) Yu, X.; Xu, D.; Xu, D.; Lv, R.; Liu, Z. *Front. Biosci.* **2006**, *11*, 983–990.

(10) Diniz, F.; Ueta, R.; Pedrosa, A.; Areias, M.; Pereira, V.; Silva, E.; Silva, J.; Ferreira, A.; Gomes, Y. *Biosens. Bioelectron.* **2003**, *19*, 79–84.

(11) Wang, R.; Wang, Y.; Lassiter, K.; Li, Y.; Hargis, B.; Tung, S.; Berghman, L.; Bottje, W. *Talanta* **2009**, *79*, 159–164.

(12) Moulton, S. E.; Barisci, J. N.; Bath, A.; Stella, R.; Wallace, G. G. *J. Colloid Interface Sci.* **2003**, *261*, 312–319.

(13) Jeyachandran, Y. L.; Mielczarski, E.; Rai, B.; Mielczarski, J. *Langmuir* **2009**, *25*, 11614–11620.

(14) Hideshima, S.; Sato, R.; Inoue, S.; Kuroiwa, S.; Osaka, T. *Sensors Actuators B Chem.* **2012**, *161*, 146–150.

(15) Fan, D.-H.; Yuan, S.-W.; Shen, Y.-M. *Colloids Surf. B. Biointerfaces* **2010**, *75*, 608–611.

(16) Maalouf, R.; Fournier-Wirth, C.; Coste, J.; Chebib, H.; Saïkali, Y.; Vittori, O.; Errachid, A.; Cloarec, J.-P.; Martelet, C.; Jaffrezic-Renault, N. *Anal. Chem.* **2007**, *79*, 4879–4886.

(17) Rossier, J. S.; Girault, H. H. *Lab Chip* **2001**, *1*, 153–157.

(18) Roscoe, S. G.; Fuller, K. L. *Food Res. Int.* **1993**, *26*, 343–353.

(19) Carelli, D.; Centonze, D.; Palermo, C.; Quinto, M.; Rotunno, T. *Biosens. Bioelectron.* **2007**, *23*, 640–647.

(20) Smiechowski, M. F.; Lvovich, V. F.; Roy, S.; Fleischman, A.; Fissell, W. H.; Riga, A. T. *Biosens. Bioelectron.* **2006**, *22*, 670–677.

(21) Labib, M.; Hedström, M.; Amin, M.; Mattiasson, B. *Biotechnol. Bioeng.* **2009**, *104*, 312–320.

(22) Oliveira, M. D. L.; Correia, M. T. S.; Diniz, F. B. *Biosens. Bioelectron.* **2009**, *25*, 728–732.

(23) Moulton, S.; Barisci, J. N.; Bath, A.; Stella, R.; Wallace, G. G. *Electrochim. Acta* **2004**, *49*, 4223–4230.

(24) Phillips, R. K. R.; Omanovic, S.; Roscoe, S. G. *Langmuir* **2001**, *17*, 2471–2477.

(25) Jhaveri, S. D.; Mauro, J. M.; Goldston, H. M.; Schauer, C. L.; Tender, L. M.; Trammell, S. *Chem. Commun.* **2003**, 338–339.

(26) Brewer, S. H.; Glomm, W. R.; Johnson, M. C.; Knag, M. K.; Franzen, S. *Langmuir* **2005**, *21*, 9303–9307.

(27) Xie, Q. *J. Colloid Interface Sci.* **2003**, *262*, 107–115.

(28) Guo, B.; Anzai, J.; Osa, T. *Chem. Pharm. Bull.* **1996**, *44*, 800–803.

(29) Daniels, J. S.; Anderson, E. P.; Lee, T. H.; Pourmand, N. *Conf. Proc. IEEE Eng. Med. Biol. Soc.* **2008**, *2008*, 5753–5756.

(30) Huang, Y.; Bell, M. C.; Suni, I. I. *Anal. Chem.* **2008**, *80*, 9157–9161.

(31) Cosman, N. P.; Fatih, K.; Roscoe, S. G. *J. Electroanal. Chem.* **2005**, *574*, 261–271.

(32) Pejcic, B.; Demarco, R. *Electrochim. Acta* **2006**, *51*, 6217–6229.

(33) Ahmed, M. U.; Hossain, M. M.; Tamiya, E. *Electroanalysis* **2008**, *20*, 616–626.

(34) Laschi, S.; Palchetti, I. *Indian J. Chem.* **2003**, *42a*, 2968–2973.

(35) Shervedani, R. K.; Mehrjardi, A. H.; Zamiri, N. *Bioelectrochemistry* **2006**, *69*, 201–208.

(36) Andreescu, S.; Luck, L. *Anal. Biochem.* **2008**, *375*, 282–290.

(37) Tsai, C.-C.; Wang, G.-J. *J. Electrochem. Soc.* **2012**, *160*, B1–B5.

(38) Le Breton, M.-H.; Beck-Henzelin, A.; Richoz-Payot, J.; Rochereau-Roulet, S.; Pinel, G.; Delatour, T.; Le Bizec, B. *Anal. Chim. Acta* **2010**, *672*, 45–49.

(39) Yin, H.; Zhou, Y.; Ai, S.; Chen, Q.; Zhu, X.; Liu, X.; Zhu, L. *J. Hazard. Mater.* **2010**, *174*, 236–243.

(40) Grabbe, E. S. E.; Buck, R. *J. Am. Chem. Soc.* **1989**, *111*, 8362–8366.

(41) Reipa, V.; Gaigalas, A.; Abramowitz, S. *J. Electroanal. Chem.* **1993**, *348*, 413–428.

(42) Wei, F.; Zhang, D.; Halas, N. J.; Hartgerink, J. D. *J. Phys. Chem. B* **2008**, *112*, 9158–9164.

(43) Das, G.; Patra, N.; Gopalakrishnan, A.; Zaccaria, R. P.; Toma, A.; Thorat, S.; Di Fabrizio, E.; Diaspro, A.; Salerno, M. *Analyst* **2012**, *137*, 1785–1792.

(44) David, C.; Guillot, N.; Shen, H.; Toury, T.; de la Chapelle, M. L. *Nanotechnology* **2010**, *21*, 475-501.

(45) Han, X. X.; Zhao, B.; Ozaki, Y. *Anal. Bioanal. Chem.* **2009**, *394*, 1719–1727.

(46) Bartlett, P.; Mahajan, S. In *Bioelectrochemistry*; 2011; pp. 269–334.

(47) Johnson, R. P.; Richardson, J. A; Brown, T.; Bartlett, P. N. *J. Am. Chem. Soc.* **2012**, *134*, 14099–14107.

(48) Asanov, A.; Wilson, W. W.; Oldham, P. B. *Anal. Chem.* **1998**, *70*, 1156–1163.

(49) Martirosyan, A.; Vardapetyan, H.; Tiratsuyan, S.; Hovhannisyan, A. In *Proc. SPIE 7715, Biophotonics: Photonic Solutions for Better Health Care II*; 2010.

(50) Heutmekers, T. H. J.; Bremer, M.; Haasnoot, W.; Nielen, M. W. F. *Anal. Chim. Acta* **2007**, *586*, 239–245.

(51) V eiseh, M.; Zareie, M. H.; Zhang, M. *Langmuir* **2002**, *18*, 6671–6678.

(52) Green, R. J.; Davies, M. C.; Roberts, C. J.; Tendler, S. J. *Biomaterials* **1999**, *20*, 385–391.

(53) Hagenhoff, B. *Biosens. Bioelectron.* **1995**, *10*, 885–894.

(54) Placzek, E.; Plebanek, M. P.; Lipchik, A. M.; Kidd, S. R.; Parker, L. L. *Anal. Biochem.* **2010**, *397*, 73–78.

(55) Henn, C.; Boettcher, S.; Steinbach, A.; Hartmann, R. W. *Anal. Biochem.* **2012**, *428*, 28–30.

(56) Nedelkov, D.; Rasooly, A; Nelson, R. W. *Int. J. Food Microbiol.* **2000**, *60*, 1–13.

(57) Rezaei, B.; Khayamian, T.; Majidi, N.; Rahmani, H. *Biosens. Bioelectron.* **2009**, *25*, 395–399.

(58) Rouhana, R.; Budge, S. *Food Res. Int.* **1997**, *30*, 303–310.

(59) Narakathu, B. B.; Atashbar, M. Z.; Bejcek, B. E. *Biosens. Bioelectron.* **2010**, *26*, 923–928.

(60) Komarova, E.; Reber, K.; Aldissi, M.; Bogomolova, A. *Biosens. Bioelectron.* **2010**, *25*, 1389–1394.

(61) Farace, G.; Lillie, G.; Hianik, T.; Payne, P.; Vadgama, P. *Bioelectrochemistry* **2002**, *55*, 1–3.

(62) K'Owino, I. O.; Sadik, O. A. *Electroanalysis* **2005**, *17*, 2101–2113.

(63) Yunfang, J.; Wencheng, N. *Solid-State Integr. Circuit Technol.* **2006**, 551–553.

(64) Ciani, I.; Schulze, H.; Corrigan, D. K.; Henihan, G.; Giraud, G.; Terry, J. G.; Walton, A. J.; Pethig, R.; Ghazal, P.; Crain, J.; Campbell, C. J.; Bachmann, T. T.; Mount, A. R. *Biosens. Bioelectron.* **2012**, *31*, 413–418.

(65) Qi, H.; Wang, C.; Cheng, N. *Microchim. Acta* **2010**, *170*, 33–38.

(66) Daniels, J. S.; Pourmand, N. *Electroanalysis* **2007**, *19*, 1239–1257.

(67) Yang, L. C.; Diaz, J. J. E.; McIntire, T. M.; Weiss, G. a; Penner, R. M. *Anal. Chem.* **2008**, *2*, 9–10.

(68) Ribaut, C.; Reybier, K.; Torbiero, B.; Launay, J.; Valentin, A.; Reynes, O.; Fabre, P.-L.; Nepveu, F. *ITBM-RBM* **2008**, *29*, 141–148.

(69) Bart, M.; Stigter, E. C. a; Stapert, H. R.; de Jong, G. J.; van Bennekom, W. P. *Biosens. Bioelectron.* **2005**, *21*, 49–59.

(70) Brosseau, C.; Roscoe, S. *Electrochim. Acta* **2006**, *51*, 2145–2152.

(71) Roscoe, S. *Mod. Asp. Electrochem.* **1996**, *29,* 319–399.

(72) Wang, W.; Mohammadi, F.; Alfantazi, A. *Corros. Sci.* **2012**, *57*, 11–21.

(73) Lassen, B.; Malmsten, M. *J. Colloid Interface Sci.* **1996**, *180*, 339–349.

(74) Bujacz, A. *Acta Crystallogr. D. Biol. Crystallogr.* **2012**, *68*, 1278–1289.

(75) Oliva, F. Y.; Avalle, L. B.; Macagno, V. A.; De Pauli, C. P. *Biophys. Chem.* **2001**, *91*, 141–155.

(76) Dolatshahi-Pirouz, A; Rechendorff, K.; Hovgaard, M. B.; Foss, M.; Chevallier, J.; Besenbacher, F. *Colloids Surf. B. Biointerfaces* **2008**, *66*, 53–59.

(77) Jackson, D. R.; Omanovic, S.; Roscoe, S. G. *Langmuir* **2000**, *16*, 5449–5457.

(78) Jin, W.-J.; Yang, G.-J.; Shao, H.-X.; Qin, A.-J. *Sensors Actuators B Chem.* **2013**, *188*, 271–279.

(79) Bhaduri, A.; Das, K. *J. Dispers. Sci. Technol.* **1999**, *20*, 37–41.

(80) Anzai, J.; Guo, B.; Osa, T. *Chem. Pharm. Bull.* **1994**, *42*, 2391–2393.

(81) Ying, P.; Viana, A. S.; Abrantes, L. M.; Jin, G. *J. Colloid Interface Sci.* **2004**, *279*, 95–99.

(82) Roscoe, S. G.; Fuller, K. L. *J. Colloid Interface Sci.* **1992**, *152*, 429–441.

(83) Pyshnov, E. Electrochemical Studies of the Adsorption of Bovine Serum Albumin on a Platinum Surface, McGill University, 2004.

(84) Valero Vidal, C.; Olmo Juan, a; Igual Muñoz, A *Colloids Surf. B. Biointerfaces* **2010**, *80*, 1–11.

(85) Omanovic, S.; Roscoe, S. G. *Langmuir* **1999**, *15*, 8315–8321.

(86) Wilhelmi, M.; Müller, C.; Ziegler, C.; Kopnarski, M. *Anal. Bioanal. Chem.* **2011**, *400*, 697–701.

(87) Fukuzaki, S.; Urano, H.; Nagata, K. *J. Ferment. Bioeng.* **1996**, *81*, 163–167.

(88) Urano, H.; Fukuzaki, S. *J. Biosci. Bioeng.* **2000**, *90*, 105–111.

(89) Su, T. J.; Lu, J. R.; Thomas, R. K.; Cui, Z. F. *J. Phys. Chem. B* **1999**, *103*, 3727–3736.

(90) Cachet, H.; Debiemme-Chouvy, C. *Electrochim. Acta* **2010**, *55*, 6233–6238.

(91) Ying, P.; Yu, Y.; Jin, G.; Tao, Z. *Colloids Surfaces B Biointerfaces* **2003**, *32*, 1–10.

(92) Jeyachandran, Y. L.; Mielczarski, J. A; Mielczarski, E.; Rai, B. *J. Coll. Int. Sci.* **2010**, *341*, 136–142.

(93) Reimhult, K.; Petersson, K.; Krozer, A. *Langmuir* **2008**, *24*, 8695–8700.

(94) Mohsen, Q.; Fadl-allah, S. A.; El-shenawy, N. S.; Nahla, S. *Int. J. Electrochem. Sci.* **2012**, *7*, 4510–4527.

(95) Yang, G.-J.; Huang, J.-L.; Meng, W.-J.; Shen, M.; Jiao, X.-A. *Anal. Chim. Acta* **2009**, *647*, 159–166.

(96) Schmidt, D. R.; Waldeck, H.; Kao, W. J. *Biological Interactions on Materials Surfaces*; Puleo, D. A.; Bizios, R., Eds.; Springer US: New York, NY, 2009.

(97) Wahlgren, M.; Arnebrant, T. *Trends in Biotechnology* **1991**, *9*, 201–208.

(98) Arnebrant, T.; Ivarsson, B.; Larsson, K. *Progress in Colloid and Polymer Science* **1985**, *70*, 62–66.

(99) Bard, A.; Faulkner, L. *Electrochemical Methods: Fundamentals and Applications*; 2nd ed.; John Wiley & Sons, Inc.: United States of America, 2001.

(100) Xie, Q.; Zhang, Y.; Xu, M.; Li, Z.; Yuan, Y.; Yao, S. *J. Electroanal. Chem.* **1999**, *478*, 1–8.

(101) Grieten, L.; Janssens, S. D.; Ethirajan, A.; Bon, N. Vanden; Ameloot, M.; Michiels, L.; Haenen, K.; Wagner, P. *Phys. Status Solidi* **2011**, *208*, 2093–2098.

(102) Campbell-Rance, D. S.; Doan, T. T.; Leopold, M. C. *J. Electroanal. Chem.* **2011**, *662*, 343–354.

(103) Pupim Ferreira, A. A.; Alves, M. J. M.; Barrozo, S.; Yamanaka, H.; Benedetti, A. V. *J. Electroanal. Chem.* **2010**, *643*, 1–8.

(104) Riegar, P. *Electrochemistry*; 2nd ed.; Prentice-Hall: United States of America, 1994.

(105) Bockris, J. O.; Reddy, A. K. N. .; Gamboa-Adelco, M. E. *Modern Electrochemistry 2A: Fundamentals of Electrodics*; Springer, 2000.

(106) Lisdat, F.; Schäfer, D. *Anal. Bioanal. Chem.* **2008**, *391*, 1555–1567.

(107) Wright, J.; Cosman, N. P.; Fatih, K.; Omanovic, S.; Roscoe, S. G. *J. Electroanal. Chem.* **2004**, *564*, 185–197.

(108) Ueta, R. R.; Diniz, F. B. *Colloids Surf. B. Biointerfaces* **2008**, *61*, 244–249.

(109) Luo, H.; Du, Y.; Guo, Z.-X. *Bioelectrochemistry* **2009**, *74*, 232–235.

(110) Lin, Z.; Chen, L.; Zhang, G.; Liu, Q.; Qiu, B.; Cai, Z.; Chen, G. *Analyst* **2012**, *137*, 819–822.

(111) Lvovich, V. F. *Impedance Spectroscopy: Applications to Electrochemical and Dielectric Phenomena*; 1st ed.; John Wiley & Sons, Inc.: Hoboken, New Jersey, 2012.

(112) Tjin, S. C. *IEEE Sensors* **2005**, 397–400.

(113) Liu, C.; Bi, Q.; Leyland, A; Matthews, A. *Corros. Sci.* **2003**, *45*, 1243–1256.

(114) *Biosensing for the 21st Century*; Renneberg, R.; Lisdat, F.; Andresen, D.; Scheller, F., Eds.; Springer Berlin Heidelberg, 2008.

(115) LeRu, E. C.; Etchegoin, P. G. *Principles of Surface-Enhanced Raman Spectroscopy*; 1st ed.; Elsevier B.V., 2009.

(116) Mahajan, S. Engineering substrates for SERS: fundamentals and applications, University of Southampton, 2008.

(117) Fleischman, A.; Hendra, P. J.; McQuillan, A. J. *Chem. Phys. Lett.* **1974**, *26*, 163–166.

(118) Jeanmaire, D. L.; Van Duyne, R. P. *J. Electroanal. Chem.* **1977**, *84*, 1–20.

(119) Albrecht, M.; Creighton, J. *J. Am. Chem. Soc.* **1977**, *99*, 5215–5217.

(120) Han, X. X.; Jia, H. Y.; Wang, Y. F.; Lu, Z. C.; Wang, C. X.; Xu, W. Q.; Zhao, B.; Ozaki, Y. *Anal. Chem.* **2008**, *80*, 2799–2804.

(121) Das, G.; Gentile, F.; Coluccio, M. L.; Perri, a. M.; Nicastri, a.; Mecarini, F.; Cojoc, G.; Candeloro, P.; Liberale, C.; De Angelis, F.; Di Fabrizio, E. *J. Mol. Struct.* **2011**, *993*, 500–505..

(122) Cao, Y. C.; Jin, R.; Nam, J.-M.; Thaxton, C. S.; Mirkin, C. *J. Am. Chem. Soc.* **2003**, *125*, 14676–14677.

(123) Stewart, S.; Fredericks, P. M. *Spectrochim. Acta Part A Mol. Biomol. Spectrosc.* **1999**, *55*, 1615–1640.

(124) Porter, M. D.; Lipert, R. J.; Siperko, L. M.; Wang, G.; Narayanan, R. *Chem. Soc. Rev.* **2008**, *37*, 1001–1011.

(125) Iosin, M.; Toderas, F.; Baldeck, P. L.; Astilean, S. *J. Mol. Struct.* **2009**, *924-926*, 196–200.

(126) Cavalu, S.; Cîntă-Pînzaru, S.; Leopold, N.; Kiefer, W. *Biopolymers* **2001**, *62*, 341–348.

(127) Chumanov, G. D.; Efremov, R. G.; Nabiev, I. R. *J. Raman Spectrosc.* **1990**, *21*, 43–48.

(128) Das, G.; Mecarini, F.; Gentile, F.; De Angelis, F.; Mohan Kumar, H.; Candeloro, P.; Liberale, C.; Cuda, G.; Di Fabrizio, E. *Biosens. Bioelectron.* **2009**, *24*, 1693–1699.

(129) Conway, B. E.; Sharp, B. A. *J. Chem. Soc. Faraday Trans. 1 Phys. Chem. Condens. Phases* **1977**, *20,* 1373-1389.

(130) Johnson, R. P.; Richardson, J.; Brown, T.; Bartlett, P. N. *Langmuir* **2012**, *28*, 5464–5470.

(131) Abdelsalam, M. E.; Bartlett, P. N.; Baumberg, J. J.; Cintra, S.; Kelf, T.; Russell, A. E. *Electrochem. Commun.* **2005**, *7*, 740–744.

(132) Orazem, M. E.; Tribollet, B. *Electrochemical Impedance Spectroscopy*; 1st ed.; Hoboken, New Jersey, 2008.

(133) Esteban, J.; Orazem, M. *J. Electrochem. Soc.* **1991**, *138,* 67-76

(134) Boukamp, B. A. *J. Electrochem. Soc.* **1995**, *142*, 1885-1894.

(135) Sadkowski, A. *J. Electroanal. Chem.* **2004**, *573*, 241–253.

(136) Boukamp, B. *Solid State Ionics* **2004**, *169*, 65–73.

(137) Macdonald, D. D.; Urquidi-Macdonald, M. *J. Electrochem. Soc.* **1985**, *132*, 2316–2319.

(138) Urquidi-Macdonald, M.; Real, S.; Macdonald, D. D. *J. Electrochem. Soc.* **1986**, 2018–2024.

(139) Macdonald, D. D.; Urquidi-Macdonald, M. *J. Electrochem. Soc.* **1990**, *137*, 20–22.

(140) Agarwal, P. *J. Electrochem. Soc.* **1992**, *139*, 1917-1927.

(141) Agarwal, P.; Crisalle, O. D.; Orazem, M. E. *J. Electrochem. Soc.* **1995**, *142*, 4149–4158.

(142) Agarwal, P. *J. Electrochem. Soc.* **1995**, *142*, 4159–4168.

(143) Labjar, N.; Lebrini, M.; Bentiss, F.; Chihib, N.-E.; Hajjaji, S. El; Jama, C. *Mater. Chem. Phys.* **2010**, *119*, 330–336.

(144) Nigam, A. K.; Balasubramaniam, R.; Bhargava, S.; Baligidad, R. G. *Corros. Sci.* **2006**, *48*, 1666–1678.

(145) Macdonald, J. *Ann. Biomed. Eng.* **1992**, *20*, 289–305.

(146) Campuzano, S.; Pedrero, M. *J. Electroanal. Chem.* **2006**, *586*, 112–121.

(147) Singh, R.; Suni, I. I. *J. Electrochem. Soc.* **2010**, *157*, J334–J337.

(148) Tsai, J.-J.; Liu, Y.-F.; Liao, E.-C.; Chen, J.-L.; Wang, G.-J. *Sensors Actuators B Chem.* **2013**, *178*, 404–411.

(149) Omanović, S.; Metikoš-Huković, M. *Thin Solid Films* **1995**, *266*, 31–37.

(150) Gu, H.; Su, X.; Loh, K. *J. Phys. Chem. B* **2005**, *109*, 13611–13618.

(151) Yu, X.; Lv, R.; Ma, Z.; Liu, Z.; Hao, Y.; Li, Q.; Xu, D. *Analyst* **2006**, *131*, 745–750.

(152) Hsu, C. H.; Mansfield, F. *Corrosion* **2001**, *57*, 747–748.

(153) Chang, B.-Y.; Park, S.-M. *Annu. Rev. Anal. Chem.* **2010**, *3*, 207–229.

(154) Jones, K. L.; O'Melia, C. R. *J. Memb. Sci.* **2000**, *165*, 31–46.

(155) Farcas, M.; Cosman, N. P.; Ting, D. K.; Roscoe, S. G.; Omanovic, S. *J. Electroanal. Chem.* **2010**, *649*, 206–218.

(156) Gilman, S. *J. Phys. Chem.* **1964**, *3*, 2098–2111.

(157) Nart, F.; Iwasita, T. *Electrochim. Acta* **1992**, *37*, 385–391.

(158) Michaels, A. M.; Brus, L. *J. Phys. Chem. B* **2000**, *104*, 11965–11971.

(159) Zhang, D.; Ansar, S. M.; Vangala, K.; Jiang, D. *J. Raman Spectrosc.* **2010**, *41*, 952–957.

(160) Vo-Dinh, T.; Allain, L. R.; Stokes, D. L. *J. Raman Spectrosc.* **2002**, *33*, 511–516.

(161) Dancil, K.; Greiner, D.; Sailor, M. *J. Am. Chem. Soc.* **1999**, 7925–7930.

(162) Graham, D.; Faulds, K. *Chem. Soc. Rev.* **2008**, *37*, 1042–51.

(163) Magner, E. *Analyst* **1998**, *123*, 1967–1970.

(164) Badihi-Mossberg, M.; Buchner, V.; Rishpon, J. *Electroanalysis* **2007**, *19*, 2015–2028.

(165) Tantipolphan, R.; Rades, T.; McQuillan, A J.; Medlicott, N. J. *Int. J. Pharm.* **2007**, *337*, 40–47.

(166) Weber, M.; Nart, F. *J. Phys. Chem.* **1996**, *3654*, 19933–19938.

(167) Urano, H.; Fukuzaki, S. *J. Ferment. Bioeng.* **1997**, *83*, 261–266.

(168) Urano, H.; Fukuzaki, S. *J. Colloid Interface Sci.* **2002**, *252*, 284–289.

(169) Bond, M.; Shuman, H. *J. Physiol.* **1984**, *357*, 185–201.

(170) Forse, R.; Shizgal, H. *J. Parenter. Enter. Nutr.* **1980**, *4*, 450–454.

(171) Cosman, N.; Roscoe, S. *Langmuir* **2004**, *20*, 1711–1720.

(172) Weingarth, D.; Foelske-Schmitz, A.; Wokaun, A.; Kötz, R. *Electrochem. Commun.* **2011**, *13*, 619–622.

APPENDIX

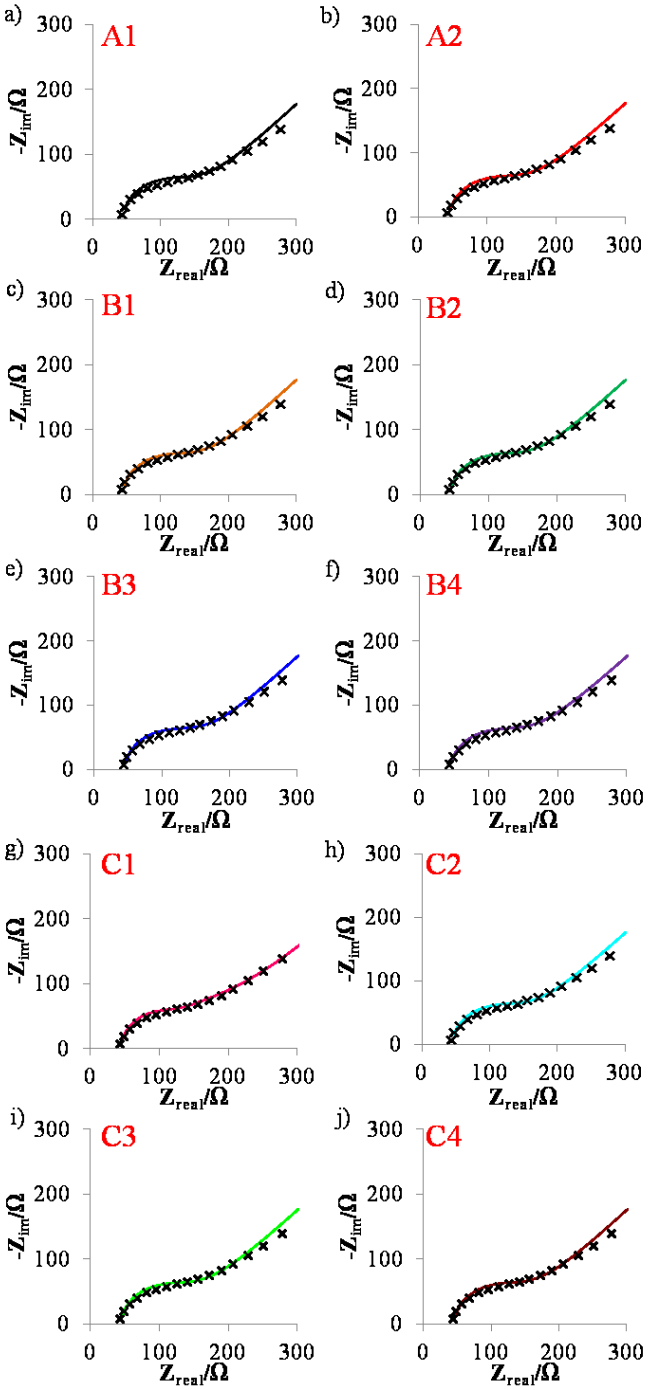

Figure A1: Nyquist plots for a Pt electrode in 0.2 M PBS with 3 mM ferri/ferrocyanide (20 h), with fit data generated from fitting experimental data to each circuit in Figure 5.2. (x) indicate experimental data and solid lines indicate fit. (Trial 2)

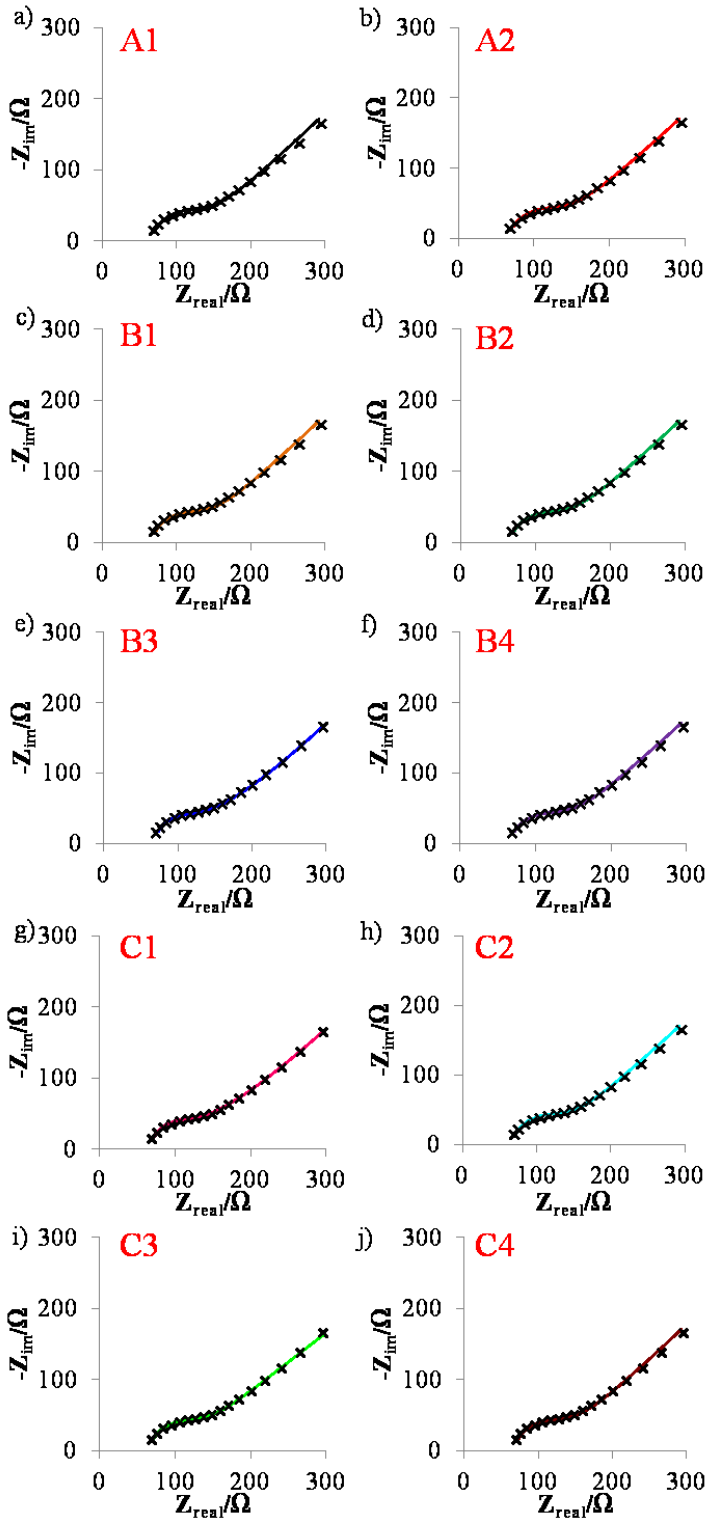

Figure A2: Nyquist plots for a Pt electrode in 0.2 M PBS with 3 mM ferri/ferrocyanide (20 h), with fit data generated from fitting experimental data to each circuit in Figure 5.2. (x) indicate experimental data and solid lines indicate fit. (Trial 3)

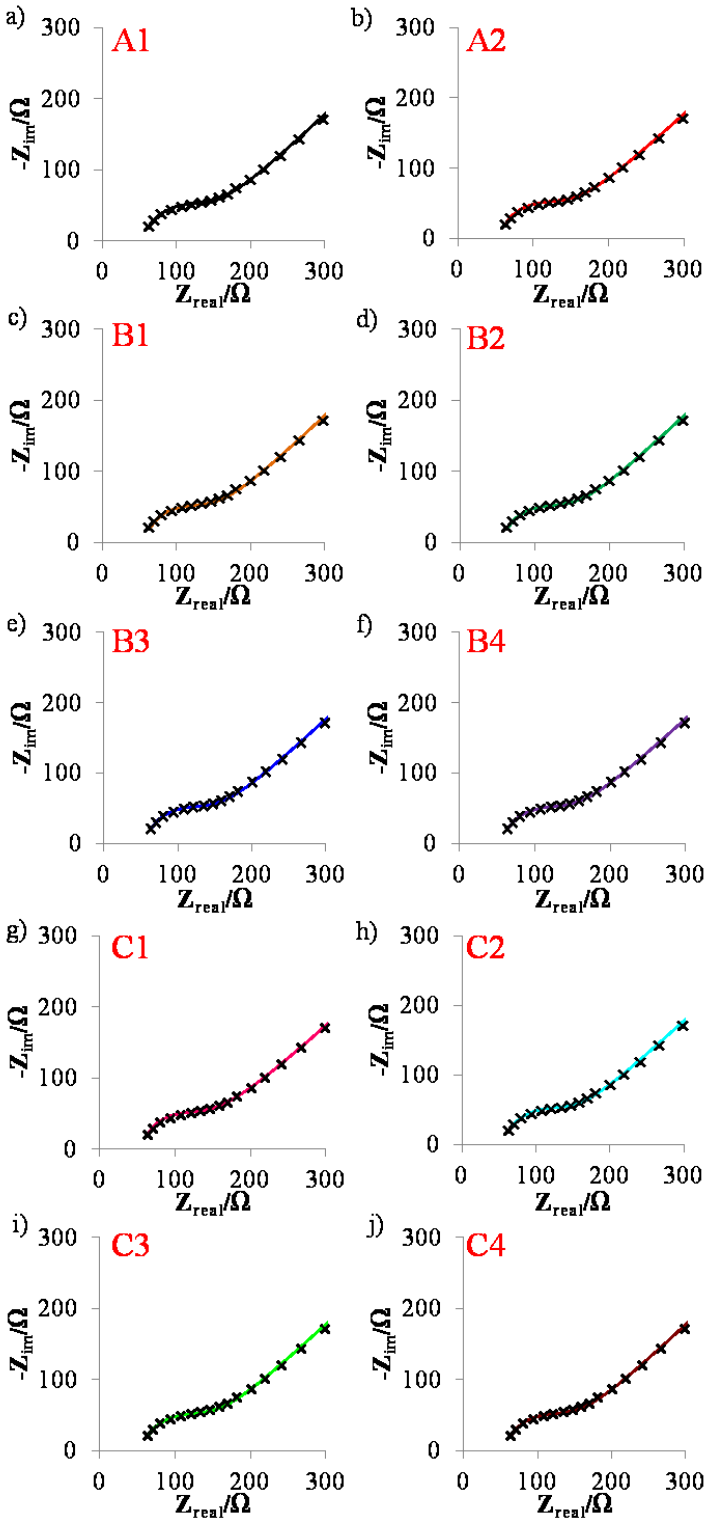

Figure A3: Nyquist plots for a Pt electrode in 0.2 M PBS with 3 mM ferri/ferrocyanide (20 h), with fit data generated from fitting experimental data to each circuit in Figure 5.2. (x) indicate experimental data and solid lines indicate fit. (Trial 4)

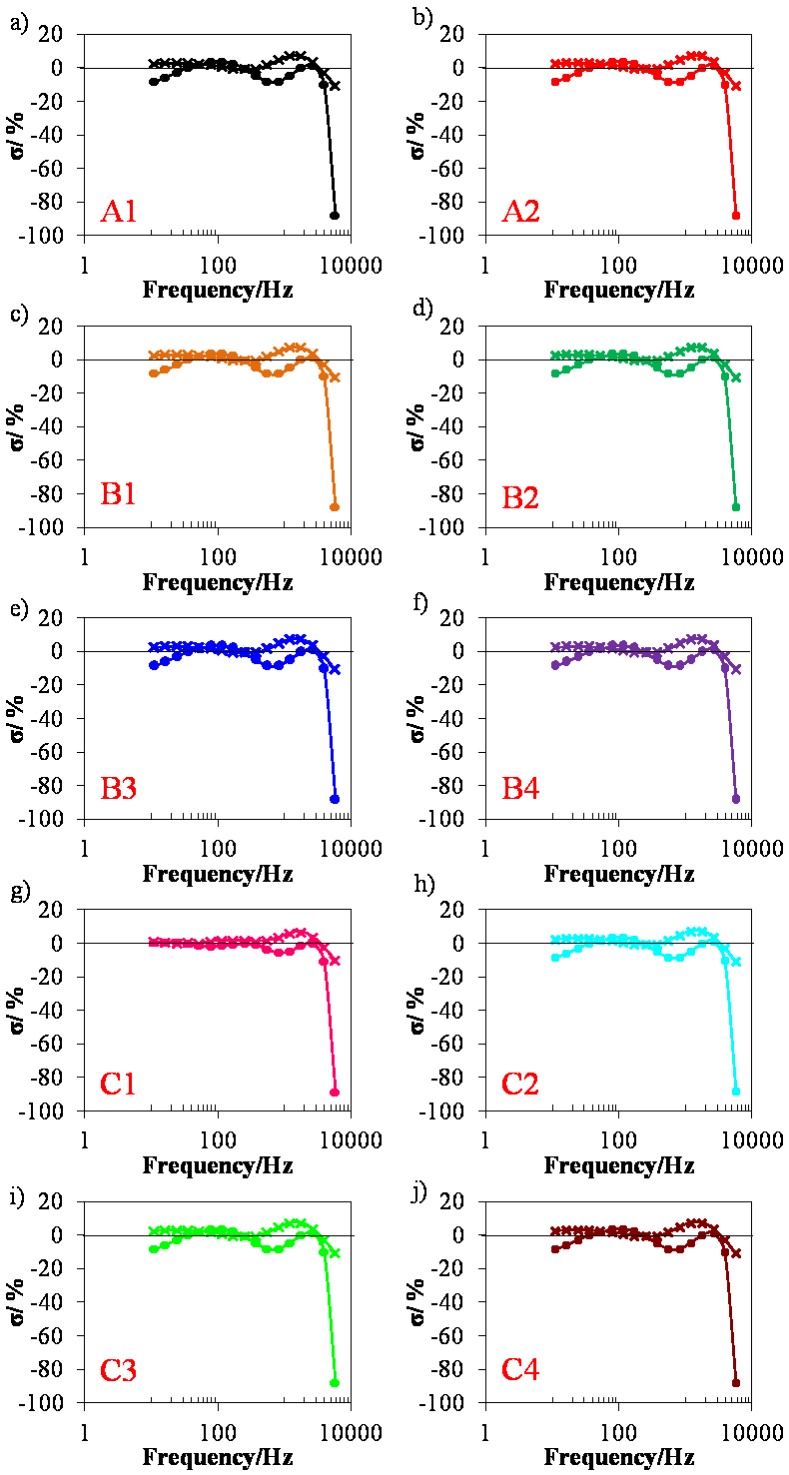

Figure A4: Relative residual errors resulting from the fit of circuits in Figure 5.2 to the 20 h data (Figure 5.3) for a Pt wire electrode in 0.2 M PBS solution with 3 mM ferri/ferrocyanide. Crosses represent σ_{real} and circles represent σ_{im}, discussed in Chapter 4. (Trial 2)

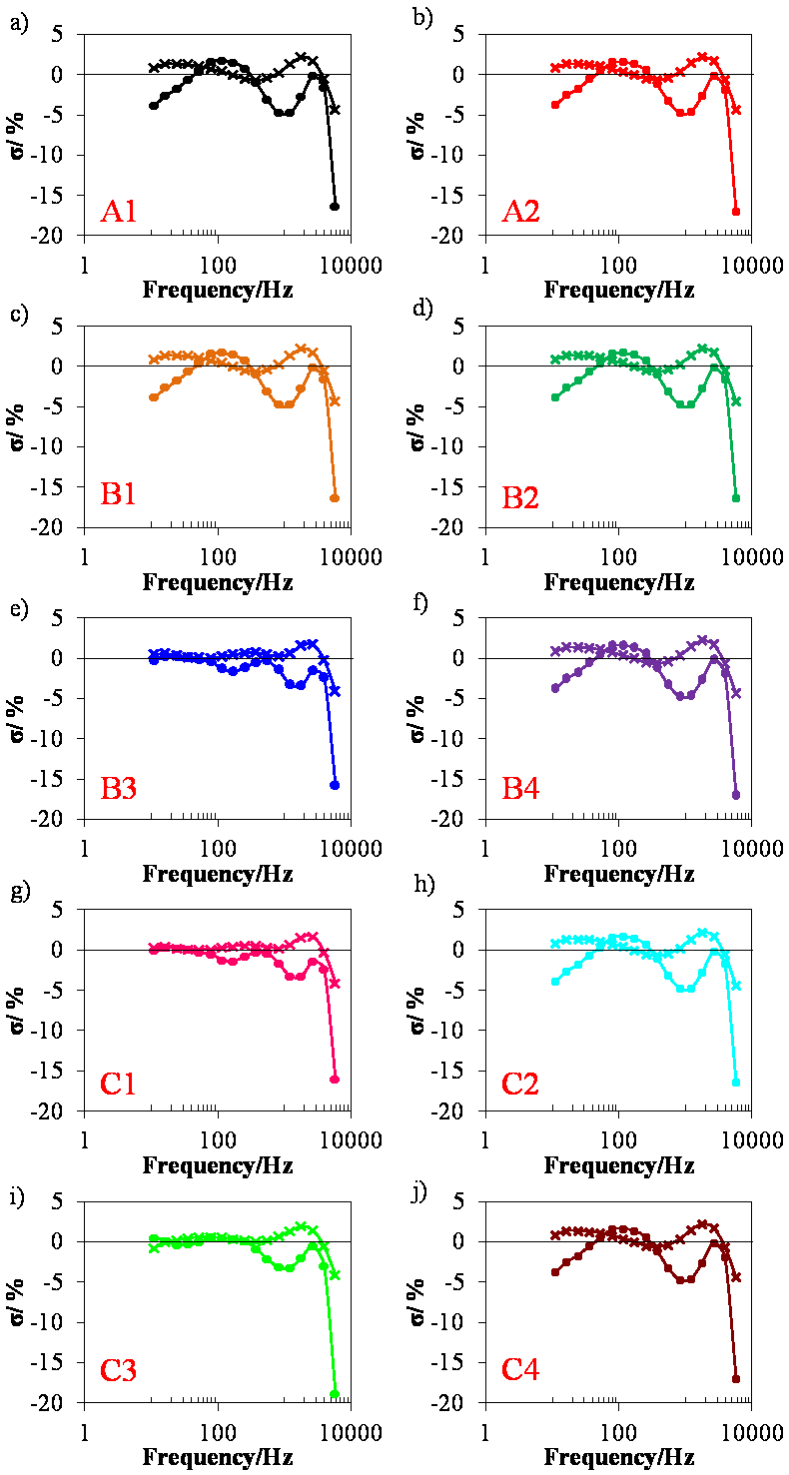

Figure A5: Relative residual errors resulting from the fit of circuits in Figure 5.2 to the 20 h data (Figure 5.3) for a Pt wire electrode in 0.2 M PBS solution with 3 mM ferri/ferrocyanide. Crosses represent σ_{real} and circles represent σ_{im}, discussed in Chapter 4. (Trial 3)

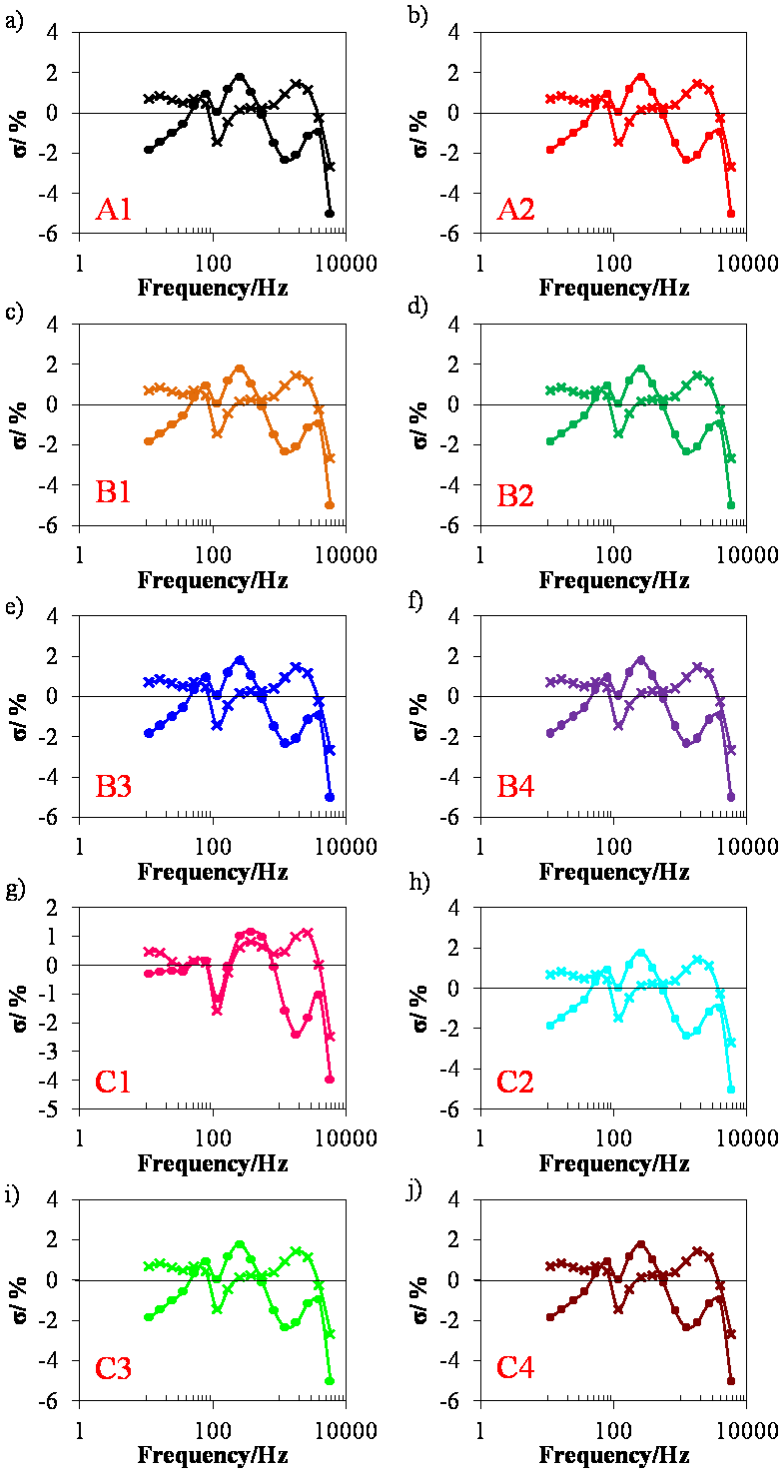

Figure A6: Relative residual errors resulting from the fit of circuits in Figure 5.2 to the 20 h data (Figure 5.3) for a Pt wire electrode in 0.2 M PBS solution with 3 mM ferri/ferrocyanide. Crosses represent σ_{real} and circles represent σ_{im}, discussed in Chapter 4. (Trial 4)

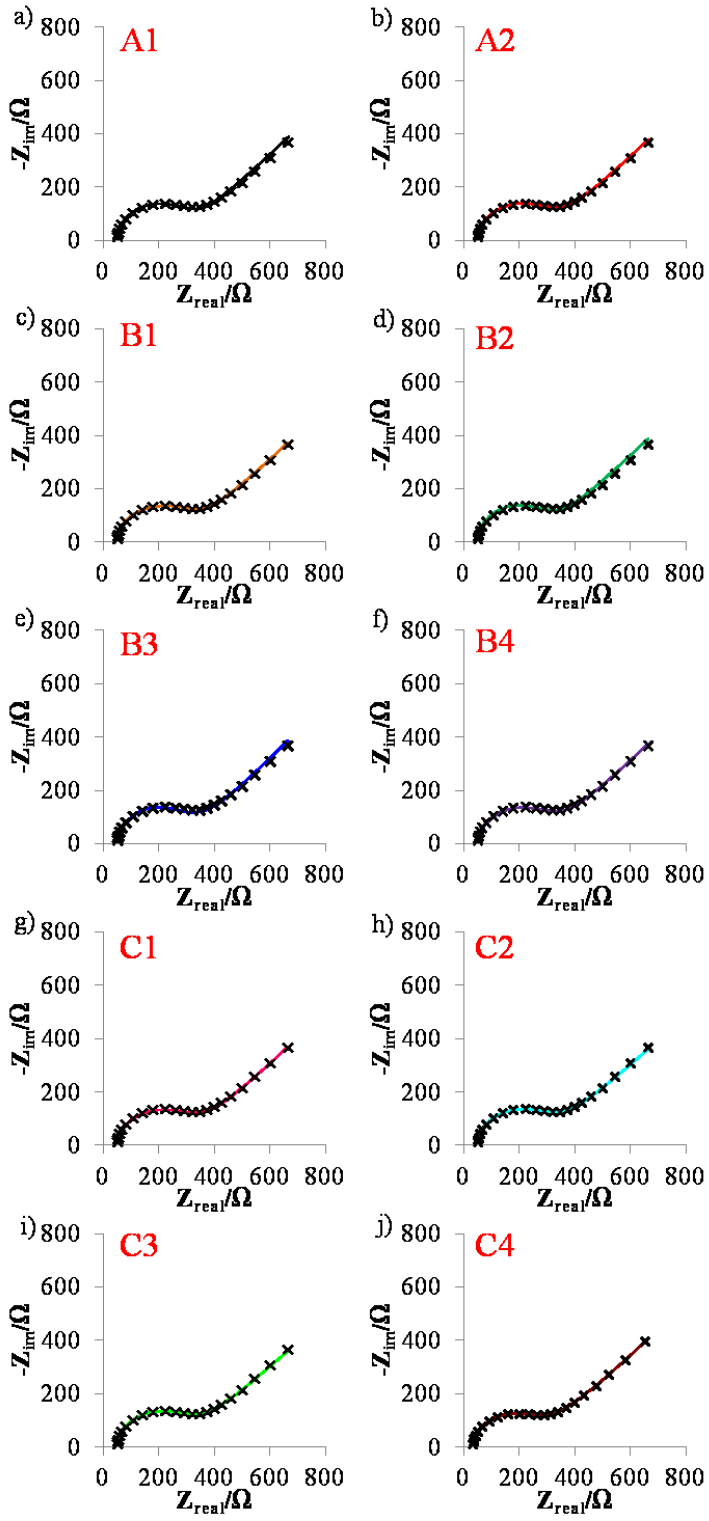

Figure A7: Nyquist plots for a Pt wire electrode incubated in 1 g L^{-1} BSA for 30 minutes, followed by EIS in a 0.2 M PBS solution with 3 mM ferri/ferrocyanide (20 h), with fit data generated from fitting experimental data (Figure 5.6) to circuits presented in Figure 5.2. (Trial 2)

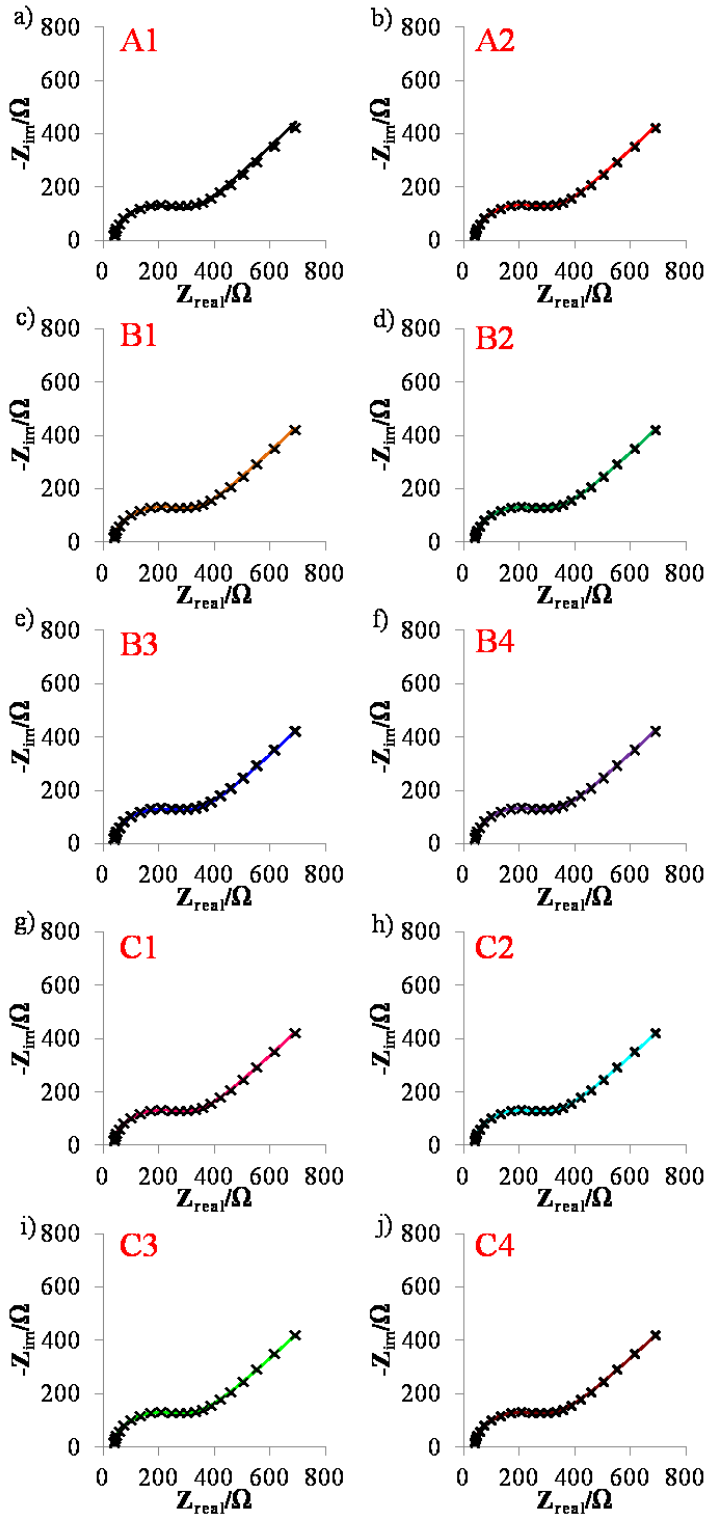

Figure A8: Nyquist plots for a Pt wire electrode incubated in 1 g L^{-1} BSA for 30 minutes, followed by EIS in a 0.2 M PBS solution with 3 mM ferri/ferrocyanide (20 h), with fit data generated from fitting experimental data (Figure 5.6) to circuits presented in Figure 5.2. (Trial 3)

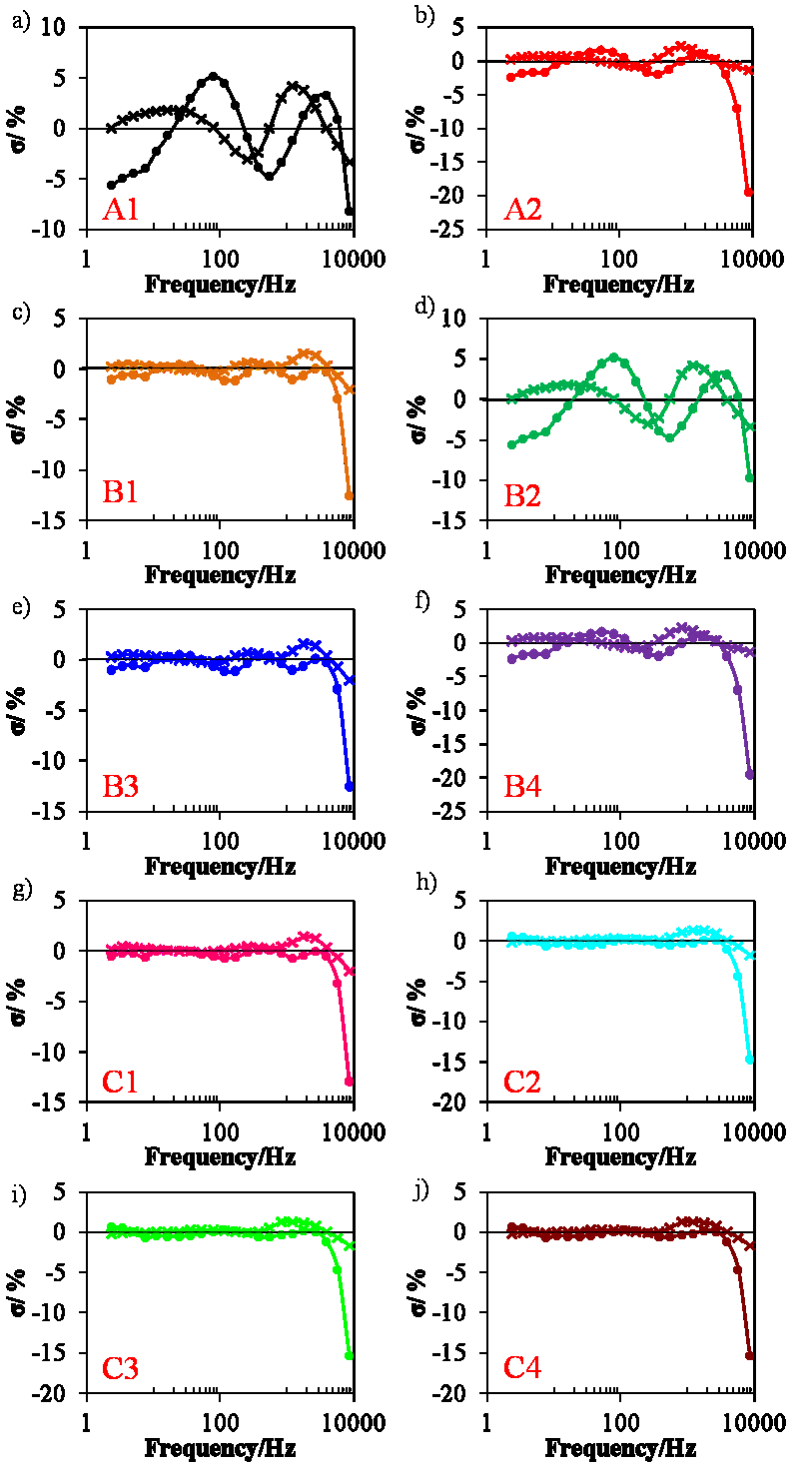

Figure A9: Relative residual errors resulting from the fit of circuits in Figure 5.2 to the data shown in shown in Figure 5.6 for a Pt wire electrode incubated in 1 g L^{-1} BSA for 30 minutes, followed by EIS in 0.2 M PBS with 3 mM ferri/ferrocyanide (20 h). Crosses represent σ_{real} and circles represent σ_{im}. (Trial 2)

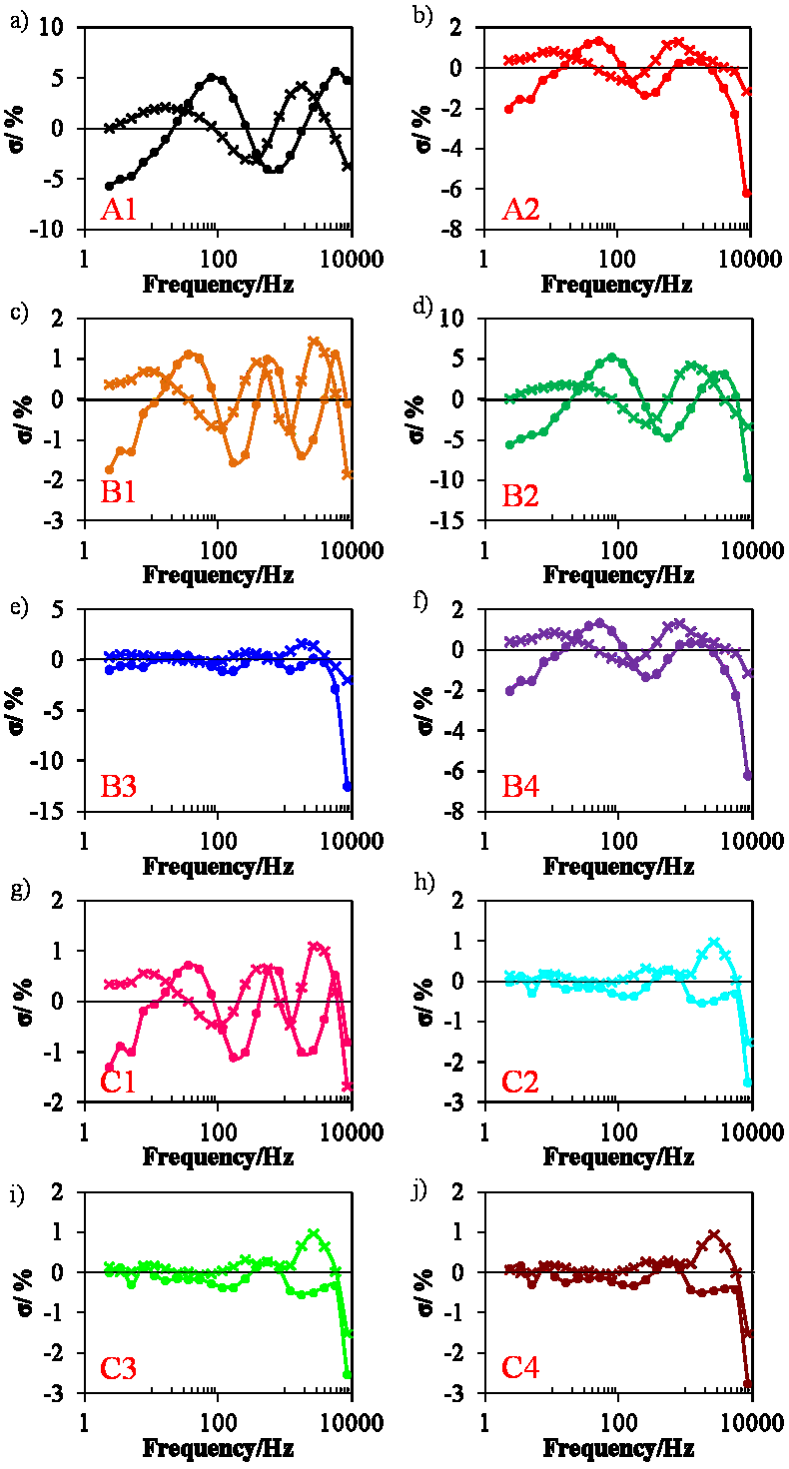

Figure A10: Relative residual errors resulting from the fit of circuits in Figure 5.2 to the data shown in shown in Figure 5.6 for a Pt wire electrode incubated in 1 g L^{-1} BSA for 30 minutes, followed by EIS in 0.2 M PBS with 3 mM ferri/ferrocyanide (20 h). Crosses represent σ_{real} and circles represent σ_{im}. (Trial 3)

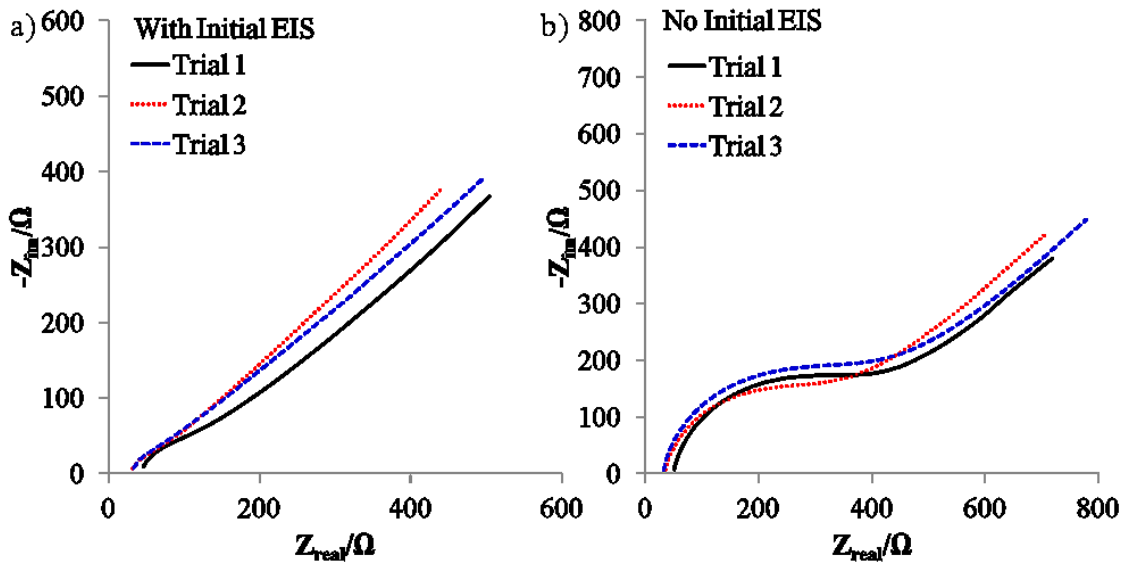

Figure A11: EIS spectra for a Pt wire electrode in 0.2 M PBS solution with 3 mM ferri/ferrocyanide after incubation in 1 g L^{-1} BSA solution for 30 minutes with (a) and without (b) initial EIS in BSA-free PBS solution.

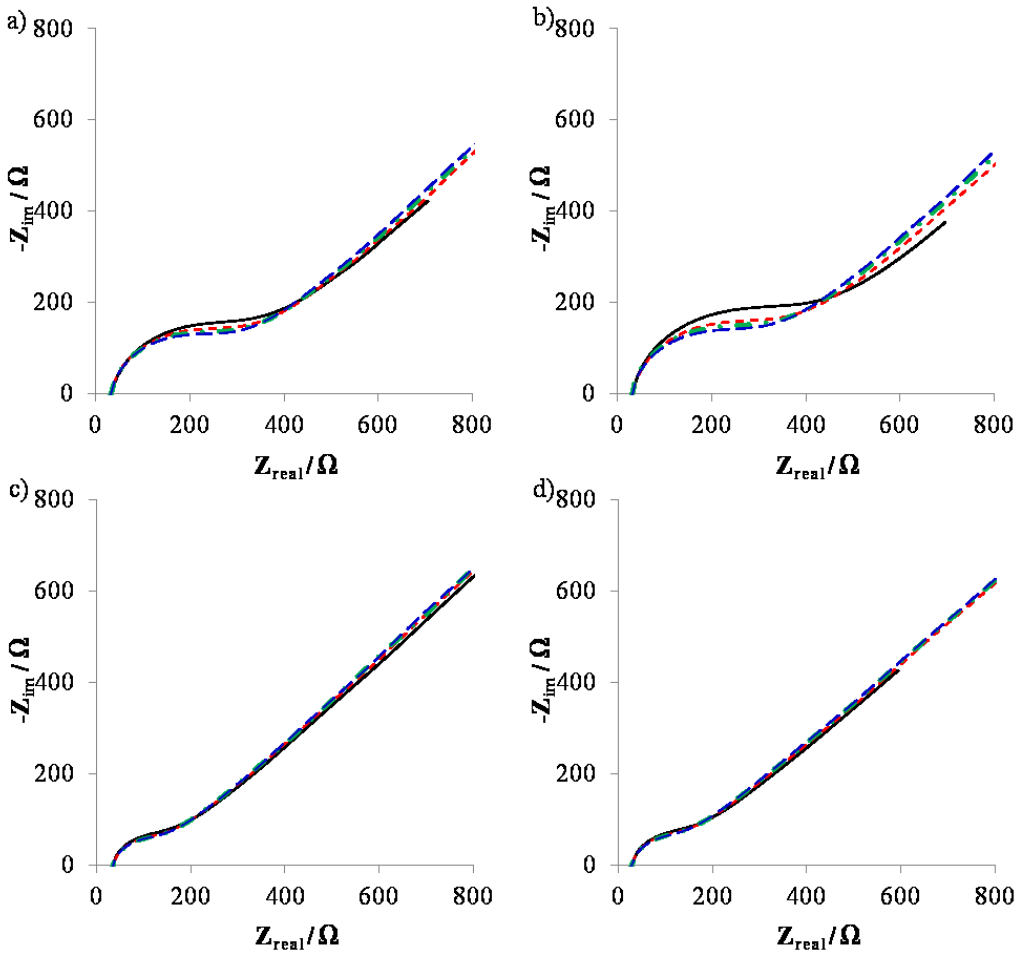

Figure A12: Four consecutive spectra recorded in 0.2 M PBS solution with 3 mM ferri/ferrocyanide after incubation at E_{oc} (a and b) and E_{eq} (c and d).Time after incubation: 0 min (solid black), 3 min (short dash red), 6 min (dot-dash green), and 9 min (long dash blue).

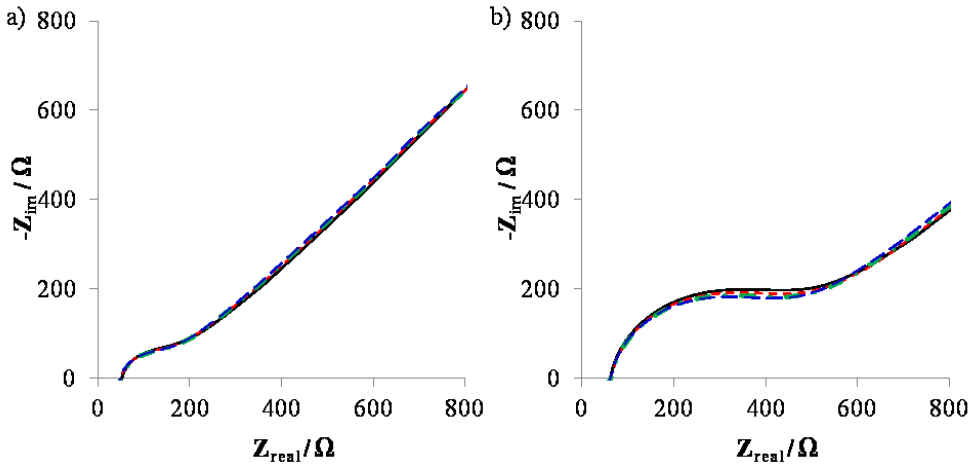

Figure A13: a) and b) Four consecutive spectra recorded in 0.2 M PBS solution with 3 mM ferri/ferrocyanide after incubation at ac 0.171 V. Time after incubation: 0 min (solid black), 3 min (short dash red), 6 min (dot-dash green), and 9 min (long dash blue).

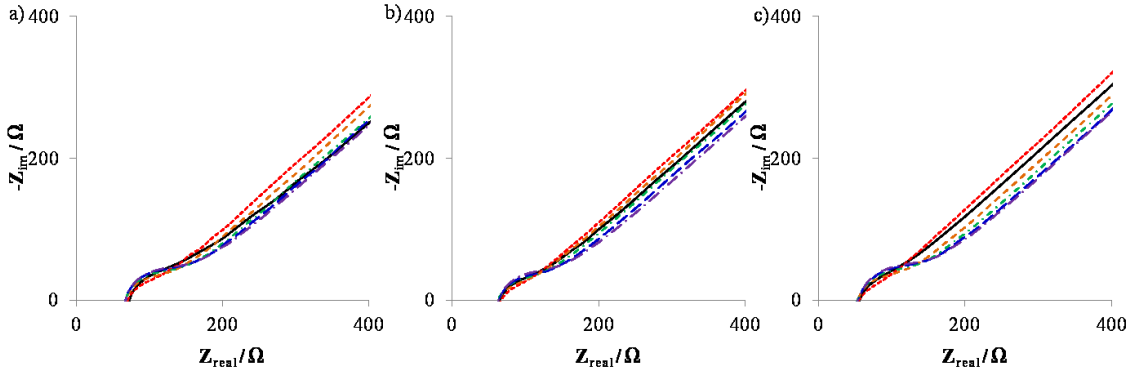

Figure A14: Nyquists plots for a Pt electrode immersed in 0.2 M PBS solution with 3 mM ferri/ferrocyanide (blank experiments). a) Trial 2, b) Trial 3, c) Trial 4

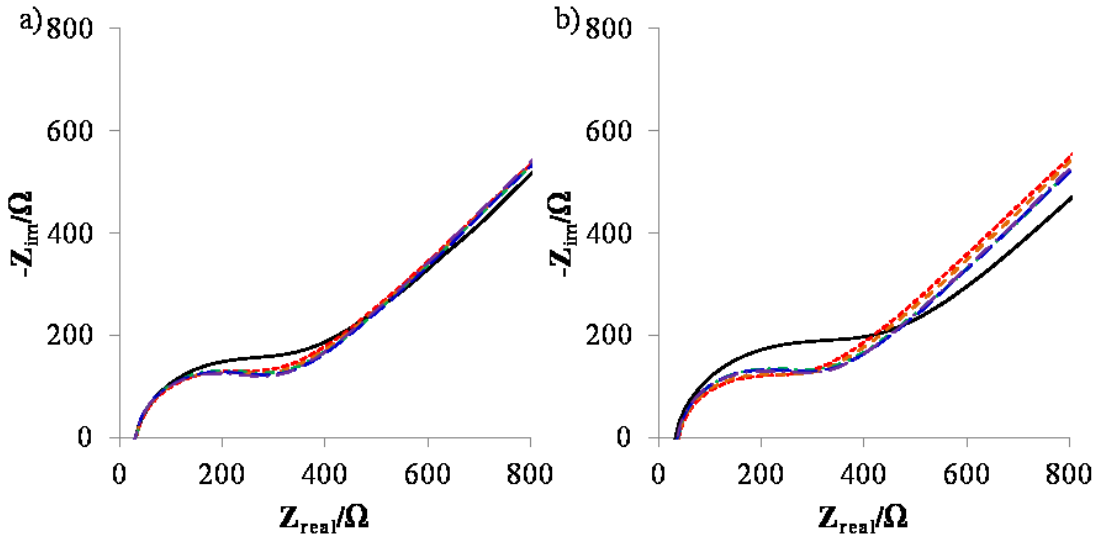

Figure A15: Nyquist plots a Pt wire electrode in 0.2 M PBS solution with 3 mM ferri/ferrocyanide, after incubation in 1 g L^{-1} BSA for 30 minutes. Time after incubation: 0 h (black, solid), 1 h (red, dotted), 5 h (orange, short dash), 10 h (green, dot dash), 15 h (blue, long dash), 20 h (purple, long dash dot). a) Trial 2, b) Trial 3

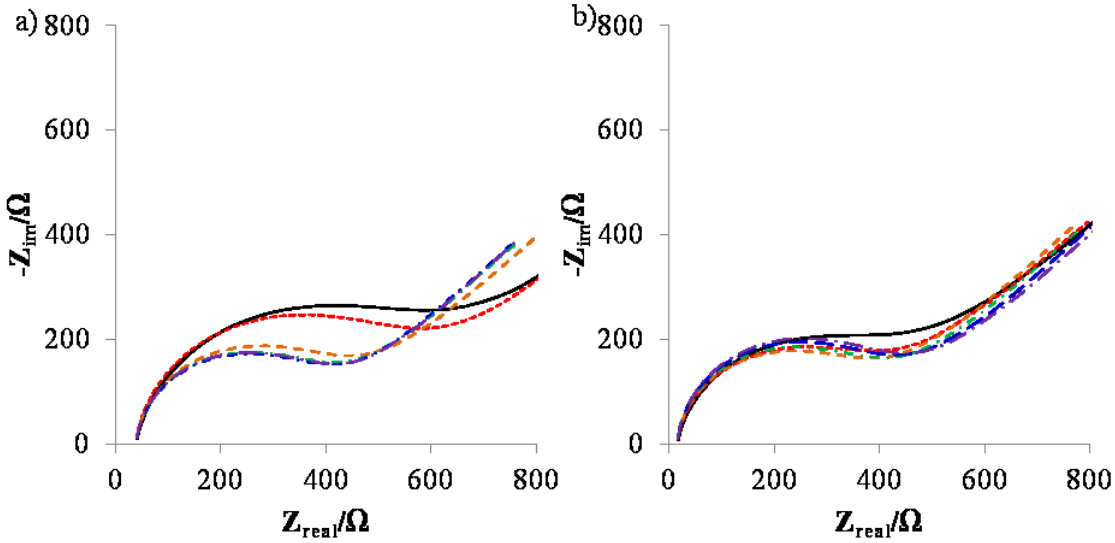

Figure A16: Nyquist plots a Pt wire electrode in 0.2 M PBS solution with 3 mM ferri/ferrocyanide and 1 g L^{-1} BSA, after 30 minutes at E_{oc}. Time after 30 minute rest at E_{oc}: 0 h (black, solid), 1 h (red, dotted), 5 h (orange, short dash), 10 h (green, dot dash), 15 h (blue, long dash), 20 h (purple, long dash dot).